



ALMA MATER STUDIORUM
UNIVERSITÀ DI BOLOGNA

DOTTORATO DI RICERCA IN
SCIENZE BIOTECNOLOGICHE, BIOCOMPUTAZIONALI,
FARMACEUTICHE E FARMACOLOGICHE

Ciclo 36

Settore Concorsuale: 03/D1 - CHIMICA E TECNOLOGIE FARMACEUTICHE,
TOSSICOLOGICHE E NUTRACEUTICO - ALIMENTARI

Settore Scientifico Disciplinare: CHIM/08 - CHIMICA FARMACEUTICA

FROM THE IDENTIFICATION OF A DRUGGABLE TARGET FOR THE
OLANZAPINE-INDUCED METABOLIC SYNDROME TO THE DEVELOPMENT OF
A NEW THERAPEUTIC APPROACH USING CRISPR/CAS7-11S.

Presentata da: Federica Veneziani

Coordinatore Dottorato

Maria Laura Bolognesi

Supervisore

Andrea Cavalli

Co-supervisore

Jean Martin Beaulieu

CONTENTS

1. BACKGROUND.....	4
1.1 OLANZAPINE AND THE METABOLIC BURDEN OF SECOND-GENERATION ANTIPSYCHOTICS (SGA).....	4
1.2 HYPOTHALAMIC CONTROL OF ENERGY METABOLISM AND HIS SUSPECTED INVOLVEMENT IN OL-INDUCED METABOLIC SYNDROME.....	7
1.3 AVAILABLE THERAPEUTIC APPROACHES FOR METS.....	11
1.4 GENE THERAPY AND THE CRISPR-CAS SYSTEM.....	13
1.5 CRISPR/Cas SYSTEM INHIBITION.....	16
2. AIMS OF THE STUDY.....	17
3. MATERIALS AND METHODS.....	18
3.1 ANIMALS.....	18
3.2 STEREOTAXIC INJECTION.....	18
3.3 IMMUNOHISTOCHEMISTRY.....	20
3.4 TREATMENT.....	21
3.5 PHENOTYPE CHARACTERIZATION.....	21
3.6 BEHAVIORAL ASSAY.....	23
3.7 TISSUES DISSECTION	23
3.8 HYPOTHALAMIC RNA EXTRACTION.....	24
3.9 STATISTICAL ANALYSIS.....	24
3.10 DEVELOPMENT OF TRUNCATED VERSION OF Cas7-11 (Cas7-11S) AND CLONING IN pcDNA3.1.....	25
3.11 MODIFICATION OF pX459V.2 PLASMID TO CHANGE THE PROMOTER DRIVING THE EXPRESSION OF THE GUIDE RNA FROM U6 TO tRNA	26
3.12 DESIGNING OF GUIDES AGAINST CB1R RNA AND CLONING.....	27
3.13 GENERATION OF STABLE CELLS EXPRESSING Cas7-11S.....	29
3.14 TRANSFECTION OF THE GUIDES TARGETING THE CB1R RNA IN N2A STABLE CELLS EXPRESSING Cas7-11S.....	29
3.15 RNA ISOLATION AND qPCR.....	29
3.16 RNA SCOPE FOR VISUALIZING CB1 AND CAS7-11S IN THE ENGINEERED N2A CELL LINE.....	29
3.17 PROTEIN PREPARATION.....	30
3.18 LIBRARIES PREPARATION.....	32
3.19 VIRTUAL SCREENING.....	32

4. RESULTS.....	33
4.1 STUDY PART 1: H1R AND CB1R INVOLVEMENT IN THE PATHOGENESIS OF OL-INDUCED METS.....	33
4.2 STUDY PART 2: EXPLORATION OF THE BIOLOGICAL MECHANISMS OF H1R AND CB1R-MEDIATED CLINICAL PHENOTYPE OF OL-INDUCED MetS.....	38
4.3 STUDY PART 3: CB1R AS A POTENTIAL DRUGGABLE TARGET: EVALUATION OF MOOD-LIKE SIDE EFFECTS AND POSSIBLE REPRODUCTIVE DISFUNCIONS.....	42
4.4 STUDY PART 4: CRISPR/Cas7-11S THERAPEUTIC APPROACH – IN VITRO VALIDATION OF THE CB1R KNOCKDOWN.....	44
5. DISCUSSION.....	48
6. CONCLUSION.....	51
7. REFERENCES.....	53
8. SUPPLEMENTAL MATERIALS.....	63
8.1 FIGURES.....	63
8.2 TABLES.....	67

1. BACKGROUND

1.1 OLANZAPINE AND THE METABOLIC BURDEN OF SECOND-GENERATION ANTIPSYCHOTICS (SGA)

Olanzapine (OL) is a second-generation antipsychotic used to treat psychotic symptoms in the context of schizophrenia and mood disorders. Its mechanism of action, same as the other drugs belonging to the same class, is mediated by the blockade of the Dopamine D2 receptor (DRD2) and the serotonin 2A receptor (5HT2A). The affinity for 5HT2A differentiates the second-generation antipsychotics from the first-generation (FGA), whose pharmacological action is only due to the DRD2 antagonism. (1)

The DRD2 blockade in the mesolimbic area of the brain seems to be responsible for the therapeutic effect of the antipsychotic medications on positive symptoms of schizophrenia, such as delusion and hallucinations. However, the broad targeting of DRD2 in the brain, involving the mesocortical, nigrostriatal and tuberoinfundibular areas, is considered the major contributor to FGA side effects, such as impaired cognitive functions, extrapyramidal symptoms (parkinsonian symptoms, dystonia, akathisia and tardive dyskinesia) and hyperprolactinemia (Figure 1). (2)

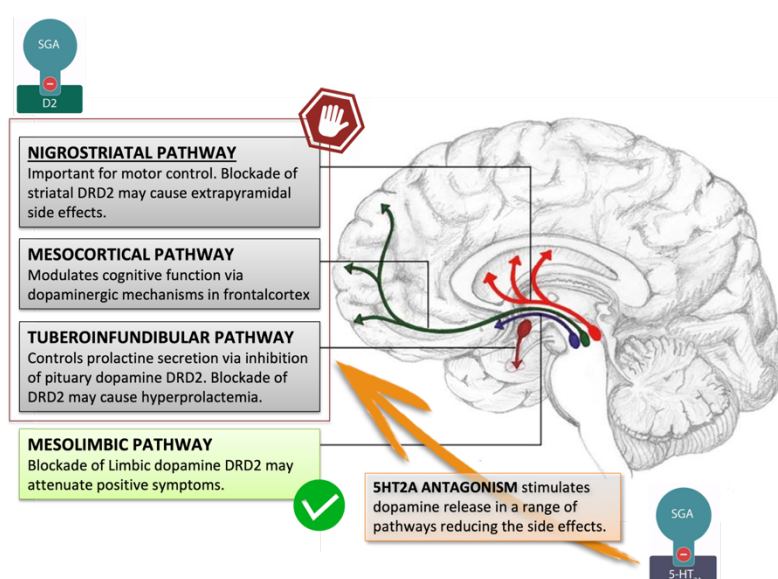


Fig.1 Representation of the mechanism of action of the second-generation antipsychotics. Here is shown the regulation by Dopamine receptor 2 (D2) and Serotonin receptor 2A (5HT2A) of the main pathways involved in the therapeutical properties and the side effects of these drugs.

The 5HT2A blockade, on the other hand, improves the side effects observed with FGA while increasing the therapeutic action on positive symptoms. Indeed, the amelioration of the motor, cognitive and hormonal functions using SGA seems to be mediated by the increase of dopamine release in a range of brain pathways induced by the 5HT2A antagonism. (3-4)

Although all the Second-generation antipsychotics share the same mechanism of action (DRD2 and 5HT2a blockade), each SGA shows a different affinity for other G protein-coupled receptors (GPCRs). (Supplement materials Table 1) Olanzapine presents a wide profile of targets affecting the Histamine receptor 1 (H1R), for which it shows a very high affinity, but also the Muscarinic receptor 1, the α -adrenergic receptor 1 and the Serotonin receptor 2C (5). The blockade of these receptors is responsible for the OL-induced main side effects (Figure 2)

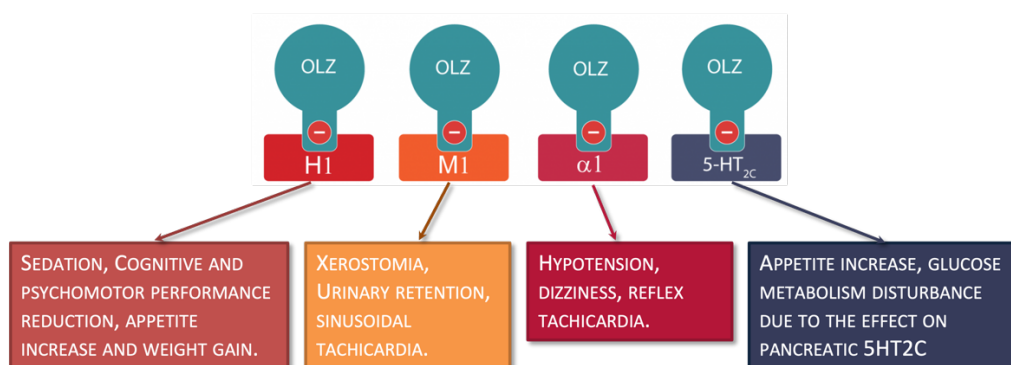


Fig.2 Schematic representation of Olanzapine side effects caused by the blockade of receptors different from the Dopamine receptor 2 (D2R) that mainly mediate its antipsychotic activity.

According to the OL affinity profile, sedation and metabolic abnormalities are the prominent disturbances reported during Olanzapine treatment. However, sedation could be used for therapeutic purposes. Low doses of OL (\approx 5mg) are prescribed to induce sleep in older adults or in patients suffering from

benzodiazepines-resistant insomnia or with major contraindications to benzodiazepines assumption. On the other hand, metabolic syndrome (MetS) represents the most significant burden of OL chronic administration.

MetS is a complex condition defined by a cluster of clinical features that include increased abdominal or visceral adiposity measured by waist circumference, atherogenic dyslipidemia with low high-density lipoprotein (HDL) and elevated fasting triglycerides (TG), hypertension, and impaired fasting glucose or overt diabetes mellitus. (6-7) Differences in the clinical presentation according to gender could be described. Increased waist circumference, hyperglycemia, and reduced HDL represent the main features of metabolic disturbance in females, while in men, hypertension and elevated triglycerides are more prevalent.

The diagnosis of Metabolic Syndrome is commonly based on the Adult Treatment Protocol Criteria (ATP-III) established by the National Cholesterol Education Program (8) or on his adapted version (ATP-IIIA) proposed by the American Heart Association following the lowering of the threshold for impaired fasting glucose to 100 mg/dl by the American Diabetes Association (9). However, a more recent definition stressing the importance of increased waist circumference has been proposed by the International Diabetes Federation (10). (Figure 3)

	ATP III (3 out of 5 criteria required)	ATP III A (3 out of 5 criteria required)	IDF (waist plus 2 criteria required)
Waist (cm)	M >102, F >88	M >102, F >88	M ≥94, F ≥80
Blood pressure	≥130/85*	≥130/85*	≥130/85*
HDL (mg/dl)	M <40, F <50	M <40, F <50	M <40, F <50
Triglycerides (≥150 mg/dl)	≥150	≥150	≥150
Glucose (mg/dl)	≥110**	≥100**	≥100**

ATP – Adult Treatment Protocol; IDF – International Diabetes Federation

*or treated with antihypertensive medication; **or treated with insulin or hypoglycaemic medication.

Fig.3 Different criteria used in the clinical practice for diagnosing Metabolic Syndrome. ATPIII: Adult Treatment Protocol Criteria; ATPIIIA: Adult Treatment Protocol Criteria adapted version; IDF: International Diabetes Federation.

Altogether, these classifications underline that no single clinical feature of the syndrome is sufficient to diagnose the complex metabolic dysfunction of MetS and

stress the idea that subgroups of endophenotypes, probably governed by alterations in different pathways, could be identified.

A comparative analysis of 689 subjects enrolled in the Clinical Antipsychotic Trials of Intervention Effectiveness Study (CATIE) reveals that patients suffering from Schizophrenia have an increased risk (odds ratio 3.5) for meeting the criteria of metabolic syndrome than demographically matched individuals from the general population (11). Metabolic abnormalities have consistently been identified as a part of the schizophrenic illness, even before the era of antipsychotic medication (12-14). However, the interest in this topic has been renewed since the introduction of second-generation antipsychotics because of the clinical relevance of the observed metabolic disturbances related to the use of these drugs (15-21). According to the data published by De Hert M. et al. (22), within the SGA, patients treated with Olanzapine show, after three years of follow-up, a prevalence of metabolic syndrome of 47,1%, three folds greater than patients treated with Risperidone or Quetiapine and five folds more than patients treated with Aripiprazole. Considering that MetS is a major risk factor for cardiovascular disorders and stroke, the increased prevalence of metabolic disturbances related to the antipsychotic administration significantly contributes to the excess mortality observed in people with Schizophrenia (23-25). Moreover, in these patients, the comorbidity with Metabolic Syndrome seems to be associated with a lower functional outcome (26), a higher prevalence of psychotic and depressive symptoms (27), worse perceived physical health (11; 27) and a lower adherence to the medications (28- 29).

The high prevalence of MetS among patients treated with Olanzapine, together with the significant clinical consequences related to this syndrome, account for the urgent need to reach a better understanding of the biological pathways involved in the Olanzapine-induced MetS and to find possible therapeutic strategies to counteract this life-threatening side effect.

1.2 HYPOTHALAMIC CONTROL OF ENERGY METABOLISM AND HIS SUSPECTED INVOLVEMENT IN OL-INDUCED METABOLIC SYNDROME.

The hypothalamus is a complex structure located in the ventral area of the brain between the pituitary gland and the third ventricle. It represents the master regulator of energy metabolism, regulating the food intake and energy expenditure homeostasis.

Two hypothalamic nuclei, the ventromedial hypothalamus (VMH) and the arcuate nucleus (ARC), are crucial in coordinating this delicate balance. They receive information on the metabolic status from the body's periphery and regulate the appropriate response accordingly, adjusting the feeding behaviour and energy expenditure.

The hypothalamic modulation of the energy balance is mainly orchestrated by two different subgroups of neurons of the ARC, known as first-order neurons: the Neuropeptide Y/Agoutirelated protein (NPY/Agrp) neurons and the Proopiomelanocortin/cocaine-and-amphetamine-related transcript (POMC/CART) neurons. Binding their receptors on the second-order neurons in VMH, the neuropeptides secreted by ARC neurons in response to the peripheral condition exert opposite effects on feeding behaviour and energy homeostasis. NPY/Agrp acts as an anorexigenic stimulus in case of energy excess, and POMC/CART gives an orexigenic signal in the presence of an energy deficit. Moreover, the ARC neurons show reciprocal regulation with POMC/CART, suppressing NPY/Agrp neurons firing (30).

Leptin and Insulin are the two main satiety signals coming from the body's periphery, affecting multiple brain systems. Leptin is secreted by adipocytes following stimulation by increases in fat deposition, while the pancreas produces Insulin in response to glucose peaks in the blood. Receptors for insulin and leptin are widely expressed on ARC neurons, and circulating concentrations of these hormones directly affect POMC and NPY/AgRP neurons, suppressing food intake and promoting

energy expenditure. On the other hand, the primary circulating orexigenic hormone is represented by Ghrelin. Ghrelin is released by the stomach following gastric emptying and directly influences hypothalamic functions, stimulating NPY/AgRP neurons firing (31- 32).

The reciprocal regulation between orexigenic and anorexigenic stimulus seems responsible for maintaining the balance of feeding behaviour. Any perturbation of this equilibrium could affect the final energy homeostasis. (Figure 4)

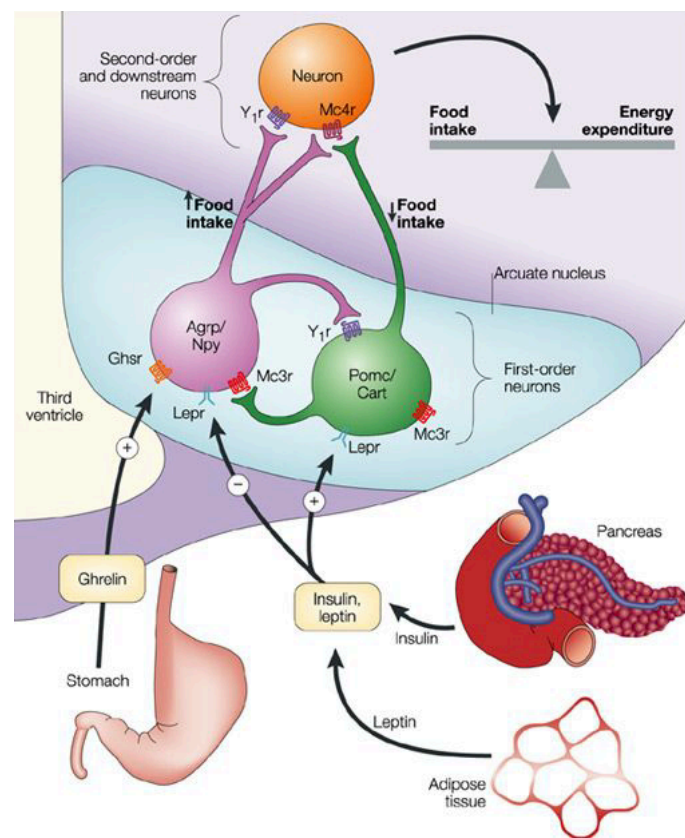


Fig.4 Representation of hypothalamic control of energy metabolism mainly orchestrated by two groups of neurons in the Arcuate Nucleus (ARC): the POMC neurons and the NPY/AgRP neurons. These two types of secreted neuropeptides regulate the energy balance in opposite directions.

Olanzapine-induced weight gain was first attributed to a direct effect of this drug on leptin signalling (33,34). Numerous prospective studies on olanzapine-treated patients suggest the possible association between the use of this medication, weight gain, and increased leptin levels in serum. (35-39) However, it was unclear

if the increased leptin level represents an effect of the adipose tissue deposition due to the weight gain or its cause.

Olanzapine-induced weight gain predominantly occurs over the first 6 months of treatment and reaches a plateau between months 6 and 12. Leptin changes do not follow in parallel with the weight changes during extended antipsychotic treatment. In fact, leptin levels peaked early in treatment, at week 2, before the establishment of the increase in fat deposition (33, 40, 41). These data support the hypothesis of a direct effect of Olanzapine on leptin signalling. Conversely, the meta-analysis published by Potvin S. et al. (42) shows that olanzapine produces a moderate-to-large increase in blood leptin levels across studies, with a high correlation between the overall leptin levels during longer-term antipsychotic treatment and weight changes. However, the association between the Olanzapine administration and leptin levels disappears when adjusted for differences in body mass index. If the involvement of leptin deregulation in the onset of MetS is still debated, the profound changes in insulin signalling have been broadly described in the literature.

Olanzapine seems to induce insulin- resistance with a double-hit mechanism. Centrally, as shown by Kowalchuc C. et al. (43), OL directly abolishes the well-established ability of central insulin to suppress hepatic glucose production at the level of VMH, resulting in hyperglycemia. Peripherally, this antipsychotic medication impairs the insulin sensitivity of the adipose tissue and skeletal muscle, explaining the abnormal responses to the oral glucose tolerance test and elevated fasting

insulin levels reported in the literature (44-46) consistent with insulin resistance. If the effect of OL treatment on the peripheral hormones controlling energy metabolism has been extensively studied, the possible role of the hypothalamic neuropeptides in OL-induced metabolic abnormalities is still poorly explored.

A recent paper by Perez-Gomez A. et al. (47) firstly analyzes the OL signature in hypothalamic gene expression, showing complete deregulation of the reciprocal

control of POMC and NPY/Agrp with a marked overexpression of both neuropeptides. The biological mechanisms by which OL interferes with POMC and NPY/Agrp gene expression and the GPCRs involved are still unknown.

From our previous work (48), using an unbiased computational approach, we identified that the hypothalamic Histamine Receptor 1 (H1R) and Cannabinoid Receptor 1 (CB1R) play a crucial role in OL-induced Metabolic Syndrome. The involvement of the histamine system was already suggested from several lines of evidence. Kroeze et al. (49), evaluating the binding of different antipsychotics to multiple neurotransmitter receptors, show that antipsychotic-induced weight gain in clinical studies is better predicted by the H1R binding affinity of the administered drug. In fact, within the antipsychotics, Olanzapine and Clozapine share the same high affinity for histamine receptor 1 and are also the medications more burdened by metabolic disturbances. Furthermore, Ratliff J.C. et al. (50) demonstrated that the antagonism of H1R due to the administration of first-generation anti-histaminergic drugs crossing the blood-brain-barrier (BBB), such as chlorpheniramine, promethazine and doxylamine, is associated with enhanced food intake and increased risk of obesity (OR, 1,70; CI, 1,23-2,31). The same side effect is not reported for the second-generation antihistamines (cetirizine, loratadine, fexofenadine), crossing the BBB to a significantly smaller extent than their predecessors. This observation suggests a direct involvement of H1R in the brain and metabolic dysfunction. Finally, H1R deficient mice are characterized by obese phenotype with increased visceral adiposity, hyperleptinemia, mildly enhanced insulin resistance and triglyceride liver deposition (51-52). The present phenotype closely resembles the clinical presentation of Metabolic Syndrome.

The involvement of the cannabinoid system in the body's metabolic control is well-established in the literature. CB1R-deficient mice present a lean phenotype (53-54) with reduced feeding behaviours and resistance to diet-induced obesity (55-57). In line with this observation, the administration of Rimonabant, a CB1 receptor antagonist, in obese mice leads to decreased body weight and food

intake with normalized plasma levels of leptin, insulin and free fatty acids and corrected insulin resistance (56, 58).

Conversely, injecting endogenous ligands of CB1R, such as Anandamide or 2-Arachidonoylglycerol, into the hypothalamus of pre-satiated rats increases dietary food intake. This increase in food intake could be prevented by pretreatment of the rats with Rimonabant. (58,59) The changes in dietary intake following the direct injection of CB1R agonists in the hypothalamus point out the importance of the cannabinoid system for the central control of energy metabolism. In humans, the treatment with Dronabinol, a CB1R agonist, significantly increases appetite and body weight compared with placebo (60,61).

However, the CB1R does not represent a known direct target of Olanzapine; therefore, the mechanism of action of OL on the cannabinoid pathways and their contribution to the pathogenesis of Olanzapine-induced MetS is still largely unknown.

Weston-Green et al. (62) show that OL chronic administration decreases the binding of the agonist, [³H] CP-55940, to CB1R in the dorsal vagal complex of the brain stem, leading to increased weight gain in rats, whereas haloperidol failed to elicit similar effects.

A deeper exploration of the way Olanzapine affects the cannabinoid system could lead to a better understanding of the hypothalamic involvement in OL-induced MetS and its underlying pathophysiological process, providing possible novel therapeutic targets for this medical condition.

1.3 AVAILABLE THERAPEUTIC APPROACHES FOR METS

The prevalence of Metabolic Syndrome has increased worldwide in the last decades, reaching 25% of the general population (63). Consequently, developing

preventive and therapeutic strategies for MetS management has become a rising public health need.

Lifestyle modifications, including dietary interventions and increased physical activity, always represent the first-line therapy for Metabolic Syndrome. However, these strategies often fail to produce sustained weight loss (64). For patients suffering from mental health disorders, adopting specific dietary indications or consistency in physical exercise could be even more challenging and frequently possible just in mental residential institutions. The periodic occurrence of depressive and manic episodes characterizes the mood swings of bipolar disorder. Depression significantly affects the motivation of patients to adhere to intervention programs. At the same time, mania causes difficulties in focusing on and completing tasks and, disorganizing thoughts, impairing the diet and planned physical activity compliance. In the context of Schizophrenia, lifestyle changes are made difficult by the presence of intruding delusions, the content of which could interfere with diet interventions (i.e. delusion of poisoning in paranoid schizophrenia) or even with the trust in medical advice (i.e. persecutory delusion). Furthermore, negative symptoms and disorganized behaviours affect the patients' motivation for physical activities and their ability to plan or follow a balanced lifestyle.

Along with dietary interventions, pharmacological treatments may be considered to manage metabolic dysfunction. Approved weight-loss medications include three types of drugs: Orlistat, Liraglutide and the association of Naltrexone and Bupropion. (65) Orlistat is an intestinal lipase inhibitor that decreases the absorption of fat ingested with the diet of about 30%. The frequent onset of gastrointestinal side effects decreases the tolerability of this drug. Despite its proven efficacy in the general population, Tchoukhine E. et al. (66) study on the long-term effects of Orlistat in patients suffering from Schizophrenia affected by OL-induced MetS shows a limited efficacy of this drug only in men with no reported benefit in women.

Liraglutide is an incretin-mimetic drug used to treat Metabolic Syndrome at a higher dose than diabetes. By binding Glucagone-like peptide-1 (GLP-1) receptors in the hypothalamic areas involved in food intake, Liraglutide increases the sense of satiety and reduces appetite. Larsen J.R. et al.'s (67) randomized clinical trial investigating the efficacy of Liraglutide on obese patients affected by Schizophrenia spectrum disorders treated with OL highlights the significant improvement of glucose tolerance, body weight and cardiometabolic disturbance after four months of drug administration. However, the administration of Liraglutide through once-daily subcutaneous injection significantly affects the compliance of the patients and frequently requires the presence of a caregiver to ensure the long-term continuation of the treatment. Another GLP-1 receptor analogue, Semaglutide, recently reached social media attention for its remarkable effectiveness in weight control in the general population. Prasad F. et al. (68) first evidence from a real-world clinical setting on using Semaglutide for treating antipsychotic-associated weight gain raises hopes for this drug's efficacy in treating OL-induced metabolic dysfunction. Furthermore, Semaglutide is administered through a weekly subcutaneous injection, partially improving the compliance observed with Liraglutide. However, randomized control trials are still needed to corroborate these findings.

On the other hand, using GLP-1 receptor analogues in Bipolar Disorder or in patients suffering from Schizoaffective disorder appears more tricky. The polypharmacotherapy frequently adopted to treat these diseases generally comprises, together with antipsychotics, the use of mood stabilizers such as Lithium or Valproic Acid. Long-term treatment with GLP-1 receptor analogues increases the risk of pancreatitis and thyroid cancer, which are already known side effects of Valproic Acid and Lithium. Therefore, the coadministration of these drugs leads to an exponential increase in the risk of life-threatening side effects. Finally, the association of Naltrexone, an opioid receptor antagonist, and Bupropion, an antidepressant belonging to the class of norepinephrine and

dopamine reuptake inhibitors (NDRIs), could be used for the treatment of MetS for their synergistic activity on the arcuate nucleus of the hypothalamus, lowering the stimulus of appetite (69). The double-blind, randomized, placebo-controlled trial on the efficacy of this therapeutic approach for treating antipsychotic-induced weight gain published by Tek C. et al. (70) demonstrates a significant weight reduction only for patients without diabetes. The remarkable prevalence of co-occurrence of glucose dysfunction and obesity in the context of Metabolic Syndrome reduced the use of this therapeutic approach to a limited specific population.

The therapeutic modulation of the Cannabinoid system for weight management deserves special mention. Rimonabant was the first selective CB1 receptor inverse agonist approved in clinical practice as an anorectic antiobesity drug. The metabolic side effects of Olanzapine treatment are fully neutralized by Rimonabant administration in female rats, as shown by Lazzari P. et al. (71) However, in 2008, Rimonabant was withdrawn from the market worldwide and is no longer available due to severe adverse effects, including anxiety, depression and suicidal ideation, probably related to the blockade of CB1R in the limbic area (72).

Bariatric surgery may represent the last option when dietary or pharmacological approaches fail. Bariatric surgery is indicated in patients with MetS with severe obesity (BMI > 35 kg/m²). (73) Although it is a viable option, the surgical approach in patients suffering from Schizophrenia and Bipolar Disorder is burdened by multiple challenges. First, the patient's functioning, treatment adherence, and psychosocial support should be assessed before surgery, considering the complex post-surgical process and the need to follow specific dietary recommendations. Moreover, as shown in the observational study by Shelby et al. (74), symptom exacerbation frequently occurs during the post-surgical observation in these patients, probably as a side effect of the prolonged anesthesia required. The heightening of the symptoms could negatively affect the management of the post-

surgical period, requiring a prolonged hospitalization. Finally, patients treated with psychotropic medications and their psychiatrists should be aware of the possible need for medication adjustments due to changes in absorption after bariatric surgery. Indeed, a lack of strict control of the symptoms for at least six months after surgery could lead to a relapse due to changes in blood concentration of the pharmacological treatments.

Altogether, these findings point out the rising need to develop more effective therapeutic options specific for antipsychotic-induced metabolic syndrome, taking into account the characteristics of people suffering from mental health issues (i.e. polypharmacotherapy, frequent lack of insight, unstable compliance) and the possible different biological pathways involved in this syndrome compared with other forms of metabolic dysfunctions.

1.4 GENE THERAPY AND THE CRISPR-CAS SYSTEM

Gene therapy is a medical approach that aims to treat clinical disorders by correcting, removing, or replacing pathogenic DNA or RNA in human cells. It represents the current frontier of precision medicine, offering new therapeutic possibilities for patients suffering from hereditary diseases or disorders with a known monogenic target (75,76).

Gene therapy originates from viral plasmids encoded with exogenous DNA to be integrated into the host genome. Unfortunately, the use of viral vectors for gene therapy is burdened by the risk of insertional oncogenesis and immunogenic toxicity. (77,78) Therefore, programmable genome editing tools have been extensively investigated, providing a safer alternate strategy for gene therapy. These systems directly correct the existing genetic aberrations rather than introducing the therapeutic gene into a novel locus. This alternative approach allows for repairing the pathological mutation while avoiding the risk of insertional oncogenesis (75).

The cutting-edge technology known as clustered regularly interspaced palindromic repeats (CRISPR)/CRISPR-associated protein (Cas), thanks to its ability to edit DNA or modulate gene expression in eukaryotic cells, represents a powerful tool for the investigation and the identification of the genetic targets implicated in specific disorders and could be a promising therapeutic strategy for gene editing (79). However, this technology is delivered with adeno-associated virus (AAV) vectors, so it does not entirely avert the risks associated with the use of viruses.

Of the CRISPR/Cas systems, CRISPR/Cas9 is the most developed and widely used tool for current genome editing. By binding to the targeted genomic locus identified through a provided single-strand RNA guide, the CRISPR/Cas9 system generates double-stranded breaks in the DNA, which are then repaired by two main repair pathways. Fixing with non-homologous end-joining (NHEJ) leads to high aberrance in the original sequence caused by frameshift mutations due to amino acid insertions or deletions. This strategy is suitable for identifying druggable targets when the blockade of specific proteins is supposed to be therapeutic or could be proposed as a gene therapy in all the cases that require a site or cell-specific blockade of a target protein. Furthermore, by providing an exogenous template, the activation of homology-directed repair (HDR) machinery can generate precise modifications at a target locus (80-85), introducing desired changes in the genome. This represents a powerful correction strategy for pathogenetic gene mutations. (Figure 5)

From the identification of a druggable target for the OL-induced MetS to the development of a new therapeutic approach using CRISPR/Cas7-11S

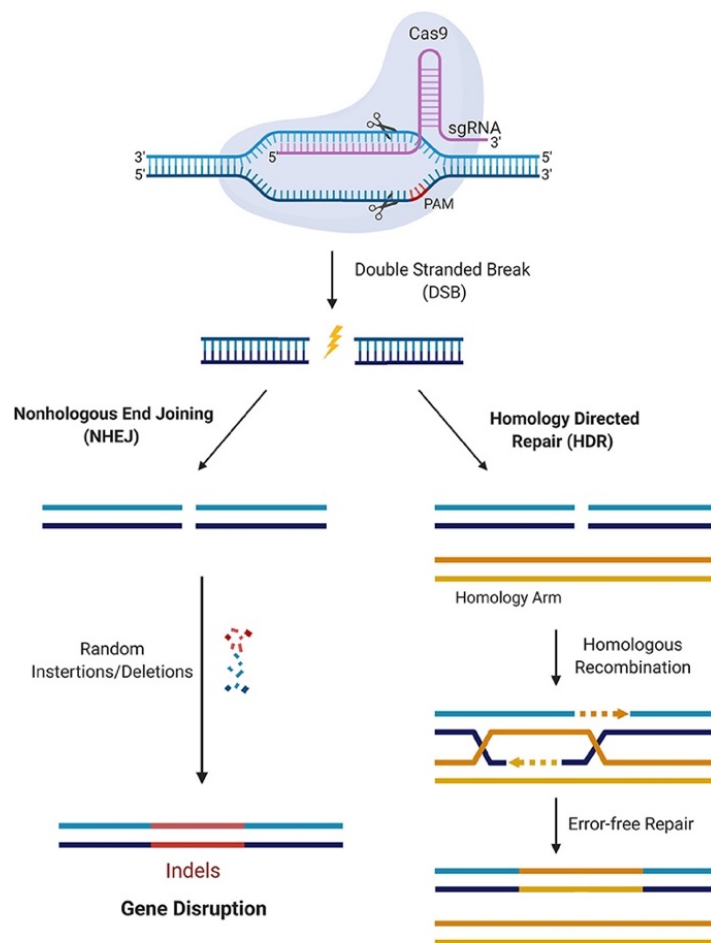


Fig.5 Mechanism of CRISPR/Cas9 genome editing. The CRISPR/Cas9 system creates double-stranded breaks in the DNA. The activation of two main DNA repair pathways is responsible for the CRISPR/Cas9 gene editing. While there are several DNA repair pathways, the key ones used for gene editing are non-homologous end joining (NHEJ) and homology-directed repair (HDR). NHEJ is exploited to render genes non-functional, while HDR is exploited to insert new genes or fragments of genetic material.

The application of CRISPR/Cas9 for gene therapy of Metabolic Syndrome appears, at the moment, still challenging considering the polygenic nature of this disorder. Conversely, different CRISPR-mediated approaches have been proposed to treat monogenic forms of Obesity. Mutations in genes involved in the control of feeding behaviours, such as the heterozygous mutation of Melanocortin Receptor 4 (MC4R), Proprotein Convertase Subtilisin/Kexin Type 1 (PCSK1), and Neurotrophic

receptor tyrosine kinase 2 (NTRK2) or homozygous mutation of Leptin (LEP), Leptin Receptor (LEPR) and Proopiomelanocortin (POMC) are associated with inherited forms of obesity characterized by early onset severe weight gain and ancillary hormonal disturbances (hyperinsulinemia, hypocortisolemia) (86,87). In all these clinical conditions, the CRISPR/Cas9 approach through the HDR machinery could correct the genomic alteration causing the disorder.

Despite the intriguing possible applications of the CRISPR/Cas9 system, the stable changes in the genomic DNA induced by this tool raise concerns about using CRISPR/Cas9 as a therapeutic approach in humans. To overcome this significant limitation while ensuring the same cell and site-selectivity of CRISPR/Cas9, the newly discovered RNA targeting CRISPR/Cas7-11 seems promising.

Cas7-11 is a Type III-E CRISPR/Cas effector that confers sequence-specific RNA cleavage using a provided RNA guide. Considering the negligible nontarget effects and low cell toxicity, this system could be used for knockdown and editing purposes with potential applications in RNA interference (88).

However, the CRISPR/Cas7-11 system has a large Cas7-11 nuclease, making its encapsulation in viral delivery systems challenging. The recently released crystal structure of CRISPR/Cas7-11 (Figure 6) provided a better structural insight into this tool, allowing the engineering of a compact Cas7-11 variant (Cas7-11S) suitable for AAV vector packaging (89). This possibility opens a new challenge for using this system as a programmable gene editing tool for transcript knockdown in human cells, enabling *in vivo* Cas7-11 applications.

The transient effect of CRISPR/Cas7-11 on the cells' transcriptome without inducing stable changes in the genomic DNA together with the cell and site-selectivity ensured by this system increases the chances that this approach has the potential of reaching the clinical trial stage for human gene therapy.

From the identification of a druggable target for the OL-induced MetS to the development of a new therapeutic approach using CRISPR/Cas7-11S

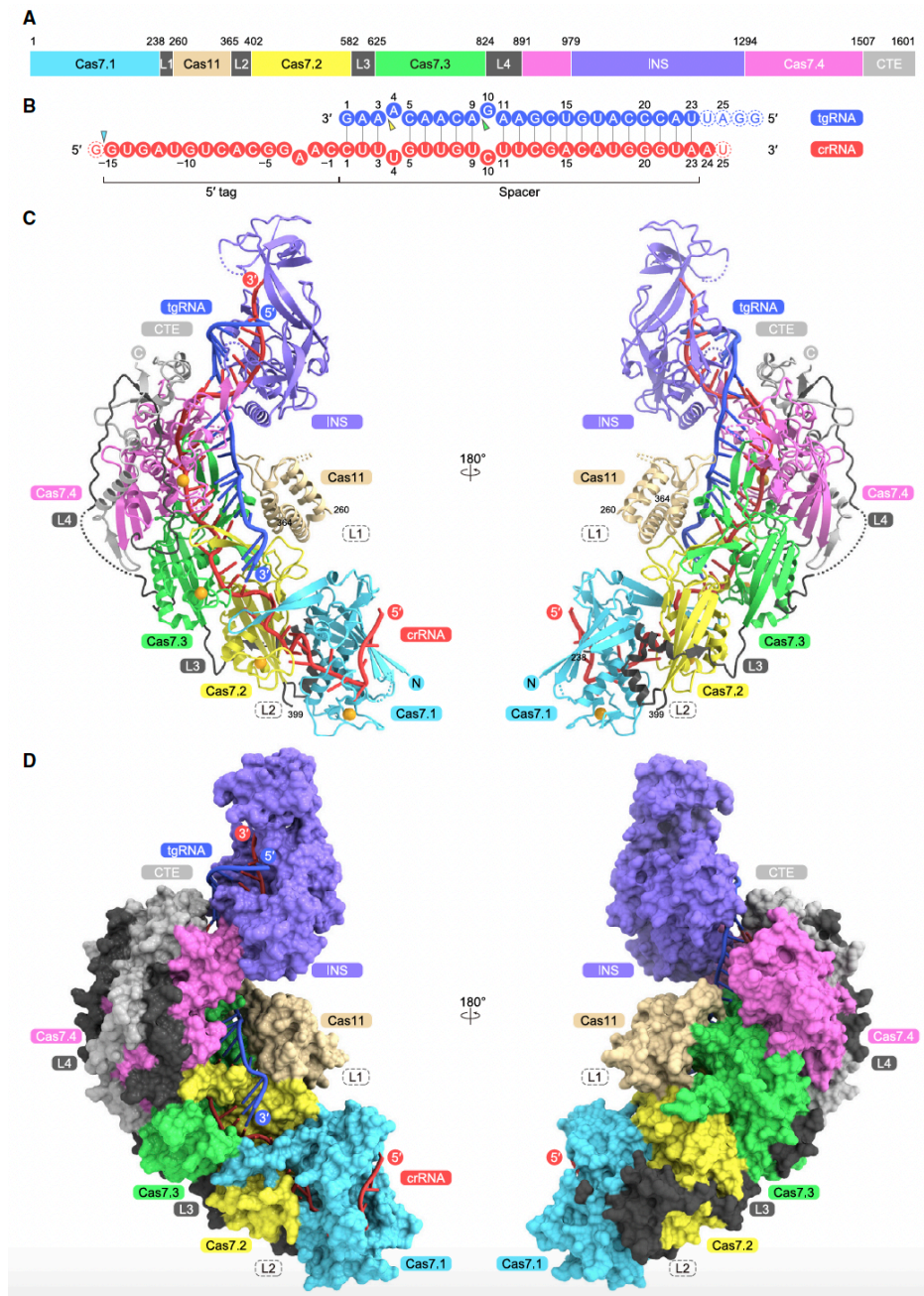


Fig.6 Cryo-EM structure of the Cas7-11–crRNA–target RNA complex. A) Domain structure of Cas7-11. B) Nucleotide sequences of the spacer RNA (crRNA) and its target RNA (tgRNA). C) Overall structure of the Cas7-11–guideRNA–targetRNA complex. D) Surface representation of the Cas7-11–guideRNA–targetRNA complex.

1.5 CRISPR/Cas SYSTEM INHIBITION

The CRISPR/Cas9 gene editing technology represents a revolutionary breakthrough in genetic engineering, offering a promising treatment of various genetic diseases. However, methods to

control of the Cas9 activity is needed to provide a safe “switch off” in case of non-specific targeting on off-target genomic sites causing unwanted mutations.

CRISPR/Cas9 system, in nature, represents a defence mechanism that provides an adaptive immunity against phage infection in bacteria and archaea (90-92). In response to these robust prokaryotic immune systems, phages have evolved proteins that bind to and inactivate Cas proteins (93-95). These proteins, altogether known as anti-CRISPRs (Acrs), have been used to control Cas9 in genome-editing applications. (96-100) While Acrs are valuable tools to control the activity of Cas9, they show some significant limitations. The large dimension of these proteins limits their membrane permeability. Moreover, their half-life and bioavailability are remarkably reduced in vivo by the quick degradation operated by cells' endogenous proteases. Furthermore, the in vivo administration of Acrs can potentially trigger undesired immune responses (101).

To overcome these problems, small molecules have been developed as an alternative strategy to the protein-based anti-CRISPR approach for genome editing applications. In fact, small molecules are relatively more permeable across the membrane (102), proteolytically stable in vivo (103), and generally non-immunogenic compared to Acrs (104), representing a more promising tool for Cas9 activity modulation. Even though Cas9 is a DNA-binding protein, a class of targets often deemed chemically intractable, a small number of anti-CRISPR/Cas9 compounds has been successfully identified. (105,106)

If small molecules to modulate the activity of the CRISPR/Cas9 system are available, for CRISPR/Cas7-11, no Acrs or inhibiting drugs are currently known. Considering the extensive structural and functional differences between Cas9 and

Cas7-11, the compounds acting as Cas9 inhibitors are unsuitable for the blockade of Cas7-11 enzymatic function. The ability to interfere with the CRISPR/Cas7-11 mode of action, inhibiting or stopping the enzymatic activity by using small molecules, represents a milestone for the use of this approach in vivo for programmable gene editing, providing a “safety switch off” in case of the onset of side effects.

2. AIMS OF THE STUDY

The first objective of the present study is to explore the relative contribution of the previously identified hypothalamic receptors H1R and CB1R to the pathogenesis of OL-induced metabolic syndrome. Indeed, the project aims to untangle the pathophysiology of each symptom of MetS, differentiating the ones due to an OL-induced dysfunction in hypothalamic neurons driven by H1R or CB1R from the ones resulting from hypothalamic functional modifications in glial cells or peripheral effects of Olanzapine. **[Study PART 1]**

Then, the study examines the underlying biological mechanism of H1R and CB1R-mediated metabolic phenotypes. Moreover, the possible direct or indirect interactions between CB1R and H1R are investigated. **[Study PART 2]**

Furthermore, the project evaluates these neuronal hypothalamic GPCRs as potential druggable targets to revert the OL-induced MetS in a pre-clinical setting, avoiding the significant side effects known for the currently available drugs. **[Study PART 3]**

Finally, the study aims to develop a novel site and cell-specific therapeutic approach for Olanzapine-induced MetS using the CRISPR/Cas7-11S s. We first engineered the CRISPR-Cas7-11S toolbox for both in vitro and in vivo RNA targeting from the wild-type Cas7-11 plasmid (pCMV huDisCas7-11). At the same time, we design and clone RNA-spacer sequences against the target transcript suitable for the knockdown in both human and mouse neuronal cells. Then, we

screen the efficiency of the CRISPR/Cas7-11S single RNA-spacer approach using the mouse neuroblastoma cell line. **[Study PART 4]** To provide a safety switch-off in case of undesired side effects of the CRISPR/Cas7-11S therapeutic system, the study aims to identify and test in vitro new ligands acting as cleavage breakers or complex formation inhibitors, arresting the enzymatic activity of CRISPR-Cas7-11S. **[Study PART 5]**

3. MATERIALS AND METHODS

3.1 ANIMALS

All animal procedures are performed in collaboration with the University of Toronto – Dept of Pharmacology and Toxicology (Jean Martin Beaulieu Lab) in accordance with Canadian Council of Animal Care guidelines and the University of Toronto animal ethics committee. The experiments are conducted on C57BL/6J wild-type mice approximately 7 weeks old (provided by Jackson Laboratory). Only female mice are used in our study because OL-induced MetS shows a sex effect on the mouse phenotype and because of the sexual dimorphism of hypothalamic structures and transcriptome. All mice are housed individually in a controlled environment in which lights are on a 12hr light/12hr dark cycle, and temperature and humidity remain constant. No changes in the corn cob layer have been made during the entire experimental period. Animals are all drug naïve and are used only for single experiments.

3.2 STEREOTAXIC INJECTION

C57BL/6J female mice (n= 108) of 7 weeks are randomized into three different batches (n =36/group): H1R Cas9-KO (H1HR-KO), CB1R Cas9-KO (CNR1-KO), and Control group (CTR). For the KO groups, an AAV5 mixture of respectively AAV5-H1HR-mCherry and AAV5-MeCP2Cas9 and AAV5-CNR1-mCherry and AAV5-MeCP2Cas9 is used for the hypothalamic bilateral stereotaxic injection. As a negative control, a mixture of AAV5-LacZ-mCherry and AAV5-MeCP2Cas9 is

injected. The specific guides for H1R and CB1R Cas9KO and the LacZ guide have been previously validated in vitro and in vivo (107). (Figure 7-8)

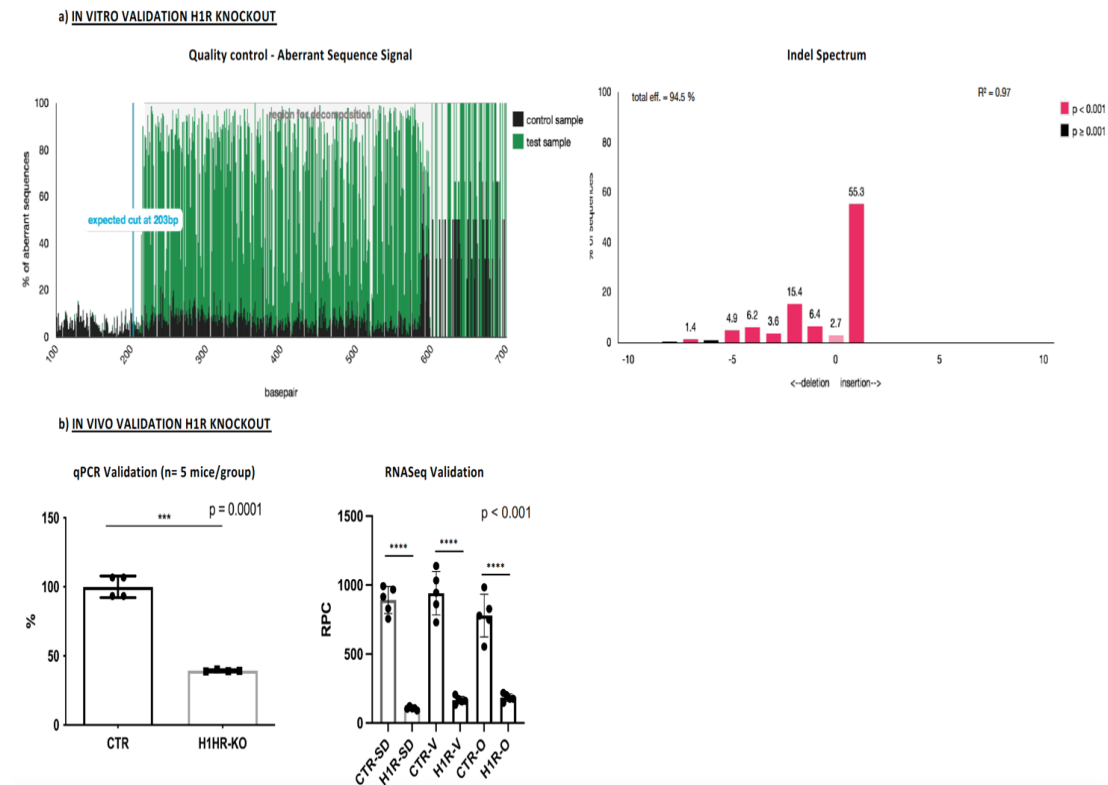


Fig.7 In vitro ed in vivo validations of H1R knockout. A) Results of TIDE analysis showing a total knockout efficiency of 94.5%. The Indel analysis highlights that the selected guide induces 55.3% of insertion of one base and 15.4% of deletion of two bases, resulting in frame-shift mutations of the H1R gene. The presence of these frame-shift mutations accounts for the significant aberration of the gene sequence of the test sample compared to the controls shown in the Quality control scheme. B) qPCR results (n=5 mice/group) and RNASeq analysis (n=5 mice/group) confirm the H1R knockout efficiency in vivo.

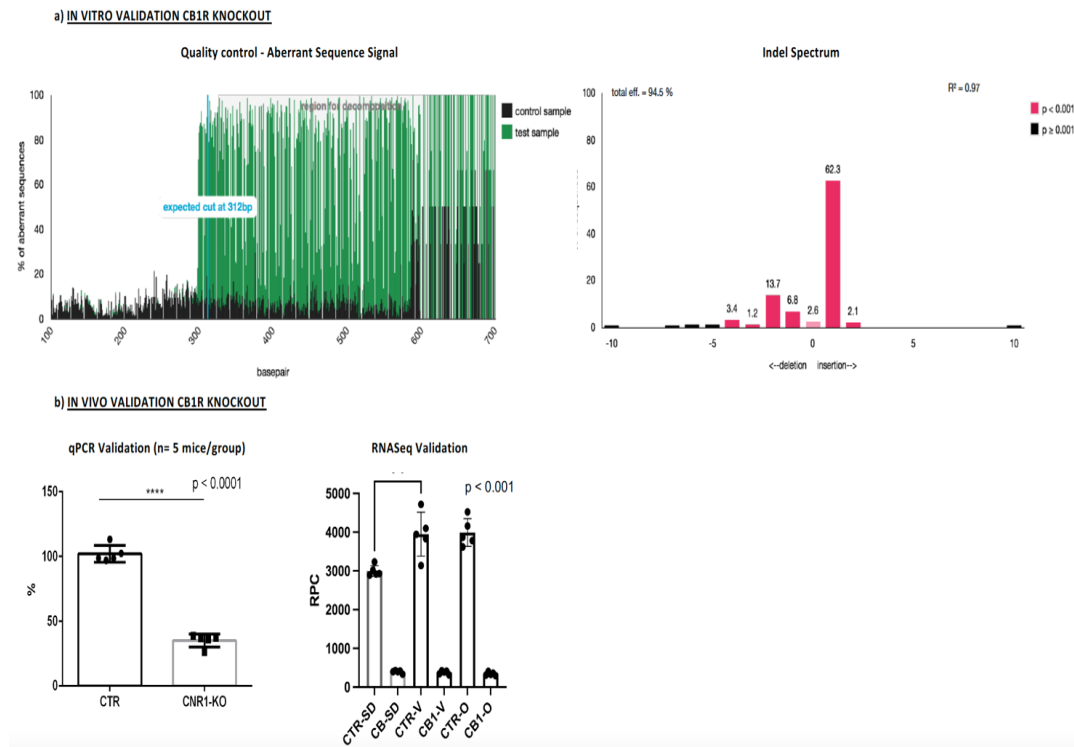


Fig.8 In vitro ed in vivo validations of CB1R knockout. A) Results of TIDE analysis showing a total knockout efficiency of 94.5%. The Indel analysis highlights that the selected guide induces 62.3% of the insertion of one base, resulting in frame-shift mutations of the CB1R gene. The presence of these frame-shift mutations accounts for the significant aberration of the gene sequence of the test sample compared to the controls shown in the Quality control scheme. B) qPCR results (n=5 mice/group) and RNASeq analysis (n=5 mice/group) confirm the CB1R knockout efficiency in vivo.

Mice are anesthetized with isoflurane (2-3%). Each animal is placed in a stereotaxic frame, and the skull surface is exposed. Bregma and lambda are used as references to align the skull. Two holes are drilled at injection sites, and 2 μ l of the virus is injected using a nanoliter injector with a micro syringe pump controller (WPI) at the speed of 10 nl per second. Following injection coordinates were used (relative to Bregma): anterior-posterior (AP), -1.50mm anterior to bregma; mediolateral (ML), \pm 0.2mm; dorsoventral (DV), -5.8mm below the surface of the brain.

3.3 IMMUNOHISTOCHEMISTRY

For the validation of the injection site and the immunohistochemical demonstration of the specificity of the knockout only in hypothalamic neurons (Supplementary Figure 1-2), 10 C57BL/6J female mice 7 weeks old undergo hypothalamic bilateral stereotaxic injection with an AAV5 mixture of AAV5-LacZ-mCherry and AAV5-MeCP2Cas9. Three weeks after the surgery, the animals are anesthetized with Avertin injection (2,5% tribromoethanol, 0,2ml/10g, i.p.) and transcardially perfused with 4% (w/v) paraformaldehyde (PFA) in 0,1 M phosphate buffer (pH7,5). Brains are extracted and incubated overnight. After 24h of fixation in 4% PFA, the brains are washed in PBS 1x and embedded in agar. Embedded brains in a wash of PBS 1x are cut into 40µm-thick slices using a sliding vibratome (Leica VT1200S). Slices containing the hypothalamic region are extensively collected in wells with PBS 1x + NaN₃. The slides are analyzed using a fluorescence microscope (Invitrogen EVOS FL Auto 2.0 Imaging System) 20x TX-Red to detect mCherry red fluorescence.

For the immunohistochemical analysis, the brain sections are washed three times for 5 min in PBS. Sections are blocked and incubated with a permeabilization solution containing 5% normal goat serum (Millipore) and 0,5% Triton X-100 (Sigma) in PBS for two hours. Sections were then incubated with primary antibodies diluted in permeabilization solution overnight at 4°C. After three washes in PBS, slices were incubated with secondary antibodies for two hours at room temperature. Sections were rinsed three times for 10 min in PBS before mounting with DAKO mounting medium. Staining was visualized using the Odyssey Imaging System (LiColor). The following primary antibodies are used: Mouse anti-NeuN (1:100, Millipore MAB377) and Rabbit anti-GFAP (1:500, Sigma G9269). As secondary antibodies, 405 Goat anti-mouse (1:500, Invitrogen) and 488 Goat anti-rabbit (1:500, Invitrogen) are used.

3.4 TREATMENT

After three weeks of post-surgical observation, 24 mice of each group (H1R Cas9-KO; CB1R Cas9-KO and Control group) are split into two batches (n= 12/each): Olanzapine or Vehicle (Figure 9).

Pure Olanzapine (Tocris Cat.N. 4349, purity 99.9%) is compounded into high fat (55 kcal% vegetable fat, 24% sucrose) food at a concentration of 54 mg/kg of diet. Olanzapine dose has been selected since it produced steady-state plasma levels (21 ± 5 ng/ml) closest to the clinically relevant range (10–50 ng/mL) in previous studies [13]. The drug is administered for 25 days. The Vehicle group received the high-fat diet (HFD) only for the same observation period.

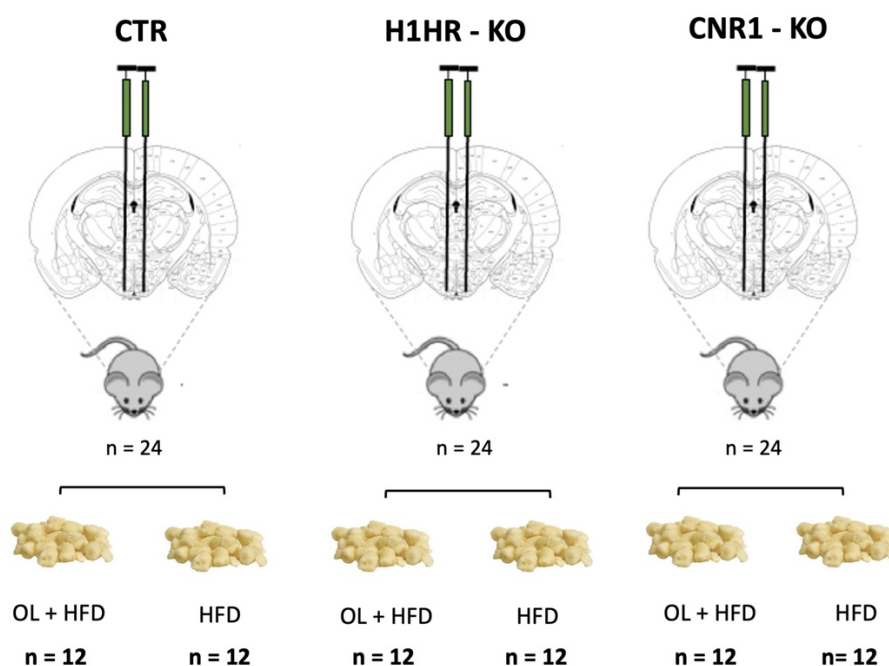


Fig.9 Schematic representation of the study design. CTR (Controls); H1HR-KO (H1R Knockout mice); CNR1-KO (CB1R Knockout mice). OL: Olanzapine; HFD: High fat diet.

The chow is provided as dough with no dyes by Envigo Company (diet TD-93075) and administered once daily in a controlled amount (9g/die). Water is provided ad libitum. The remaining 12 mice of each group (H1R Cas9-KO; CB1R Cas9-KO and Control group) are kept under a standard chow diet (SD) for an additional 25 days.

3.5 PHENOTYPE CHARACTERIZATION

The weight is evaluated every five days, and the food intake is measured daily to the nearest 0.01 g using an electronic balance. Food consumption during day/night periods is checked at established time points (baseline and after three weeks of treatment) to assess possible changes in the feeding pattern. Blood glucose is measured with a glucometer (Roche, Accu-Chek) immediately after the decapitation. Serum insulin and leptin are quantified with the ultra-sensitive mouse insulin ELISA kit (Crystal Chem #90080) and the mouse leptin ELISA kit (Crystal Chem #90030), according to the kit manual. Serum HDL and LDL are measured with the specific ELISA kits (Crystal Chem #79980 e #79990). Triglycerides are evaluated on serum and liver with a Triglyceride Assay Kit (Abcam #Ab65336). Corticosterone levels in serum are quantified using DetectX Corticosterone Enzyme Immunoassay Kit (Arbor Assays #K014-H5). The presence of Fatty liver disease is assessed using the Oil-Red-O staining histological technique according to the protocol previously standardized by Mehlem et al. (108) and with Masson's Trichrome staining for fibrosis detection (109).

Rectal temperature is measured with a rectal probe daily for ten days at established time points (baseline and last ten days of treatment). For each mouse, the data are analyzed as the difference between the mean temperature recorded at the end of the treatment minus the mean temperature observed at the baseline (Delta rectal temperature).

The estrous cycle phases (proestrus, estrus, metestrus, and diestrus) are evaluated by analyzing the appearance of the vagina (110) and vaginal smears through vaginal lavage (111,112) twice per day (9:00 am and 6:00 pm) for ten days after the surgery and before the sacrifice. (Figure 10) Vaginal lavage was performed by flushing the vagina with 20 μ L of saline (0.9% saline, pH 7.4) until cloudy. Samples were dry-fixed overnight on charged microscope slides and stained with 0.1% Toluidine Blue O (Sigma-Aldrich, Cat#89640-5G) diluted in double-distilled

deionized water (ddH₂O) for two minutes, then sequentially incubated in ddH₂O, 100% 200 proof ethanol (Decon Laboratories, CAS#64-17-5, Cat#2701), and 100% ClearRite-3 (Thermo Scientific, Cat#6901TS) for 1 minute each. Slides were mounted with EMS DPX Mountant for Microscopy and analyzed at 5× and 20× magnification. Estrus cycle phases were classified by the cytology described by Cora et al. (112).

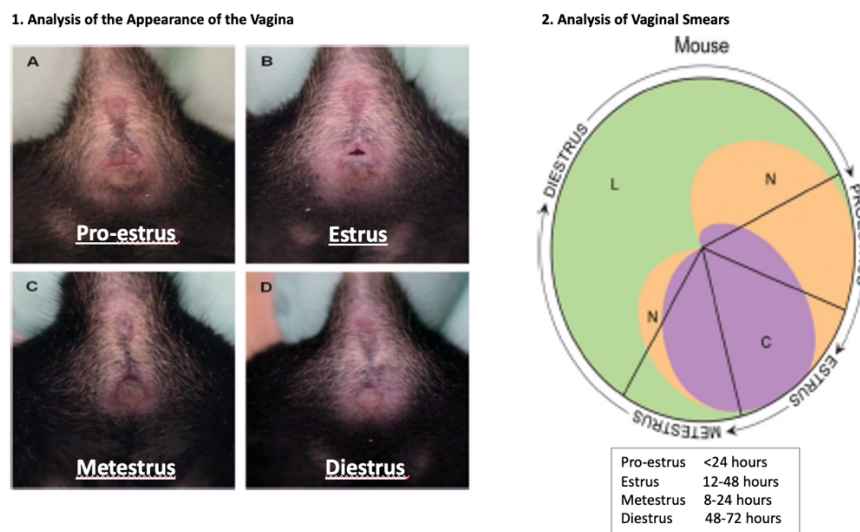


Fig.10 Assessment of estrous cycle phases (proestrus, estrus, metestrus, and diestrus). 1) Evaluation of vagina appearance in the different phases. 2) Estrous Cycle identification tool for the analysis of the cytology of vaginal smear in the four stages of the estrous cycle. Each cell type and its relative proportion in the different phases are shown in a different color (Green= Leucocyte; Orange= nucleated epithelial cells; Purple= cornified epithelial cells). The size of each quadrant is a rough estimation of the length of each stage. The total cycle takes about 4–5 days.

3.6 BEHAVIORAL ASSAY

Open field Test (OFT)

OFT is performed for 30 min in an automated Omnitech Digiscan apparatus (AccuScan Instrument, Columbus, OH, United States). Each mouse is placed in a corner of the large plexiglass box, and the exploratory activity was recorded. Time spent in the center, number of entries and latency to enter were recorded separately for the central (25% of the total surface) and peripheral areas.

Dark-Light Emergence Test (DLET)

DLET is performed for 5 min using an automated open field activity apparatus with light/dark insert (Med-Associates, St Albans, VE, United States) with the light compartment illuminated at 800 lux. Mice are placed initially at the center of the dark chamber. The total time spent in the dark and light compartments, the total distance travelled, and the delay in crossing from the dark to the light chamber are recorded.

Elevated Plus Maze (EPM)

EPM is performed for 10 min. The EPM apparatus is constituted as follows: two open arms (30 x 5 x 0.25 cm) and two enclosed arms (30 x 5 x 15 cm) extended from a common central platform (5 x 5 cm). The mice are initially placed at the far end of the close arm. The time spent in the open arm is measured by the observer unaware of the treatment and the KO.

3.7 TISSUES DISSECTION

Mice are sacrificed one hour after the last meal by rapid cervical dislocation. Blood is collected during mice decapitation and allows clotting in 1.5mL tubes. Blood is then centrifuged, and the obtained serum is stored at -70°C. The serum quality check for interfering hemolysis is performed by evaluating the absorbance at 414 nm. The considered cutoff is 0.072, as previously reported in the literature (113). After cervical dislocation, the heads of animals are immediately cooled by immersion in liquid nitrogen. The brain and the liver are rapidly dissected on an ice-cold surface. Hypothalamic 500 nm thick serial coronal sections are prepared using an ice-cold adult slicer, and the hypothalamus is cut with a microsurgical knife. One lobe of the liver is fast-frozen in OCT by immersion in liquid nitrogen for staining procedures. All the samples are stored at -80°C until they are analyzed.

3.8 HYPOTHALAMIC RNA EXTRACTION

For RNA preparation, hypothalamic tissue is rapidly homogenized in Trizol (ThermoFisher) and proceeded for RNA isolation following the manufacturer's protocol (Zymo Research). RNA is resuspended in elution buffer or water. Total RNA was monitored for quality control using the Nanodrop absorbance ratios for 260/280nm.

For RNA sequencing, the library preparation and sequencing were performed at the Centre for Applied Genomics (TCAG) at the Hospital for Sick Children. Library construction was performed according to the Illumina NovaSeq – S4 flowcell guide. RNA quality control and alignment were conducted at TCAG at the Hospital for Sick Children. Read quality was assessed by FastQC v.0.11.5 (<http://www.bioinformatics.babraham.ac.uk/projects/fastqc/>). Adapter trimming and removal of lower quality ends was performed using Trim Galore v. 0.5.0. All raw FASTQC files were aligned to the *Mus musculus* GENCODE reference genome (GRCm39) using the STAR aligner, v.2.6.0c software. The STAR alignments were processed to extract raw gene read counts using htseq-count v.0.6.1p2 (HTSeq).

3.9 STATISTICAL ANALYSIS

The data are presented as means \pm SEM. The normality of the data is assessed using the Shapiro-Wilk test, and the check for outliers is performed with Grubb's test. The two-tailed t-test is used to compare two groups, while comparisons between multiple groups are performed with one-way ANOVA followed by Bonferroni corrected pair-wise comparisons.

The results of the three different behavioural assessments of anxiety are summarized in the Emotionality Score according to the method previously described by Guilloux et al. (114)

Differential expression analysis is performed using DESeq2 v.1.26.0s, using R v.3.6.1. (115). Initial minimal filtering of 10 reads per gene for all samples is applied to the datasets. Normalized read counts are converted into log-read counts, which are then used for identifying differentially expressed genes (DEGs). Selected DEGs, corrected for multiple testing (Benjamini-Hochberg), are used as an input for pathway analysis (p-adjusted, $p_{adj} \leq 0.05$). Ingenuity Pathway Analysis (IPA, Qiagen) is used for gene set enrichment and pathway enrichment analyses filtering for hypothalamic pathways only (116). RNASeq data of the different experimental groups are used to perform separate Genome-wide Weighted Genes Co-expression Network Analyses (WGCNA), obtaining a co-expression network in each condition (117). The datasets used as inputs for IPA and WGCNA analysis are summarized in Table 2.

3.10 DEVELOPMENT OF TRUNCATED VERSION OF Cas7-11 (Cas7-11S) AND CLONING IN pcDNA3.1

pDF0159 pCMV - huDisCas7-11 mammalian expression vector is ordered from Addgene (cat #172507). Primers are designed to amplify the region between restriction sites Not1 and Kpn1; the amplified products are digested with Not1 and Kpn1 restriction enzymes (Thermo Fisher #ER0591 and #ER0521). Gene block sequence as Msc1-DeltaINS-GGGS-PolyA terminator-Bbs1 is ordered from Integrated Genome Technologies (IDT). This gene block presents the deletion of the INS region of the wild-type Cas7-11. (Figure 11) The gene block is digested with Kpn1 and Bbs1 restriction enzymes. The PCR amplified fragments, and the gene block are ligated using the T4 ligase (Thermo Fisher #EL0011) to generate a single shorter Cas7-11 fragment with the INS region deleted.

pcDNA3.1 vector (Invitrogen #V70020) is designed for high-level, constitutive expression in mammalian cell lines. Here, pcDNA3.1 is digested with Not1 and Bbs1

(Thermo Fisher #ER1011). The shorter Cas7-11 fragment with Not1 and Bbs1 overhangs is ligated with pCDNA3.1 (Figure 12).

The ligated products are transformed into BL21 competent Escherichia coli (E. coli) strain, a widely used bacterial host for high-level recombinant protein production. The colonies were screened, and a positive clone was picked by Sanger sequencing.

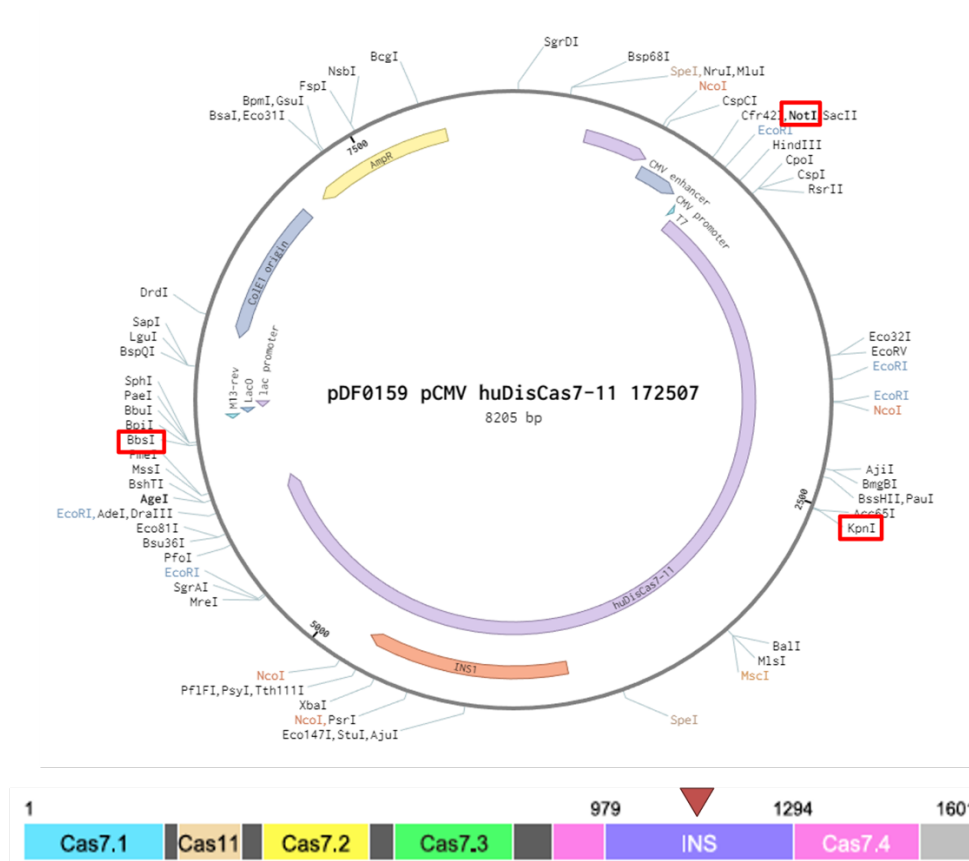


Fig.11 Engineering strategy of Cas7-11S starting from the wild-type version of Cas-11 (pCMV huDisCas7-11).

From the identification of a druggable target for the OL-induced MetS to the development of a new therapeutic approach using CRISPR/Cas7-11S

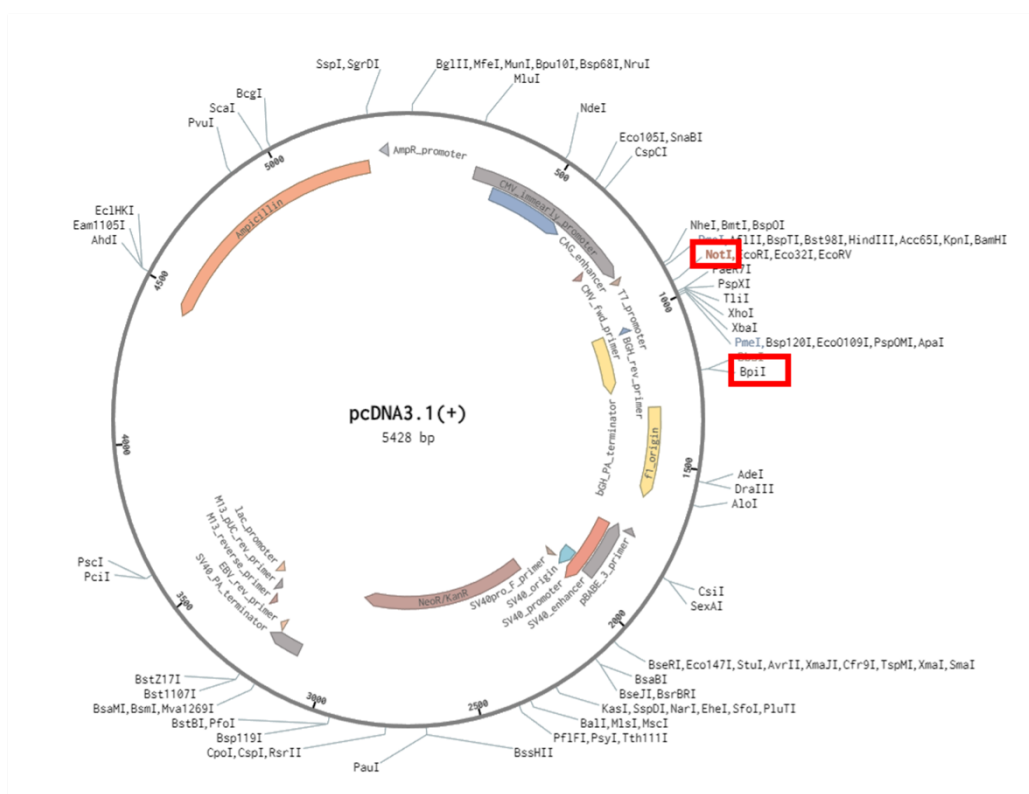


Fig.12 Cloning approach of Cas7-11S in a pcDNA3.1 vector for high-level, constitutive expression in mammalian cell lines.

3.11 MODIFICATION OF pX459V.2 PLASMID TO CHANGE THE PROMOTER DRIVING THE EXPRESSION OF THE GUIDE RNA FROM U6 TO tRNA

The plasmid of Cas9 from *S. pyogenes* with the cloning backbone for single guide RNA (sgRNA) (pX459V.2) is ordered from Addgene (#62988). The plasmid is digested with Age1 (NEB #R3552) and Fse1 (NEB #R0588L) restriction enzymes to remove Cas9. The linearized plasmid is circularized using Mung bean nucleases (NEB #M0250L) followed by T4 ligation, obtaining px459-deltaCas9 plasmid.

To change the promoter driving the expression of the sgRNA from U6 to tRNA, a gene block containing the tRNA promoter with the sequence as pcil-TRNAPromoter-goldengateBbs1site-NheI is synthesized from IDT. The circularized px459-deltaCas9 plasmid and the gene block are digested with PciI (Thermo Fisher #ER1871) and NheI (Thermo Fisher #ER0972) restriction enzymes. The digested

products are ligated together, and the ligated products are transformed into BL21 E. coli. Positive clones are selected by Sanger sequencing. (Figure 13)

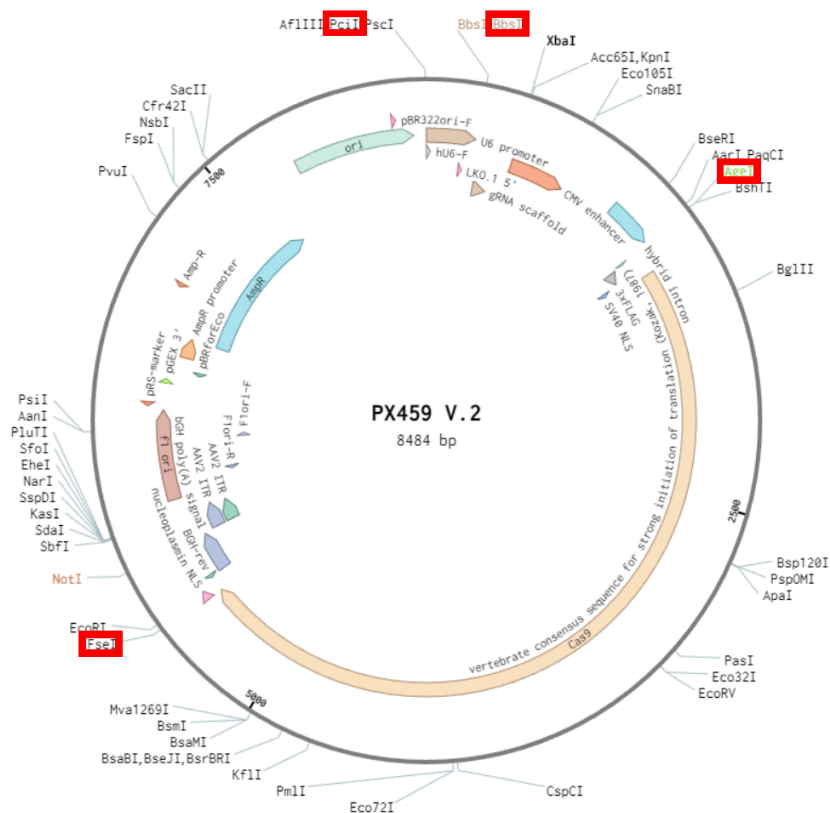


Fig.13 Modification strategy to change the promoter driving the expression of the sgRNA in a pX459V.2 plasmid.

3.12 DESIGNING OF GUIDES AGAINST CB1R RNA AND CLONING

Seventeen guides were designed targeting both the mice and the human CB1R RNA using an in-house generated randomization code of the cDNA sequence. Off-target analysis was performed to minimize the risk of undesired cell transcriptome changes. Each guide is 31 nucleotides long and is flanked by Bbs1 restriction site overhangs to enable Gibson assembly (Figure 14). The guides were customized and ordered from Thermo Fisher Scientific.

1) **CACC**GATCGCAGGACCCCTAGAGTTCAGTAAGTTC
AAACGAACTTACTGAACTCTAGGGGTCCTGCGATC**C**

- 2) CACC GAACTAGAGACCTAGTTCTCATCTGGTAATTG
AAAC CAATTACCAGATGAGAAGCTAGGTCTCTAGTT C
- 3) CACC GGTGGTTTTCTATGGGTAGTTAGGCTTCAGAT
AAAC ATCTGAAGCCTAACTACCCATAGAAAACCAC C
- 4) CACC GATATATAACCGATGAGACAACAGACTTCTAA
AAAC TTAGAAGTCTGTTGTCTCATCGGTTATATAT C
- 5) CACC GGGCTGTGTTATTGGCGTGCTTGTGCAGGCAG
AAAC CTGCCTGCACAAGCACGCCAATAACACAGCC C
- 6) CACC GCTTCTTGCTGAACGCTGGCCTTACAGAACAC
AAAC GTGTTCTGTAAGGCCAGCGTTCAGCAAGAAG C
- 7) CACC GTTTTTGGCCATCGAGGCCGAAATCTACTTA
AAAC TAAGTAGATTTTCAGGCCTCGATGGCCAAAAA C
- 8) CACC GCTCTTATGAGGGCTATATTCTGTTTTTGCTA
AAAC TAGCAAAAACAGAATATAGCCCTCATAAGAG C
- 9) CACC GCAGGCCAAATCTAGACATATCCTAGTTTGGC
AAAC GCCAAACTAGGATATGTCTAGATTTGGCCTG C
- 10) CACC GAGACATGTCGGTTGATATTCAGGTTTCATGT
AAAC ACATGAACCTGAATATCAACCGACATGTCTC C
- 11) CACC GCCTGACAGTATCCGACAGCTTTGGAGTCATC
AAAC GATGACTCCAAAGCTGTCGGATACTGTCAGG C
- 12) CACC GAACTAGAGACCTAGTTCTCATCTGGTAATTG
AAAC CAATTACCAGATGAGAAGCTAGGTCTCTAGTT C
- 13) CACC GTAGCACCCGTGCGCCACGGCCCTGGGACTG
AAAC CAGTCCAGGGGCCGTGGCGCACGGGTGCTA C
- 14) CACC GTTTGGGAATTGGCCCTTTTAAAGATGAGTA
AAAC TACTCATCTTAAAAGGGGCCAATTCCTCAA C
- 15) CACC GTAATACTCACTAGGGAGAATGTTTGGTCAG
AAAC CTGACCAAACATTTCTCCCTAGTGAGATTAT C
- 16) CACC GATGAAGGTAGCTTAACGCACACATGATGATA
AAAC TATCATCATGTGTGCGTTAAGCTACCTTCAT C

```
17) CACC AAAAGTTCAATACACTATAAAATCTTATCACT  
AAAC AGTGATAAGATTTTATAGTGTATTGAACTTT C
```

Fig.14. Sequences of the generated guides targeting CB1R RNA.

The forward and the reverse guide pairs are annealed and then ligated in a single-step digestion-ligation reaction with Bbs1 and T4 ligase.

The obtained double-strand CB1R RNA targeting guides are cloned with pX459delta cas9 plasmid under both U6 and tRNA promotor to compare the efficiency of knockdown of mCB1 in these two conditions. The previous in vitro application of the CRISPR-Cas7-11S approach published by Kato et al. [89], in fact, demonstrates a better efficiency of this system with a tRNA promoter-driven guide expression. The positive clones for all the seventeen guides were confirmed by Sanger sequencing.

3.13 GENERATION OF STABLE CELLS EXPRESSING Cas7-11S

To overcome the efficiency limitations due to the double transfection of Cas7-11S and the guide, a mouse neuronal cell line (N2A) is used for generating stable cells expressing Cas7-11S. These cells express CB1 innately. N2A cells are grown in high glucose DMEM containing 10% FBS, penicillin/streptomycin and L-glutamine (HyClone-GE Healthcare, Logan, UT). Cells are maintained at 37°C in a 5% CO₂ atmosphere. 50-70% confluent N2A cells are transfected with pCMV-huDisCas7-11S using Lipofectamine 2000 (Thermo Fisher Scientific, Waltham, MA) according to the manufacturer's protocols. To select only transfected cells, 48 hours after transfection, cells are incubated with 200ug/ml of Hygromycin for 20 days. Finally, the selected cells are cryopreserved.

3.14 TRANSFECTION OF THE GUIDES TARGETING THE CB1R RNA IN N2A STABLE CELLS EXPRESSING Cas7-11S.

N2A stable cells expressing cas7-11S are transfected with 200ng of the guides using lipofectamine according to the manufacturer's protocol. The scramble sequence pX459-deltacas9 without the guide is used as a control. Then, the transfected cells are double-selected with 200ug/ml of Hygromycin and 2ug/ml of Puromycin 48 hours post-transfection for 4 days.

3.15 RNA ISOLATION AND qPCR.

RNA extraction was performed using TRI reagent and the Direct-zol RNA Microprep from Zymo per the kit protocol. The RNA was quantified and checked for its quality using a nanodrop. Complementary DNA (cDNA) is synthesized using a reverse transcriptase SuperScript IV VILO Master Mix for Thermo. RT-qPCR was performed using TaqMan™ Fast Advanced Master Mix (Applied Biosystems) per the manufacturer's protocol. The CB1R probe (cat #Mm01212171_s1) and GAPDH probe (cat #Mm99999915_g1) are procured from Thermo Fisher. Data were acquired by QuantStudio 3 Real-Time PCR System (Thermo Fisher Scientific). Relative expression analysis calculated by normalizing CB1R expression over scramble was performed using data from biological triplicates of each sample by QuantStudio™ Design and Analysis Software (Thermo Fisher Scientific).

3.16 RNA SCOPE FOR VISUALIZING CB1 AND CAS7-11S IN THE ENGINEERED N2A CELL LINE.

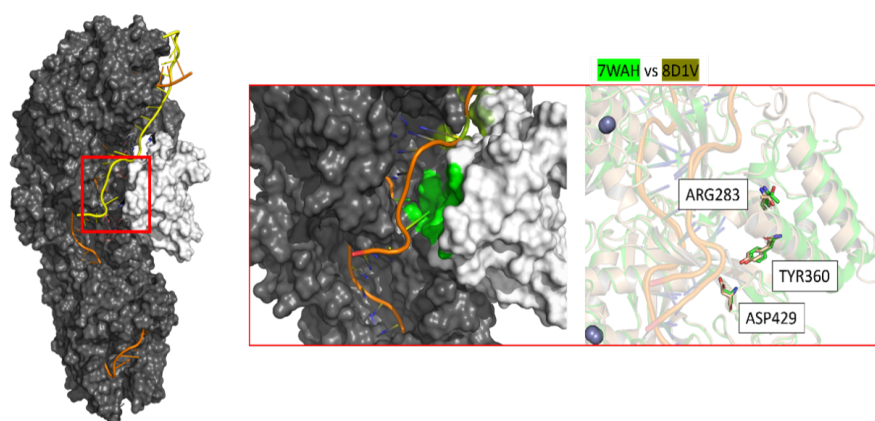
Stable N2A cells expressing Cas7-11s are transfected with 200ng of scramble guide, Guide 2, Guide 8, and Guide 13. The cells are selected using 200ug/ml of hygromycin and 2ug/ml of puromycin for six days. Probe - syn-CAS7-11-C1: The Probe for mapping cas7-11S is custom synthesized from Advanced Cell Diagnostic

Inc. (ACD Inc.). The RNAscope Probe - Mm-Cnr1-C3 (9420721-C3) and RNAscope® Multiplex Fluorescent Reagent Kit v2 with TSA Vivid Dyes (323270) are obtained from ACD Inc. The fixed and dehydrated cells are hybridized as per the manufacturer's protocol, and the cells are observed and images captured using Zeiss live cell imager at a 63X zoom.

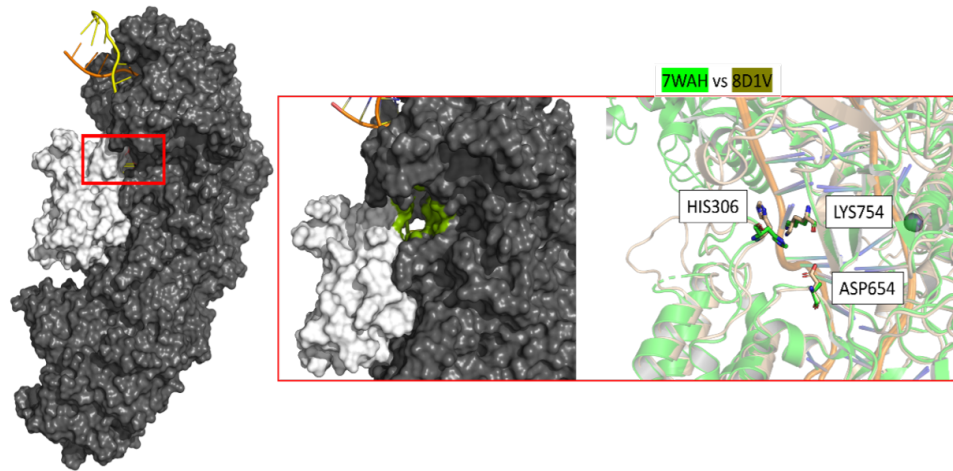
3.17 PROTEIN PREPARATION

The X-ray coordinates of CRISPR CAS 7-11 in complex with guide and target RNA are extracted from the Protein Data Bank (PDB code 8D1V). The structure is then processed with the Schrödinger Suite 2022-2 Protein Preparation Wizard tool. Water molecules are removed, and an exhaustive sampling of the orientations of groups whose hydrogen bonding network needs to be optimized is performed. Finally, the protein structure is refined to relieve steric clashes with a restrained minimization with the OPLS4 force field until a final rmsd of 0.30 Å concerning the input protein coordinates. The RNA coordinates are subtracted to the final minimized crystal, and three main putative binding sites (BS) are selected to conduct the screening: Cleavage Site 1, Cleavage Site 2, and the Protein-Protein interaction Interface on the Sub11 side (Figure 15 – 16)

CLEAVAGE_SITE1



CLEAVAGE_SITE2



PUTATIVE BINDING SITE TO EXPLORE

• Inhibitor binding sites



• Protein-Protein Disruptors binding sites



Fig.15 Identification of the putative binding sites (BS) selected for the virtual screening.

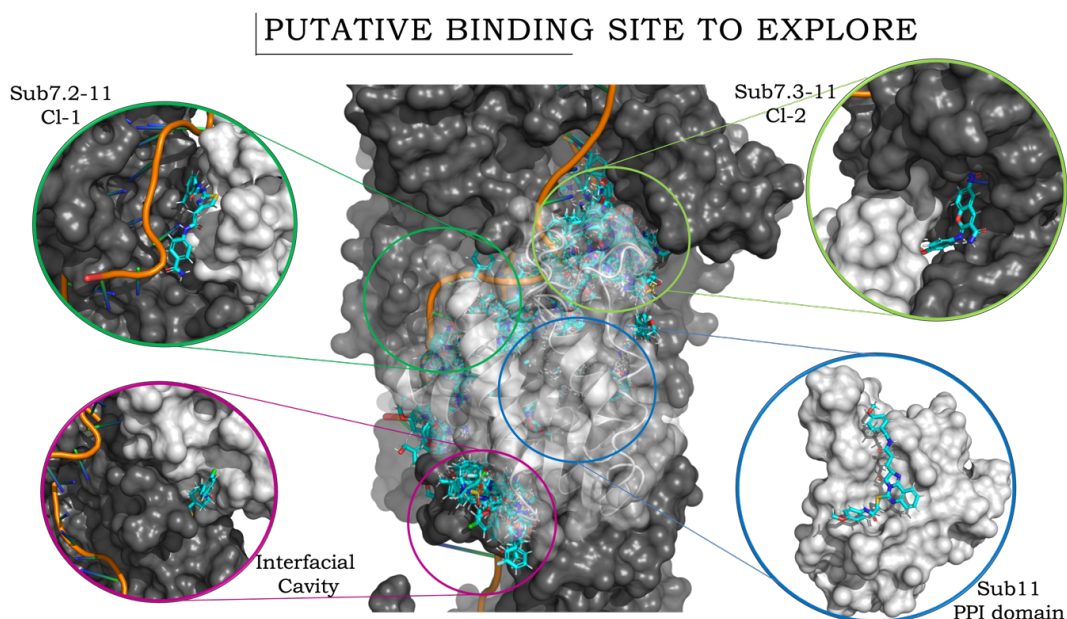


Fig.16 Putative binding sites (BS) selected for the virtual screening.

3.18 LIBRARIES PREPARATION

Two different ligand libraries, the IIT in-house library, accounting for ≈ 56000 compounds, and the Life-Chemicals library, with ≈ 760000 compounds, are screened on the four selected putative binding sites identified on the CRISPR/Cas7-11 complex. The entire library consists of 730k compounds, prepared with the LigPrep tool available on the Schrödinger Suite 2022-2. Ionization states are generated at $\text{pH } 7.0 \pm 2.0$ with Epik.

3.19 VIRTUAL SCREENING

The Virtual Screening (VS) study is performed using Glide v95128. The protein structure, prepared as described above, is used to build the energy grid. The enclosing boxes for the four VS are centred around the following residues:

- ARG283, TYR360, ASP429 (Cleavage Site 1)
- HIS306, ASP654, LYS754 (Cleavage Site 2)
- LEU284, SER291, TRP315 (Sub7.3 – Sub11 Protein-Protein Interface)

A size of 15 Å and 35 Å is used for the INNERBOX and OUTERBOX, respectively. The Standard Precision docking protocol is used, and all parameters are set to their default value. The top-scored binding pose for each compound is selected; the compounds are then clustered using the Tanimoto fingerprint similarity, using 64-bit precision. The final pool of 200 molecules, targeting the three BS, was visually inspected to complete the molecule selection of the top 25 compounds.

4. RESULTS

4.1 STUDY PART 1: H1R AND CB1R INVOLVEMENT IN THE PATHOGENESIS OF OL-INDUCED METS.

The hypothalamic-neuronal KO of H1R explains the weight gain but not the glucose impairment or the changes in lipid metabolism.

The H1R-KO mice show a statistically significant increase in weight compared to the control mice ($p < 0.01$). The present weight gain appears fully comparable to the effect of the treatment with Olanzapine in control mice. Moreover, the treatment with OL in H1R-KO mice does not result in a further increase in weight (Figure 17).

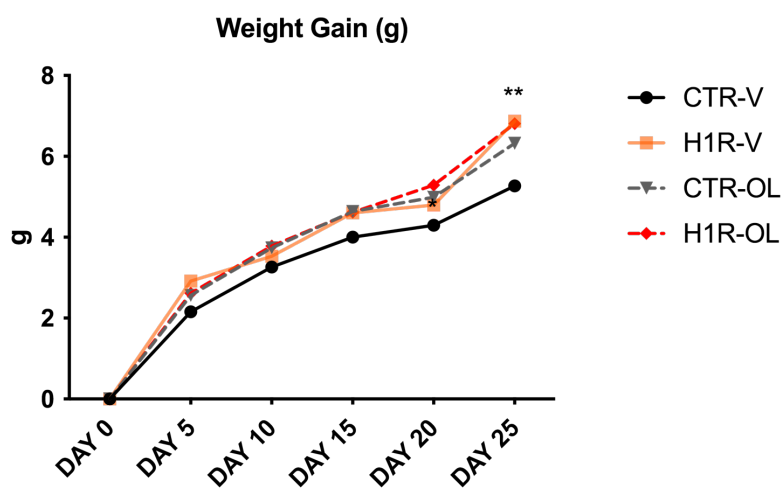


Fig.17 Weight gain induced by Olanzapine vs Vehicle in the different study groups (H1R-KO and Controls) fed with a high-fat diet. Repeated measure ANOVA with Bonferroni correction. (* $p < 0.05$; ** $p < 0.01$; *** $p < 0.001$; **** $p < 0.0001$). CTR-V (Controls treated with Vehicle), CTR-O (Controls treated with Olanzapine), H1R-V (H1R-KO mice treated with Vehicle), H1R-O (H1R-KO mice treated with Olanzapine)

The analysis of the other metabolic parameters (glucose, insulin, triglycerides, LDL, HDL) indicates that the Knockout of H1R in hypothalamic neurons does not lead to glucose impairment or lipid dysfunctions. In fact, no statistically significant differences between H1R-KO mice and Control mice are observed. Additionally, the treatment with Olanzapine in both H1R-KO mice and CTR increases glucose, insulin, triglycerides and LDL and decreases HDL levels. No differences are reported between H1R-KO treated mice and Control treated mice [Figure 18].

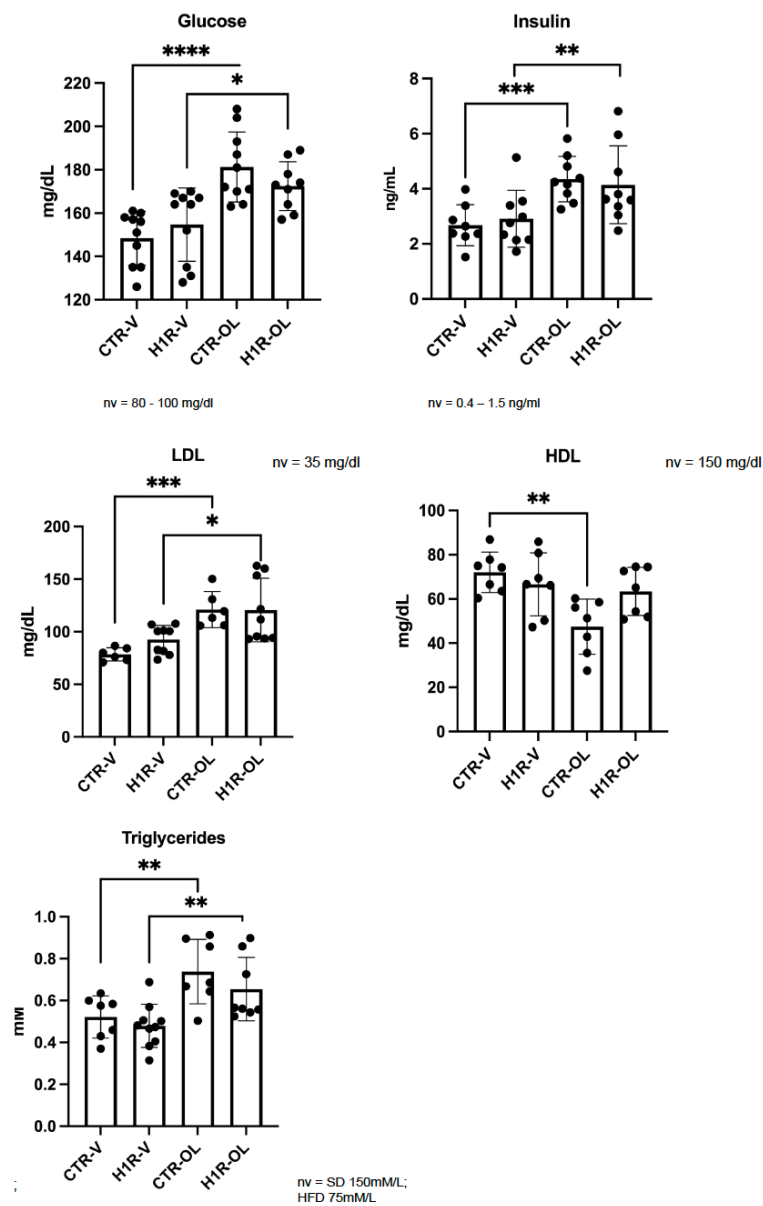


Fig.18 Differences in metabolic parameters between H1R-KO mice compared to the controls after 25 days of treatment with Olanzapine or Vehicle. The animals are all on a high-fat diet. One-way ANOVA (* $p < 0.05$; ** $p < 0.01$; *** $p < 0.001$; **** $p < 0.0001$). CTR-V (Controls treated with Vehicle), CTR-O (Controls treated with Olanzapine), H1R-V (H1R-KO mice treated with Vehicle), H1R-O (H1R-KO mice treated with Olanzapine)

The results obtained by evaluating the lipid profile are confirmed by analyzing the histological patterns of fatty liver disease in the different study groups (Supplementary Figure 3-4). Altogether, all these findings support the hypothesis that the H1R in hypothalamic neurons is the primary regulator of fat deposition. However, this receptor seems not involved in the dysfunction of peripheral organs caused by olanzapine. Therefore, the clinical features of MetS other than weight gain could be mediated by other hypothalamic receptors or H1R in hypothalamic glial cells.

The KO of CB1R hypothalamic neurons restores the complete phenotype of OL-induced MetS.

In mice fed with a high-fat diet of 25 days, the knockout of CB1R in hypothalamic neurons does not show any difference in terms of weight gain compared with control mice. However, when Olanzapine is compounded into the HFD chow and administered to both groups, the CB1R-KO treated mice have a statistically significant less increase in weight compared with control-treated mice ($p < 0,01$). The weight changes in the CB1R-KO treated mice are in line with what is observed in CB1R-KO untreated mice (Figure 19).

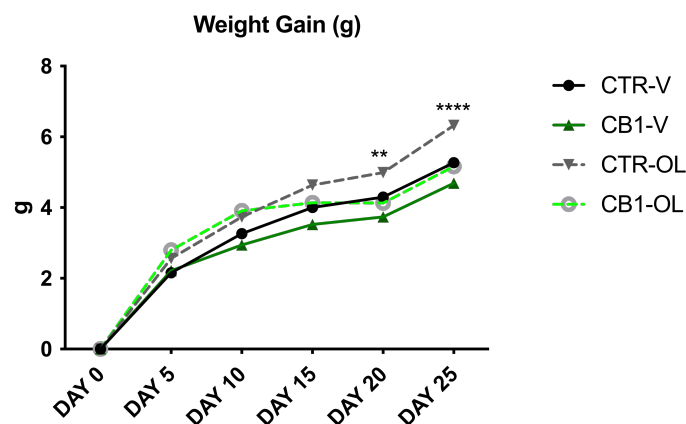


Fig.19 Weight gain induced by Olanzapine vs Vehicle in the different study groups (CB1R-KO and Controls) fed with a high-fat diet. Repeated measure ANOVA with Bonferroni correction. (* $p < 0.05$; ** $p < 0.01$; *** $p < 0.001$; **** $p < 0.0001$). CTR-V (Controls treated with Vehicle), CTR-O (Controls treated with Olanzapine), CB1-V (CB1R-KO mice treated with Vehicle), CB1-O (CB1R-KO mice treated with Olanzapine)

The present results highlight that the hypothalamic neuronal KO of CB1R neutralizes the increase in weight due to Olanzapine treatment. However, it seems to have no effect on the fat deposition caused by the lipid diet. This suggests that the HFD induces the storage of fat acting through different hypothalamic receptors, or CB1R of hypothalamic glial cells or even through peripheral receptors. These mechanisms are different from the fat deposition caused by OL treatment.

The evaluation of the pre-diabetic phenotype (an observed increase of blood glucose and insulin) in mice fed with HFD shows that the knockout of CB1R in hypothalamic neurons reduced the glycemic dysfunction induced by the OL treatment ($p < 0,001$). However, as for the weight gain, the CB1R-KO does not correct the glycemic impairment due to the HFD only. In fact, analyzing the cohort of mice fed with HFD, the CB1R-KO in mice treated with Olanzapine leads to a decrease in glucose and insulin blood levels compared with controls treated with the antipsychotic, while CB1R-KO mice treated with vehicle do not have any difference compared with the control mice (Figure. 20). Therefore, seems that the dysfunction in glucose metabolism due to the fats contained in the HFD involves different pathogenetic pathways than Olanzapine-induced diabetes.

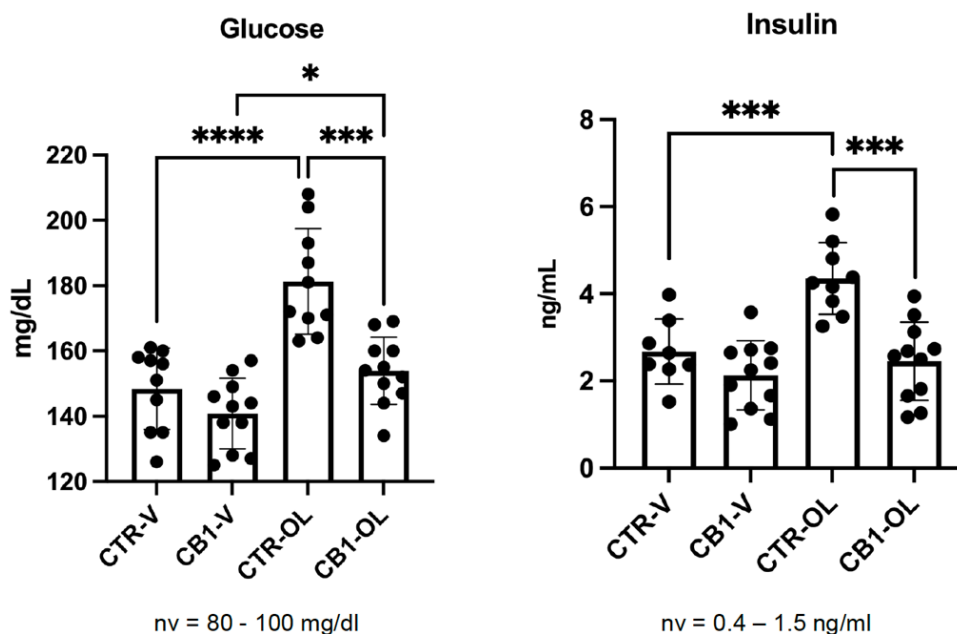


Fig.20 Differences in glycemia and insulin levels in CB1-R-KO mice compared to the controls fed with high-fat diet after 25 days of treatment with Olanzapine or Vehicle. One-way ANOVA (* $p < 0.05$; ** $p < 0.01$; *** $p < 0.001$; **** $p < 0.0001$). CTR-V (Controls treated with Vehicle), CTR-O (Controls treated with Olanzapine), CB1-V (CB1R-KO mice treated with Vehicle), CB1-O (CB1R-KO mice treated with Olanzapine)

The analysis of the lipid profile (Triglycerides, HDL, LDL) highlights that the CB1R-KO in hypothalamic neurons ameliorates the lipid dysfunction caused by Olanzapine with a statistically significant decrease of the levels of triglycerides ($p < 0,001$) and LDL ($p < 0,001$) and a statistically significant increase of the level of HDL ($p < 0,0001$) in CB1R-KO treated mice compared to the treated controls. In this case, the improvement is also statistically significant in the absence of OL treatment. In fact, the CB1R-KO mice fed with HFD show lower triglycerides $p < 0,01$ and increased HDL $p < 0,05$ in blood compared with the matched controls (Figure 21).

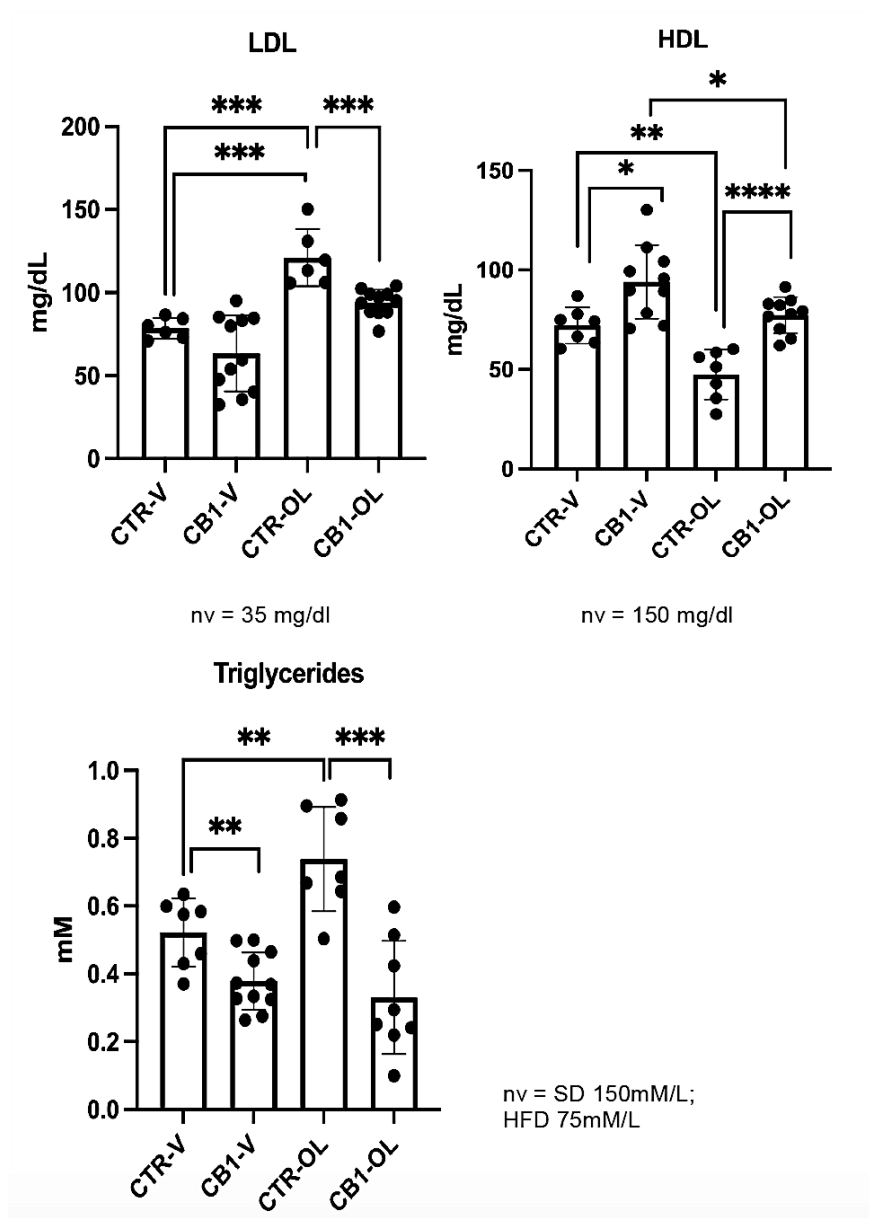


Fig.21 Differences in the lipid profile in CB1-R-KO mice compared to the controls fed with high-fat diet after 25 days of treatment with Olanzapine or Vehicle. One-way ANOVA (* p < 0.05; ** p < 0.01; *** p < 0.001; **** p < 0.0001). CTR-V (Controls treated with Vehicle), CTR-O (Controls treated with Olanzapine), CB1-V (CB1R-KO mice treated with Vehicle), CB1-O (CB1R-KO mice treated with Olanzapine)

The findings obtained by evaluating the lipid profile are confirmed by analyzing the histological patterns of fatty liver disease in the different study groups (Supplementary Figure 5- 6). The present results elucidate that the KO of CB1R in

According to the observed deregulation in the hypothalamic sensing of the metabolic status, the H1R-KO mice, although shown an increased weight, do not present any decrease in the daily food intake as expected. Furthermore, no increase in thermogenesis is observed in H1R-KO mice in response to the enhanced weight gain. Conversely, the rectal temperature in H1R-KO mice is lower than in control mice (Figure 23).

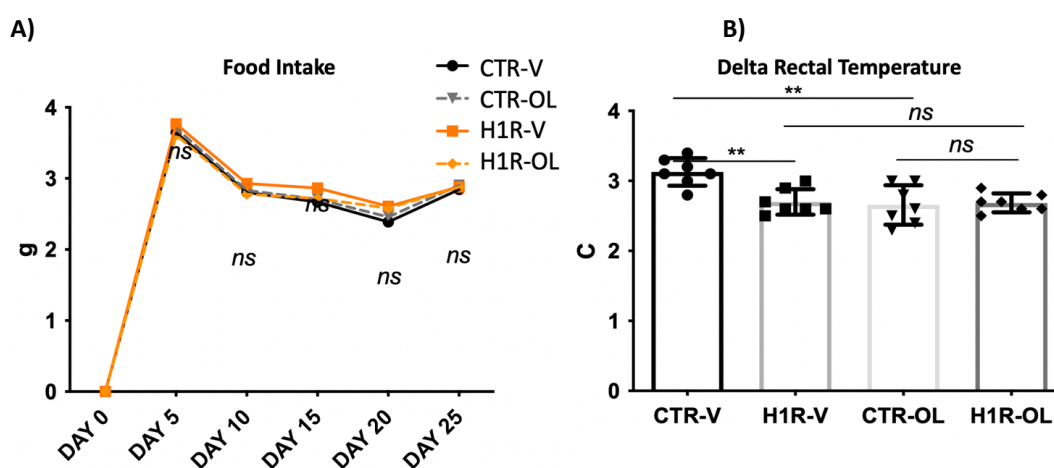


Fig.23 A) Evaluation of the food intake. Repeated measure ANOVA with Bonferroni correction. B) Assessment of the delta rectal temperature (difference between end-point mean temperature and baseline mean temperature). One-way ANOVA. (* $p < 0.05$; ** $p < 0.01$; *** $p < 0.001$; **** $p < 0.0001$). CTR-V (Controls treated with Vehicle), CTR-O (Controls treated with Olanzapine), H1R-V (H1R-KO mice treated with Vehicle), H1R-O (H1R-KO mice treated with Olanzapine)

The treatment with OL of the H1R-KO mice seems to boost the effect of H1R-KO with a further increase of NPY expression (IPA analysis performed on Dataset3 Table 2; Figure 24).

From the identification of a druggable target for the OL-induced MetS to the development of a new therapeutic approach using CRISPR/Cas7-11S

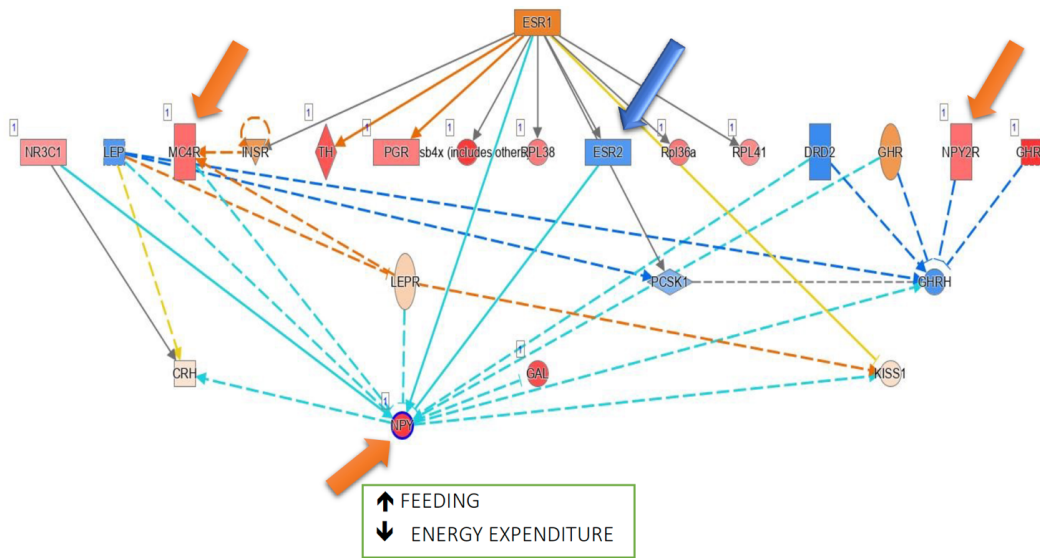


Fig.24 Olanzapine treatment boosts the effect of H1R-KO in hypothalamic neurons on the NPY pathway. IPA analysis of DEG between H1RKO-HFD-Vehicle vs H1RKO-HFD-Olanzapine.

Moreover, Olanzapine treatment directly affects the expression of both the Cannabinoid receptor 1 and the POMC/CART pathway, inducing a significant increase in their transcription levels (IPA analysis performed on Dataset3 table2 ; Figure 25).

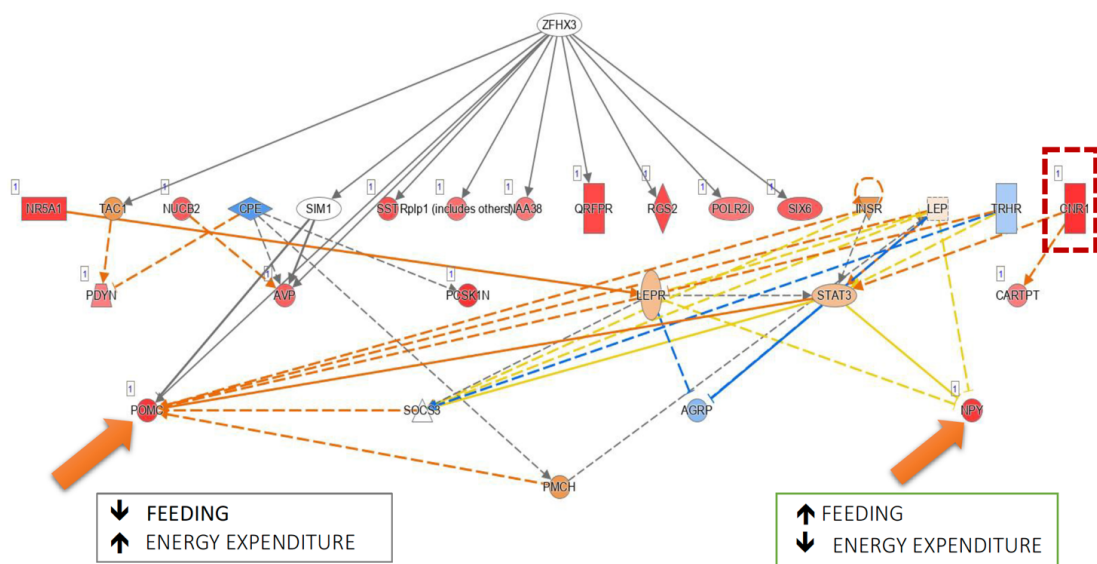


Fig.25 Olanzapine treatment additive effect of H1R-KO in hypothalamic neurons on NPY pathway. IPA analysis of DEG between H1RKO-HFD-Vehicle vs H1RKO-HFD-Olanzapine.

Therefore, the complete Olanzapine-induced metabolic deregulation represents the consequence of the disruption of the reciprocal POMC/NPY hypothalamic regulation. In line with H1R-KO mice, the Olanzapine treatment in control mice does not reduce the feeding behaviors or increase the energy expenditure through the thermogenesis in response to the observed increase in weight, as expected in physiological conditions. Finally, although Olanzapine exacerbates the alteration in the NPY pathway due to the H1R-KO, the administration of this drug to H1R-KO mice does not have an additive effect on food intake or energy expenditure (Figure 23).

Finally, the Ingenuity pathway analysis highlights that the knockout of CB1R could counteract the effect of Olanzapine, restoring the normal response to the calory intake with an observed decrease of the expression of the NPY/Agpr pathway (Figure 26). In line with this finding, the CB1-KO mice show a pronounced reduction in food intake and a significant increase in thermogenesis that correlates with weight gain (IPA analysis performed on Dataset4 Table 2; Figure 27).

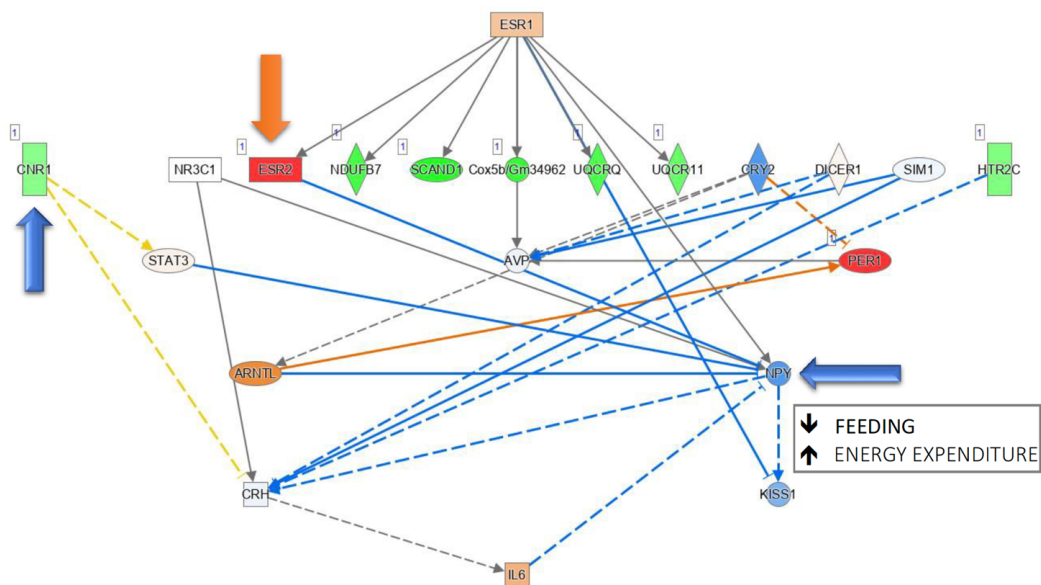


Fig.26 The CB1R-KO in hypothalamic neurons reverts the OL-induced MetS, down-regulating the NPY pathway. IPA analysis of DEG between CTR-HFD-Olanzapine and CB1RKO-HFD-Olanzapine.

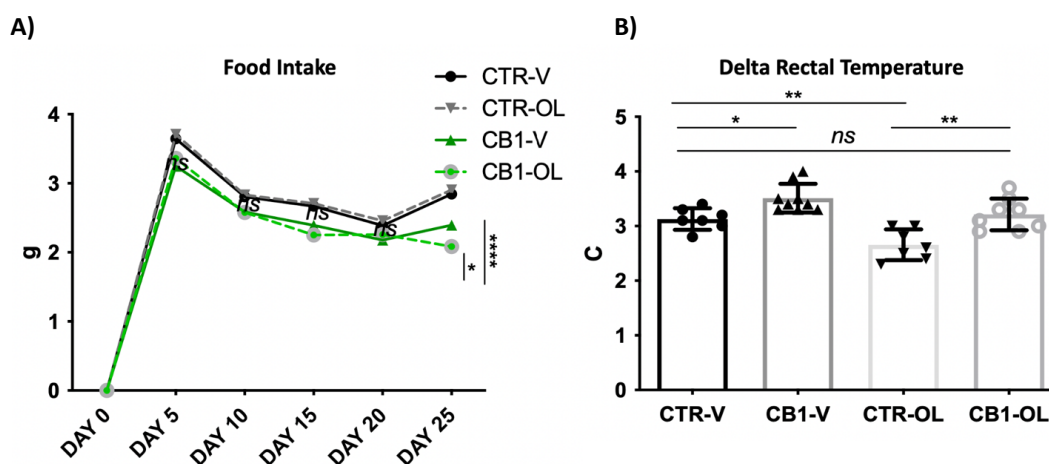
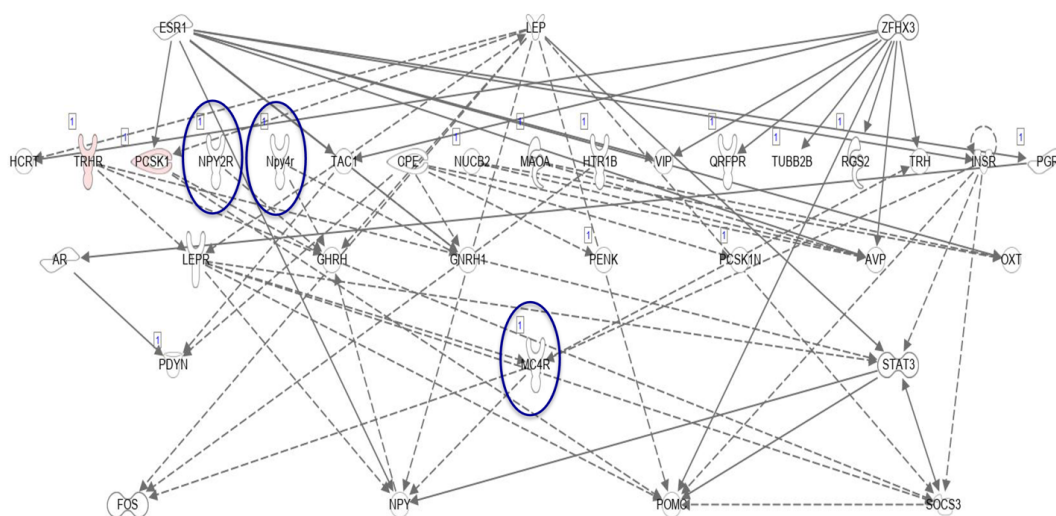


Fig.27 A) Evaluation of the food intake. Repeated measure ANOVA with Bonferroni correction. B) Assessment of the delta rectal temperature (difference between end-point mean temperature and baseline mean temperature). One-way ANOVA. (* $p < 0.05$; ** $p < 0.01$; *** $p < 0.001$; **** $p < 0.0001$). CTR-V (Controls treated with Vehicle), CTR-O (Controls treated with Olanzapine), CB1R-V (CB1R-KO mice treated with Vehicle), CB1R-O (CB1R-KO mice treated with Olanzapine)

The present results elucidate that the KO of CB1R in hypothalamic neurons can considerably reduce the metabolic side effects of Olanzapine treatment, restoring the NPY-mediated hypothalamic signalling.

The Knockout of CB1R in hypothalamic neurons restores the phenotype of OL-induced MetS by dissociating the expression of H1R and the NPY pathway.

Exploring the connectivity in the hypothalamic co-expression network of Control mice treated with Olanzapine (Dataset 5 Table 2), it appears that H1R is co-expressed in the same module with NPY, NPY receptor 2 (NPY2R) NPY receptor 4 (NPY4R) and Melanocortin receptor 4 (MC4R) (Figure 28). Therefore, the blockade of H1R due to Olanzapine treatment could result in the observed changes in the hypothalamic NPY signalling and the ability of POMC to suppress the NPY release, thus explaining the complete deregulation observed in the Ingenuity Pathway Analysis.



© 2000-2022 QIAGEN. All rights reserved.

Fig 28 Graphical representation of the H1R co-expression module in Control mice.

The Knockout of the CB1 receptor in Olanzapine-treated mice (WGCNA performed on Dataset 6 Table 2) doesn't affect the connectivity of CB1R by itself. Still, it leads to a dissociation between the H1R expression and NPY/Agrp signalling, belonging to different co-expression modules in this case. The present finding could represent a putative mechanism for the CB1-KO ability to restore OL-induced metabolic dysfunction.

4.3 STUDY PART 3: CB1R AS A POTENTIAL DRUGGABLE TARGET: EVALUATION OF MOOD-LIKE SIDE EFFECTS AND POSSIBLE REPRODUCTIVE DISFUNCIONS.

The blockade of CB1R in hypothalamic neurons does not cause any anxiety-like side effects, as observed during Rimonabant treatment, and does not induce any change in the estrous cycle.

From the results above, the CB1R in hypothalamic neurons represents a potential target for the treatment of OL-induced MetS. However, the onset of severe mood side effects, as observed in the case of Rimonabant administration, in response to the blockade of CB1R in the hypothalamus should be excluded. The assessment of the effect on mood of the knockout of CB1R is performed on mice fed with a Standard Diet to avoid any confounding effect of the diet on behaviours. In fact,

Dutheil S. et al. (118) demonstrate that rodents chronically exposed to high-fat content diets develop anxiety and anhedonia. This finding is also confirmed by the increase in corticosterone levels observed in rats by De Souza et al. following prolonged HFD (119).

In our study, CB1R-KO mice show no significant change in the anxiety levels evaluated by three different behavioural paradigms (Open Field Test, Dark/Light test, Elevated Plus Maze) and summarized in the Emotionality Score (Figure 29). In line with this finding, comparing CB1-KO mice and controls, no differences in corticosterone levels are described (Supplemental Figure 8).

These results confirm that targeting the CB1R specifically in hypothalamic neurons represents an effective therapeutic strategy to obtain the reduction of the metabolic dysfunction caused by OL, avoiding the severe mood changes observed with the Rimonabant administration.

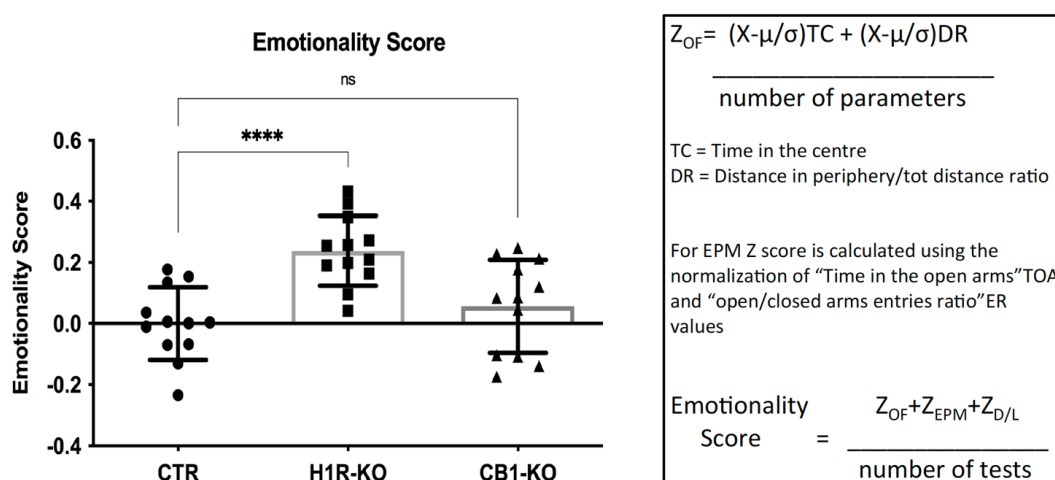


Fig.29 Differences in anxiety levels in the different study groups (H1R-KO, CB1R-KO and Controls) fed with standard diet assessed with three different behavioural paradigms (OFT, D/L test, EPM) and summarized as Emotionality Score. One-way ANOVA (* p < 0.05; ** p < 0.01; *** p < 0.001; **** p < 0.0001)

Similarly, the estrous cycle is evaluated on mice fed with a Standard diet. Indeed, both acute and chronic intake of HFD results in an impairment of the estrous

cyclicality as a homeostatic regulation of body weight, protecting from diet-induced metabolic abnormalities (120,121).

In our study, the knockout of the CB1R in hypothalamic neurons does not change the estrous cycle duration compared to the controls (Figure 30). This finding confirms that the observed amelioration of the OL-induced metabolic abnormalities in CB1R-KO mice is not the consequence of a sexual hormones' deregulation having orexigenic effects. On the other hand, the present finding ensures that targeting the CB1R in hypothalamic neurons is safe, preserving the normal function of the hypothalamic-pituitary-gonadal axis.

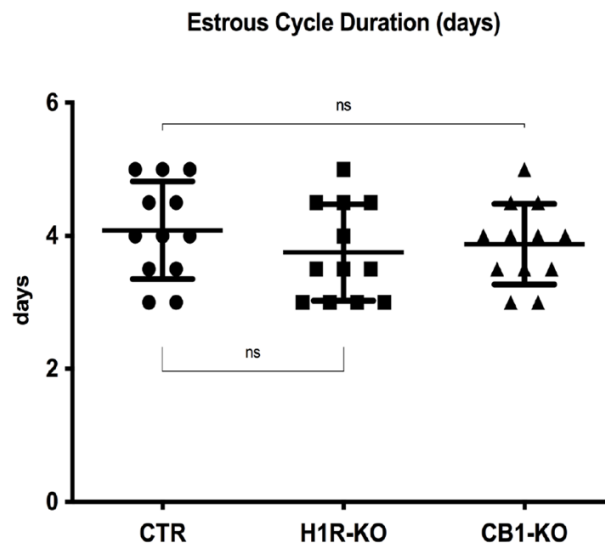


Fig.30 Differences in the estrous cycle duration (days) in the study groups (H1R-KO, CB1R-KO and Controls) fed with standard diet. One-way ANOVA (* $p < 0.05$; ** $p < 0.01$; *** $p < 0.001$; **** $p < 0.0001$).

4.4 STUDY PART 4: CRISPR/Cas7-11S THERAPEUTIC APPROACH – IN VITRO VALIDATION OF THE CB1R KNOCKDOWN.

CRISPR/Cas7-11S approach generates an efficient knockdown of the CB1R RNA in N2A cells.

The analysis of the qPCR data obtained from N2A stable cells expressing cas7-11S transfected with each CB1R-RNA targeting guide reveals that 7 of the 17 guides

perform significantly beyond the best knockdown efficiency described in the literature for Cas7-11S (50% of drop of the RNA). (Figure 31).

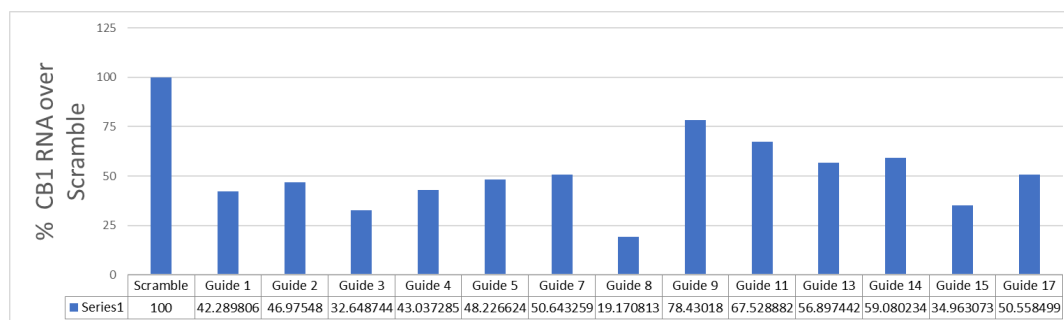


Fig.31 Plot of qPCR results of the CB1R knockdown performance of each designed guide in N2A

Guide 8 was selected as the best-performing guide according to the 81% drop in the CB1R RNA registered. No differences between the U6 and the tRNA promotor expressing guides are shown. This result contrasts the previously published data (89) where 50% of Knockdown was obtained only with tRNA promotor expressing guides. The U6 promotor expressing guides were only able to determine a 30% drop in the target RNA. Moreover, the comparative analysis of the knockdown performances of the different guides highlights that spacers targeting the first portion of the CB1R-RNA induce a more dramatic drop in CB1R expression than guides targeting other parts of the ribonucleic acid. The qPCR data were confirmed using RNAScope (Figures 32-33).

The present results show that Cas7-11S could represent a powerful tool for modulating the transcription of target genes in site and cell-specific manner.

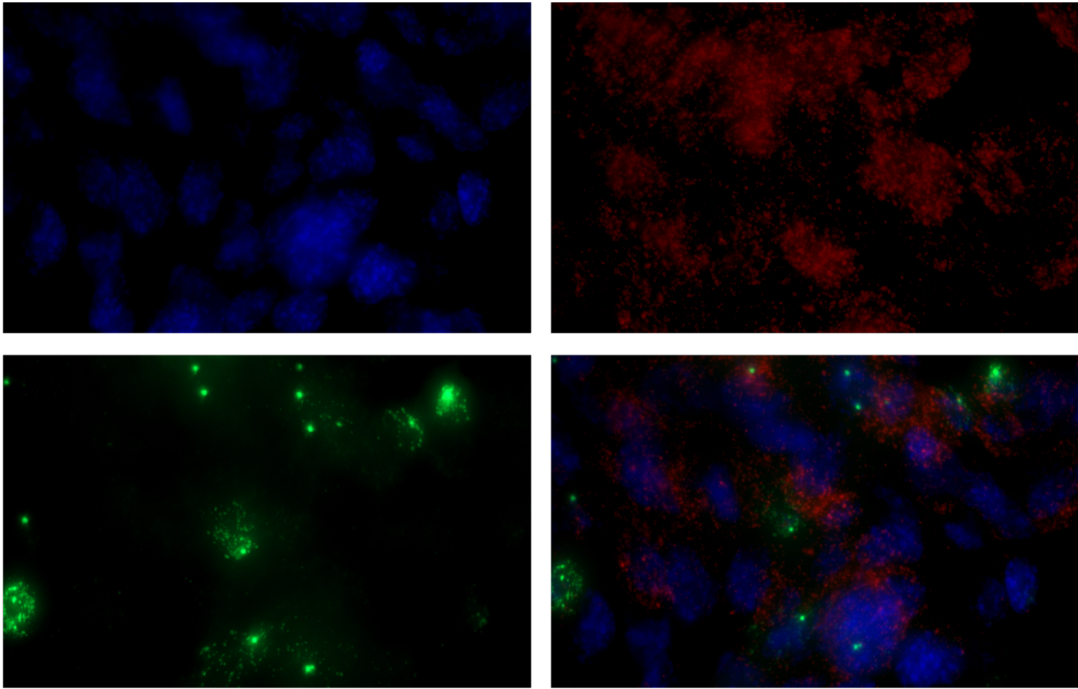


Fig.32 RNAScope of N2A cells expressing Δ CAS7-11 (63X). Blue-DAPI, Red-CB1R(Endogenous), Green- Δ CAS7-11.

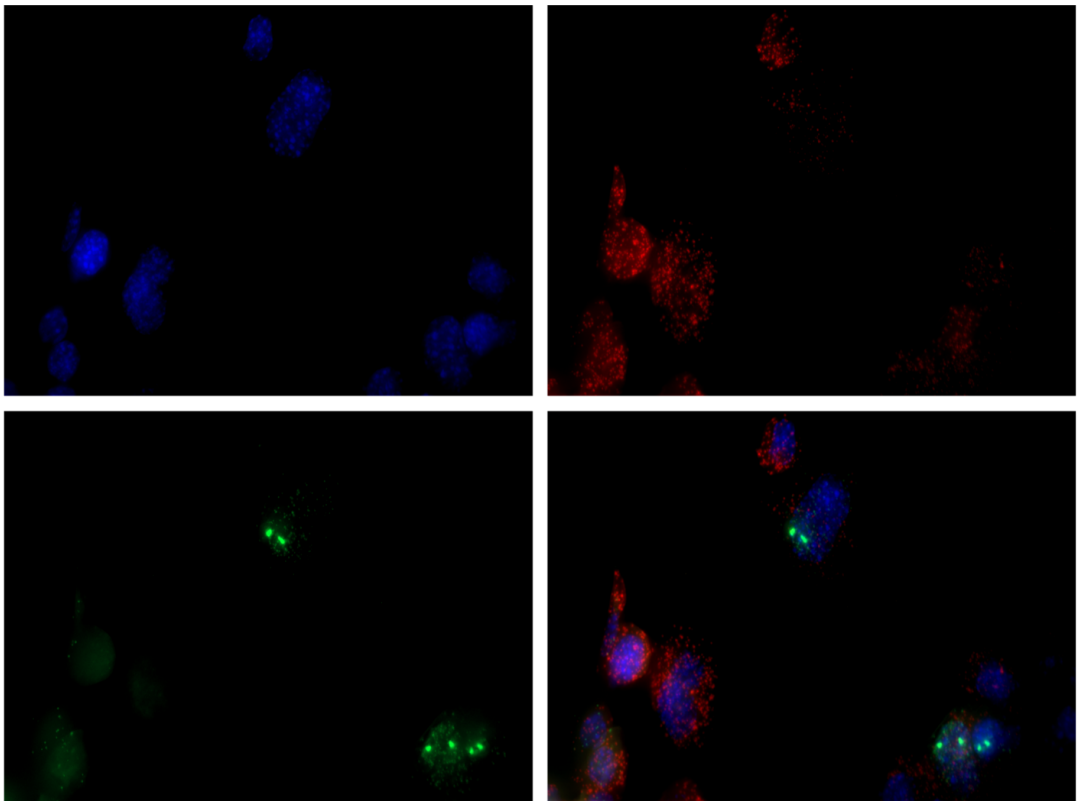


Fig.33 N2A cells expressing Δ CAS7-11 (63X) and Guide 8 targeting CB1R. Blue-DAPI, Red-CB1R(Endogenous), Green- Δ CAS7-11.

4.5 STUDY PART 5: DRUG DISCOVERY PROCESS FOR CRISPR/Cas7-11S SAFETY SWITCH-OFF.

A list of ligands acting as antagonists of Cas7-11S has been identified.

If in literature were described compounds antagonizing the activity of CRISPR-Cas9, no ligands targeting Cas7-11 are known. Considering the extensive structural and functional differences between Cas9 and Cas7-11, the compounds acting as Cas9 inhibitors are not suitable for the blockade of Cas7-11 enzymatic function. Here, we describe the first group of compounds specifically studied as Cas7-11S inhibitors. From the 200 molecules resulting from the virtual screening (Supplemental Table 2), a list of 25 compounds with higher binding affinity and QPlogBB scores and with a lower number of chiral centers was extracted. The present list accounts for fourteen compounds interacting with cleavage site 1 and five with cleavage site 2. The remaining six compounds are PPI disruptors; five of them act by binding the subunit 11, and one interacts at the level of the interface between subunit 11 and subunit 7.2 (Figure. 34). The first test of the efficiency of these compounds on N2A cells is currently on-going.

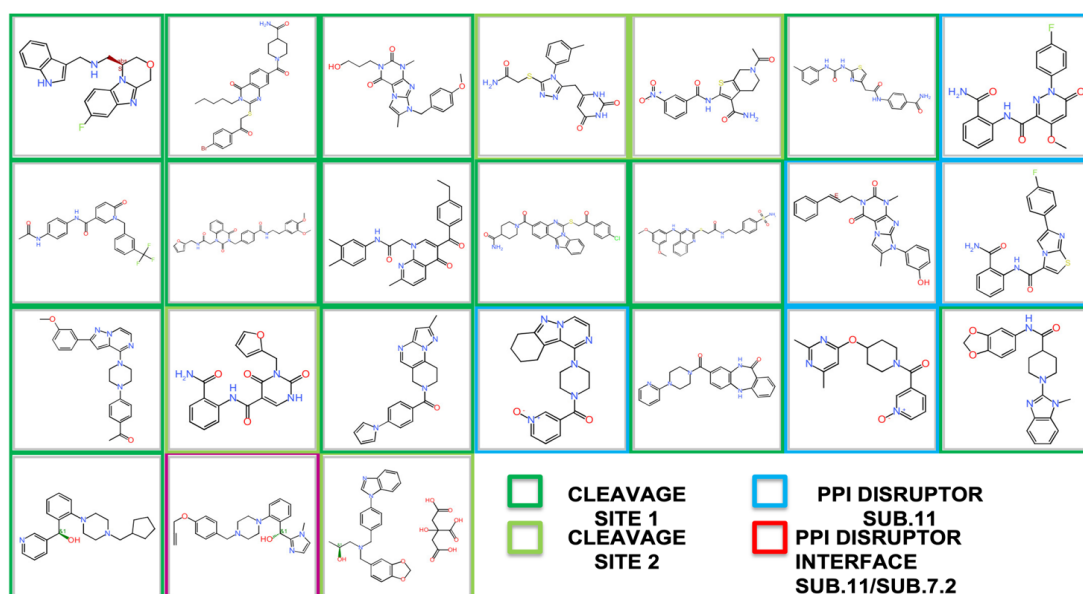


Fig.34 Top 25 compounds inhibiting Cas7-11S selected for the first screening on N2A cells.

5. DISCUSSION

The study of the biology of Olanzapine-induced metabolic syndrome represents a rising need for modern medicine, considering the limited therapeutic strategies currently available for this clinical condition and the frailty of the population involved. However, it presents a major scientific challenge due to the multifactorial complexity of this disease. In this project, we first dissect the biological architecture underlying this complex disease using an integrated biological and biocomputational approach. In fact, the combination of biocomputational analysis, such as DEG, Ingenuity Pathway Analysis, and WGCNA, with the CRISPR/Cas9 manipulation of gene expression enables the investigation of the impact of single GPCRs and their interactions in a specific brain area on the clinical features of the studied phenotype. The cell type and the brain region selectivity of CRISPR/Cas9- mediated gene targeting differentiate not only the phenotypical effect resulting from the knockout of the studied GPCRs in a target part of the brain but also dissect the cross-talk between different populations of cells within the investigated brain area.

Our results show that the hypothalamic neuronal H1R, but not the glial histamine receptor 1, is responsible for the weight gain induced by Olanzapine through changes in the NPY signalling. The overexpression of the NPY pathway affects the hypothalamus's ability to sense the body's metabolic status and coordinate the appropriate response regarding food intake and energy expenditure. In fact, the blockade of H1R, on the one hand, causes an increase in weight; on the other hand, it mimics an energy deficiency scenario, altering feeding behaviour and reducing energy utilization with enhanced fat deposition and thermogenesis. As previously shown in the literature (122-126), the NPY overexpression in ARC and VMH inhibits sympathetic nerve system (SNS) outflow and suppresses norepinephrine release. The decrease in sympathetic NA reduces the binding of this catecholamine to the β -adrenergic receptors in white adipose tissue (WAT) and brown adipose tissue (BAT). This results in an inhibition of the cAMP-PKA

pathway-associated lipolysis in the WAT and a down-regulation of the expression of the uncoupling protein 1 (UCP1) in the BAT, causing a deficit thermogenic potential. Furthermore, adrenal medullary catecholamines, primarily epinephrine (EPI), compensate for the reduced SNS outflow. The enhanced EPI levels stimulate adipogenesis through the binding to the α_2 -adrenergic receptors in the WAT.

The blockade of histamine receptor 1 in hypothalamic neurons, however, is not sufficient to explain the complete phenotype of OL-induced MetS. In fact, neuronal H1R seems to be not involved in the glucose and lipid abnormalities due to this antipsychotic chronic treatment, suggesting that glial H1R or other neuronal, glial receptors, peripheral mechanisms or a combination of more than one of these processes are related with the development of glucose intolerance and dyslipidemia in OL-induced MetS. The highly selective deconstruction of the circuitry involved in the metabolic dysfunction due to Olanzapine treatment is essential for understanding this complex disorder where multiple organs or brain regions and different cell types contribute to the final clinical presentation. Moreover, exploring the detailed biological map underlying each symptom provides relevant information for the target identification in the drug design process.

In fact, the treatment with Olanzapine of H1R knockout mice highlights the hypothalamic upregulation of the expression of the Cannabinoid receptor 1 induced by this drug as part of the disrupted metabolic pathway of POMC and NPY/Agrp.

The performed CRISPR/Cas9 mediated knockout of the CB1R then validates the efficacy of the blockade of the Cannabinoid receptor 1 in hypothalamic neurons in reverting the complete phenotype of the OL-induced metabolic syndrome, re-modulating the NPY expression. Conversely, the inability of the CB1R KO to re-establish a healthy phenotype in diet-induced obesity underlines that the onset of OL-induced MetS follows the dysfunction in different biological pathways than

other forms of metabolic disorders. Therefore, our study emphasizes the need to develop specific treatments for this medical condition.

The present finding does not lead to the detection of a novel druggable target, considering that the CB1R antagonist Rimonabant was already used as an anorexigenic drug to treat Olanzapine-induced metabolic syndrome. However, our study, topologically dividing the effect of the cannabinoid receptor 1 in the hypothalamus and other brain regions, demonstrates that the blockade of the CB1R in the hypothalamus is sufficient to treat the metabolic dysfunction without causing any behavioural side effects observed with Rimonabant treatment such as anxiety, depression, and suicidal ideation (72). Our results suggest that other brain regions, such as the limbic areas, could be involved in the unwanted mood changes observed during Rimonabant administration. This evidence opens the question of how brain-area specificity could be achieved with our therapeutic options. The present issue represents one of the major recent challenges for the development of new medical approaches for treating complex disorders, especially in neuropsychopharmacology.

To meet this problem, here we develop an innovative therapeutic approach for OL-induced MetS targeting CB1R in hypothalamic neurons using the RNA targeting CRISPR/Cas7-11. This tool was first described by Gootenberg and Abudayyeh's team (88) in 2021, displaying substantial RNA interference (knockdown) properties in *E. coli* and mammalian cells. The development by the same group in 2022 of a smaller version of Cas7-11 (Cas7-11S) suitable for AAVs packaging enables its potential translation to clinical use. In fact, given that many concerns regarding CRISPR-mediated editing revolve around the permanency and heritability associated with DNA editing, this RNA-targeting nuclease appears to be a promising approach for human therapeutic applications.

In our study, combining an in-house re-engineering of the wild-type CRISPR/Cas7-11 to obtain the Cas7-11S with a comparative analysis of the performance of the spacers, we obtain a high-efficiency knockdown tool reaching an 81% drop in the

CB1R RNA in N2A cells. This level of knockdown is considerably higher than the best performance described by Kato et al. (89) in the only other mammalian cell application of the CRISPR/Cas7-11S system reported in the literature.

Furthermore, to improve the safety of our therapeutic strategy, here we develop a method of switching off the Cas7-11S system in case of any undesired side effects, using small molecules. Following a drug-discovery process, we identify a list of twenty-five compounds inhibiting the enzymatic activity of the CRISPR-Cas7-11S system. Considering the desired application of the CRISPR/Cas7-11S tool for the modulation of the CB1R in the hypothalamus, the Cas7-11S targeting drugs are selected to be highly permeable to the blood-brain barrier. The present result represents the first described list of compounds predicted to inhibit specifically Cas7-11S. The *in vitro* validation of these small molecules is currently ongoing.

Altogether, our RNA-editing approach, ensuring a reversible strategy for the fine modulation of target protein in specific brain circuitry in a cell and site-selective manner, provides an innovative strategy applicable to the treatment of a large number of disorders with the potential of reaching the human clinical-trial stage. This CRISPR/Cas7-11 strategy, although developed here as a therapy for the OL-induced MetS, could be widely applied in neuropsychopharmacology in all the conditions that require the blockade of a known GPCR in a specific part of the brain. Considering, for example, the treatment of Schizophrenia, the CRISPR/Cas7-11S tool could be used to target the D2 receptor in the mesolimbic area without reaching the Dopamine receptors of the nigrostriatal and tuberoinfundibular pathways, thus attenuating the positive symptoms avoiding extrapyramidal or pituitary mediated side effects. Similarly, this approach targeting the SCL6A4 transcription levels in the amygdala, could result in an inhibition of 5-HT reuptake in the presynapse from the synaptic cleft, mimicking the effect of Selective Serotonin Reuptake Inhibitors (SSRI) without the common side-effect on weight and on sexual functions commonly experienced during the antidepressant treatment.

Reducing the burden of the currently prescribed drugs, the CRISPR/Cas7-11S approach could improve the patient's adherence and compliance to the treatment, ensuring a long-term, well-tolerated therapy.

Despite the promising results, the present study represents just the first step toward developing highly selective, alternative strategies for the treatment of neuropsychiatric conditions. Further studies are still needed to validate the safe translatability of this approach and to overcome the limitation of the AAV vector delivery of this system.

6. CONCLUSIONS

The present project is a comprehensive pharmacological study that meets the urgent need to find an effective treatment for OL-induced MetS, a life-threatening clinical syndrome affecting a frail population. Starting from a mechanistic open question emerging from the clinical practice, we investigate, using a combined biocomputational-biotechnological approach, the main GPCRs involved in this specific type of metabolic dysfunction, dissecting the role of each one on the onset of the clinical features characterizing the MetS. The systematic deconstruction of the complex biological architecture underlying this complex disorder led us to identify a suitable druggable- target: the cannabinoid receptor 1. To overcome the known side effects of the CB1R blockade in the whole brain, we developed an innovative therapeutic approach using CRISPR/Cas7-11S, a cutting-edge cell and site-selective RNA-editing tool. Our engineering of the wild type Cas7-11 (pCMV - huDisCas7-11) to obtain the short version (Cas7-11S) combined with a comparative analysis of the efficiency of the spacers allowed us to reach a highly efficient (81% drop of CB1R-RNA) knockdown in N2A cells. Finally, to ensure the reversibility of the CRISPR/Cas7-11S RNA interference, we applied a drug-discovery process to uncover a list of Cas7-11S selective inhibitors that potentially could block the enzymatic activity of this nuclease in case of side effects. The present results open promising perspectives for the application of the

CRISPR/Cas7-11S system as a safe tool for human gene therapy. The use of different unbiased biocomputational paradigms followed by a required biological validation of the findings empowers the overall scientific process, offering an integrated approach to capture the biological complexity of multifactorial disorders, maximizing the possibilities to develop translatable therapeutic strategies.

In conclusion, the trajectory of our study highlights the importance for clinical settings to meet the more advanced knowledge in the biotechnological field to address still open medical questions and to provide innovative therapeutic options for diseases with currently limited available therapies.

REFERENCES

- 1) Zhang JP et al. Pharmacogenetics and antipsychotics: Therapeutic efficacy and side effects prediction *Expert Opin. Drug Metab Toxicol.* (2011) 7(1): 9–37.
- 2) Brisch R et al. The Role of Dopamine in Schizophrenia from a Neurobiological and Evolutionary Perspective: Old Fashioned, but Still in Vogue. *Front Psychiatry* (2014) 5:47.
- 3) Mocci, G. et al. Expression of 5-HT_{2A} receptors in prefrontal cortex pyramidal neurons projecting to nucleus accumbens. Potential relevance for atypical antipsychotic action. *Neuropharmacology*, (2014) 79, 49-58.
- 4) Meltzer HY et al. The role of serotonin receptors in the action of atypical antipsychotic drugs. *Curr. Opin. Pharmacol.*, (2011) 11 (1), 59-67.
- 5) Correll CU et al. From receptor pharmacology to improved outcomes: individualizing the selection, dosing, and switching of antipsychotics. *Eur. Psychiatry.* (2010) 25(Suppl 2): S12–S21.
- 6) Eckel RH, et al. The metabolic syndrome. *Lancet* (2005) 365: 1415–28.
- 7) Alberti KGMM, et al. Metabolic syndrome – a new world-wide definition. A consensus statement from the International Diabetes Federation. *Lancet* (2006) 23:469-80.
- 8) Expert Panel on Detection and Evaluation of Treatment of High Blood Cholesterol in Adults. Executive summary of the third report of the National Cholesterol Education Program (NCEP) expert panel on detection, evaluation and treatment of high blood cholesterol in adults (Adult Treatment Panel III). *JAMA* (2001) 285: 2486-97.
- 9) Grundy SM, et al. Diagnosis and management of the metabolic syndrome: an American Heart Association/ National Heart, Lung, and Blood Institute Scientific Statement. *Circulation* (2005) 112: 2735-52.
- 10) International Diabetes Federation. The IDF consensus worldwide definition of the metabolic syndrome. Brussels: International Diabetes Federation (2005).
- 11) McEvoy JP et al. Prevalence of the metabolic syndrome in patients with schizophrenia: baseline results from the clinical antipsychotic trials of intervention

effectiveness (CATIE) schizophrenia trial and comparison with national estimates from NHANES III. *Schizophr Res* (2005) 80:19–32.

12) Allison DB et al. Antipsychotic-induced weight gain: a comprehensive research synthesis. *Am J Psychiatry*. 1999 Nov;156(11):1686-96. doi: 10.1176/ajp.156.11.1686. PMID: 10553730.

13) Homel P et al. Changes in body mass index for individuals with and without schizophrenia, 1987-1996. *Schizophr. Res.* (2002) Jun 1;55(3):277-84. doi: 10.1016/s0920-9964(01)00256-0. PMID: 12048151.

14) Meduna LJ et al. Biochemical disturbances in mental disorders: I. Anti-insulin effect of blood in cases of Schizophrenia. *Arch NeurPsych.* (1942) 47(1):38–52.

15) Allison DB, Casey DE. Antipsychotic-induced weight gain: a review of the literature. *J Clin Psychiatry.* (2001) 62 Suppl 7:22-31. PMID: 11346192.

16) Henderson DC. Schizophrenia and comorbid metabolic disorders. *J Clin. Psychiatry.* (2005) 66 Suppl. 6:11-20. PMID: 16107179.

17) Newcomer JW. Second-generation (atypical) antipsychotics and metabolic effects: a comprehensive literature review. *CNS Drugs.* (2005) 19 Suppl. 1:1-93. doi: 10.2165/00023210-200519001-00001. PMID: 15998156.

18) Newcomer JW. Metabolic considerations in the use of antipsychotic medications: a review of recent evidence. *J Clin Psychiatry.* (2007) 68 Suppl 1:20-7. PMID: 17286524.

19) Scheen AJ, De Hert M. Drug-induced diabetes mellitus: the example of atypical antipsychotics. *Rev Med Liege.* (2005) 60(5-6):455-60. PMID: 16035311.

20) Scheen AJ, De Hert MA. Abnormal glucose metabolism in patients treated with antipsychotics. *Diabetes Metab.* (2007) Jun;33(3):169-75. doi: 10.1016/j.diabet.2007.01.003. Epub 2007 Apr 6. PMID: 17412628.

21) Tschoner A, et al. Metabolic side effects of antipsychotic medication. *Int J Clin Pract.* 2007 Aug;61(8):1356-70. doi: 10.1111/j.1742-1241.2007.01416.x. PMID: 17627711.

22) De Hert M, et al. Typical and atypical antipsychotics differentially affect long-term incidence rates of the metabolic syndrome in first-episode patients with schizophrenia: A retrospective chart review *Schizophrenia Research* (2008), vol. 101, iss. 1-3, pp. 295-303.

- 23) Brown S. Excess mortality of schizophrenia. A meta-analysis. *Br J Psychiatry* (1997) 171:502–8.
- 24) Khan A, Faucett J, Morrison S, Brown WA. Comparative mortality risk in adult patients with schizophrenia, depression, bipolar disorder, anxiety disorders, and attention deficit/hyperactivity disorder participating in psychopharmacology clinical trials. *JAMA Psychiatry* (2013) 70:1091–9.
- 25) Osby U et al. Mortality and causes of death in schizophrenia in Stockholm County, Sweden. *Schizophr. Res* (2000) 45:21–8.
- 26) Lyketsos, C.G et al. Medical comorbidity in psychiatric inpatients: relation to clinical outcomes and hospital length of stay. *Psychosomatics* (2002) 43 (1), 24-30.
- 27) Dixon, L. et al. The association of medical comorbidity in schizophrenia with poor physical and mental health. *J. Nerv. Ment. Dis.* 187 (8), 496-502.
- 28) Robinson, D.G. et al. Predictors of medication discontinuation by patients with first- episode schizophrenia and schizoaffective disorder. *Schizophr. Res.* (2002) 57 (2-3), 209-219.
- 29) Weiden, P.J. et al. Obesity as a risk factor for antipsychotic noncompliance. *Schizophr. Res.*(2004) 66 (1), 51-57.
- 30) Schwartz MW, Morton GJ. Obesity: keeping hunger at bay. *Nature.* (2002) Aug 8;418(6898):595-7. doi: 10.1038/418595a. PMID: 12167841.
- 31) Meier, U & Gressner, AM. Endocrine regulation of energy metabolism: review of pathobiochemical and clinical chemical aspects of leptin, ghrelin, adiponectin, and resistin. *Clin Chem* (2004) 50(9), 1511–1525.
- 32) Higgins SC, et al. Ghrelin, the peripheral hunger hormone, *Annals of Medicine* (2007) 39:2, 116-136, DOI: 10.1080/07853890601149179
- 33) Bromel T et al. Serum leptin levels increase rapidly after initiation of clozapine therapy. *Molecular Psychiatry.* (1998) 3: 76–80.
- 34) Kraus T et al. Body weight and leptin plasma levels during treatment with antipsychotic drugs. *American Journal of Psychiatry.* (1999) 156: 312–4.
- 35) Graham KA et al. Effect of olanzapine on body composition and energy expenditure in adults with first-episode psychosis. *American Journal of Psychiatry.* (2005) 162: 118–23.

- 36) Eder U et al. Association of olanzapine-induced weight gain with an increase in body fat. *American Journal of Psychiatry*. (2001) 158:1719–22.
- 37) Ebenbichler C, et al. The soluble leptin receptor in olanzapine-induced weight gain: results from a prospective study. *Schizophrenia Research*. (2005) 75: 143–6.
- 38) Murashita M, et al. Olanzapine increases plasma ghrelin level in patients with schizophrenia. *Psychoneuroendocrinology*. (2005) 30: 106–10.
- 39) Hosojima H et al. Early effects of olanzapine on serum levels of ghrelin, adiponectin and leptin in patients with schizophrenia. *Journal of Psychopharmacology*. (2006) 20: 75–9.
- 40) Monteleone P et al. Pronounced early increase in circulating leptin predicts a lower weight gain during clozapine treatment. *Journal of Clinical Psychopharmacology*. (2002) 22: 424–6.
- 41) Theisen FM, et al. A prospective study of serum ghrelin levels in patients treated with clozapine. *Journal of Neural Transmission*. (2005) 112: 1411–6.
- 42) Potvin S et al. Antipsychotic-Induced Changes in Blood Levels of Leptin in Schizophrenia: A Meta-Analysis. *Can J Psychiatry* (2015) 60(3): S26–S34.
- 43) Kowalchuk C. et al. In male rats, the ability of central insulin to suppress glucose production is impaired by olanzapine, whereas glucose uptake is left intact. *J Psychiatry Neurosci*. (2017) 42(6): 424-431.
- 44) Newcomer JW, et al. Abnormalities in glucose regulation during antipsychotic treatment of schizophrenia. *Arch Gen Psychiatry*. (2002) 59: 337-345.
- 45) Melkersson KI et al. Relationship between levels of insulin or triglycerides and serum concentrations of the atypical antipsychotics clozapine and olanzapine in patients on treatment with therapeutic doses. *Psychopharmacology (Berl)*. (2003) 170: 157-166.
- 46) Simpson GM et al. Randomized, controlled double-blind multicentre comparison of the efficacy and tolerability of ziprasidone and olanzapine in acutely ill inpatients with schizophrenia or schizoaffective disorder. *Am J Psychiatry*. (2005) 161: 1837-1847.

- 47) Perez-Gomez et al. A phenotypic *Caenorhabditis elegans* screen identifies a selective suppressor of antipsychotic-induced hyperphagia. *Nat Comm* (2018) 9: 5272-83
- 48) Veneziani F. et al. Dissecting hypothalamic dysfunction in the Olanzapine-induced Metabolic Syndrome. *Neuropsychopharmacology* (2022) 47 Suppl1 164-165. <https://doi.org/10.1038/s41386-022-01484-1>
- 49) Kroeze WK, et al. H1-histamine receptor affinity predicts short-term weight gain for typical and atypical antipsychotic drugs. *Neuropsychopharmacology* (2003) 28: 519–526.
- 50) Ratliff JC, et al. Association of prescription H1 antihistamine use with obesity: results from the National Health and Nutrition Examination Survey. *Obesity*. (2010) Dec;18(12):2398-400. doi: 10.1038/oby.2010.176. Epub 2010 Aug 12. PMID: 20706200; PMCID: PMC3221329.
- 51) Masaki T, et al. Involvement of hypothalamic histamine H1 receptor in the regulation of feeding rhythm and obesity. *Diabetes*. 2004 Sep;53(9):2250-60. doi: 10.2337/diabetes.53.9.2250. PMID: 15331534.
- 52) Jørgensen EA, et al. Increased susceptibility to diet-induced obesity in histamine-deficient mice. *Neuroendocrinology*. (2006) 83(5-6):289-94. doi: 10.1159/000095339. Epub 2006 Aug 22. PMID: 16926531.
- 53) Cota D et al. The endogenous cannabinoid system affects energy balance via central orexigenic drive and peripheral lipogenesis. *J Clin Invest* (2003) 112: 423–431.
- 54) Di Marzo V et al. Leptin-regulated endocannabinoids are involved in maintaining food intake. *Nature* (2001) 410: 822–825.
- 55) Osei-Hyiaman D et al. Endocannabinoid activation at hepatic CB1 receptors stimulates fatty acid synthesis and contributes to diet-induced obesity. *J Clin Invest* (2005) 115: 1298–1305.
- 56) Ravinet Trillou C et al. Anti-obesity effect of SR141716, a CB1 receptor antagonist, in diet-induced obese mice. *Am J Physiol Regul Integr Comp Physiol* (2003) 284: R345–R353.

- 57) Ravinet Trillou C et al. CB1 cannabinoid receptor knockout in mice leads to leanness, resistance to diet-induced obesity and enhanced leptin sensitivity. *Int J Obes Relat Metab Disord* (2004) 28: 640–648.
- 58) Jamshidi N et al. Anandamide administration into the ventromedial hypothalamus stimulates appetite in rats. *Br J Pharmacol* (2001) 134: 1151–1154.
- 59) Kirkham TC, et al. Endocannabinoid levels in rat limbic forebrain and hypothalamus in relation to fasting, feeding and satiation: stimulation of eating by 2-arachidonoyl glycerol. *Br J Pharmacol* (2002) 136: 550–557.
- 60) Beal JE, et al. Dronabinol as a treatment for anorexia associated with weight loss in patients with AIDS. *J Pain Symptom Manage* (1995) 10: 89–97.
- 61) Nelson K et al. A phase II study of delta-9-tetrahydrocannabinol for appetite stimulation in cancer-associated anorexia. *J Palliat Care* (1994) 10: 14–18.
- 62) Weston-Green K, et al. The effects of antipsychotics on the density of cannabinoid receptors in the dorsal vagal complex of rats: implications for olanzapine-induced weight gain. *Int J Neuropsychopharmacol* (2008) 11: 827–835.
- 63) Chew NWS, et al. The global burden of metabolic disease: Data from 2000 to 2019. *Cell Metab.* 2023 Mar 7;35(3):414-428.e3. doi: 10.1016/j.cmet.2023.02.003. PMID: 36889281.
- 64) Montesi L, et al. Long-term weight loss maintenance for obesity: a multidisciplinary approach. *Diabetes Metab Syndr Obesity J* (2016) 9:37–46
- 65) Khera R, et al. Association of Pharmacological Treatments for Obesity with Weight Loss and Adverse Events: A Systematic Review and Meta-analysis. *JAMA.* 2016 Jun 14;315(22):2424-34. doi: 10.1001/jama.2016.7602. Erratum in: *JAMA.* (2016) Sep 6;316(9):995. PMID: 27299618; PMCID: PMC5617638.
- 66) Tchoukhine E, et al. Orlistat in clozapine- or olanzapine-treated patients with overweight or obesity: a 16-week open-label extension phase and both phases of a randomized controlled trial. *J Clin Psychiatry.* (2011) Mar;72(3):326-30. doi: 10.4088/JCP.09m05283yel. Epub 2010 Aug 24. PMID: 20816037.
- 67) Larsen JR, et al. Effect of Liraglutide Treatment on Prediabetes and Overweight or Obesity in Clozapine- or Olanzapine-Treated Patients with Schizophrenia

Spectrum Disorder: A Randomized Clinical Trial. *JAMA Psychiatry*. (2017) Jul 1;74(7):719-728. doi: 10.1001/jamapsychiatry.2017.1220. PMID: 28601891; PMCID: PMC5710254.

68) Prasad F, et al. Semaglutide for the treatment of antipsychotic-associated weight gain in patients not responding to metformin - a case series. *Ther Adv Psychopharmacol*. (2023) Apr 19;13:20451253231165169. doi: 10.1177/20451253231165169. PMID: 37113745; PMCID: PMC10126648.

69) Tek C. et al. Naltrexone HCl/bupropion HCl for chronic weight management in obese adults: patient selection and perspectives. *Patient Prefer Adherence*. (2016) May 4;10:751-9. doi: 10.2147/PPA.S84778. PMID: 27217728; PMCID: PMC4862388.

70) Tek C, et al. A randomized, double-blind, placebo-controlled pilot study of naltrexone to counteract antipsychotic-associated weight gain: proof of concept. *J Clin Psychopharmacol*. (2014) Oct;34(5):608-12. doi: 10.1097/JCP.000000000000192. PMID: 25102328; PMCID: PMC4149840.

71) Lazzari P, et al. Weight loss induced by rimonabant is associated with an altered leptin expression and hypothalamic leptin signalling in diet-induced obese mice. *Behav Brain Res*. (2011) Mar 1;217(2):432-8. doi: 10.1016/j.bbr.2010.11.022. Epub 2010 Nov 11. PMID: 21074566.

72) Moreira FA and Crippa JA. The psychiatric side-effects of rimonabant. *Braz J Psychiatry*. (2009) Jun;31(2):145-53. doi: 10.1590/s1516-44462009000200012. PMID: 19578688.

73) Nguyen NT and Varela JE. Bariatric surgery for obesity and metabolic disorders: state of the art. *Nat Rev Gastroenterol Hepatol* (2017) 14(3):160–169.

74) Shelby SR, et al. Bariatric surgery: a viable treatment option for patients with severe mental illness. *Surg Obes Relat Dis*. (2015) Nov-Dec;11(6):1342-8. doi: 10.1016/j.soard.2015.05.016. Epub 2015 Jun 3. PMID: 26363716.

75) Li H, et al. Applications of genome editing technology in the targeted therapy of human diseases: mechanisms, advances and prospects. *Signal Transduct Target Ther*. 2020 Jan 3;5(1):1. doi: 10.1038/s41392-019-0089-y. PMID: 32296011; PMCID: PMC6946647.

76) Carroll D. Genome editing: progress and challenges for medical applications. *Genome Med*. 2016 Nov 15;8(1):120. doi: 10.1186/s13073-016-0378-9. PMID: 27846896; PMCID: PMC5111268.

- 77) Kohn DB and Candotti F. Gene therapy fulfilling its promise. *N. Engl. J. Med.* (2009) 360(5):518–21
- 78) Hacein-Bey-Abina S, et al. LMO2- associated clonal T cell proliferation in two patients after gene therapy for SCID-X1. *Science* (2003) 302(5644):415–19
- 79) Savić N and Schwank G. Advances in therapeutic CRISPR/Cas9 genome editing. *Transl Res.* (2016) Feb;168:15-21. doi: 10.1016/j.trsl.2015.09.008. Epub 2015 Sep 26. PMID: 26470680.
- 80) Barrangou R. The roles of CRISPR-Cas systems in adaptive immunity and beyond. *Curr Opin Immunol* (2015) 32:36–41
- 81) Jinek M, et al A programmable dual-RNA-guided DNA endonuclease in adaptive bacterial immunity. *Science* (2012) 337:816–821
- 82) Cong L, et al. Multiplex genome engineering using CRISPR/Cas systems. *Science* (2013) 339:819–823
- 83) Mali P, et al. RNA-guided human genome engineering via Cas9. *Science* (2013) 339:823–826
- 84) Hsu PD, et al. Development and applications of CRISPR-Cas9 for genome engineering. *Cell* (2014) 157:1262–1278
- 85) Shin HY et al. CRISPR/Cas9 targeting events cause complex deletions and insertions at 17 sites in the mouse genome. *Nat Commun* (2017) 8:15464.
- 86) Farooqi IS. and O'Rahilly S. Monogenic human obesity syndromes. *Recent Prog Horm Res* (2004) 59:409–424.
- 87) Gray J, et al. Functional characterization of human NTRK2 mutations identified in patients with severe early-onset obesity. *Int J Obes* (2007) 31(2):359–364.
- 88) Özcan A, et al. Programmable RNA targeting with the single-protein CRISPR effector Cas7-11. *Nature.* 2021 Sep;597(7878):720-725. doi: 10.1038/s41586-021-03886-5. Epub 2021 Sep 6. Erratum in: *Nature.* (2022) Aug;608(7923):E30. PMID: 34489594.
- 89) Kato K, et al. Structure and engineering of the type III-E CRISPR-Cas7-11 effector complex. *Cell.* (2022) Jun 23;185(13):2324-2337.e16. doi: 10.1016/j.cell.2022.05.003. Epub 2022 May 27. PMID: 35643083.

- 90) Barrangou, R, et al. CRISPR provides acquired resistance against viruses in prokaryotes. *Science* (2007) 315, 1709–1712.
- 91) Brouns, S.J. et al. Small CRISPR RNAs guide antiviral defence in prokaryotes. *Science* (2008) 321,960–964.
- 92) Marraffini, L.A., and Sontheimer, E.J. CRISPR interference limits horizontal gene transfer in staphylococci by targeting DNA. *Science* (2008) 322, 1843–1845.
- 93) Bondy-Denomy, et al. Bacteriophage genes that inactivate the CRISPR/Cas bacterial immune system. *Nature* (2013) 493, 429–432.
- 94) Bondy-Denomy, J., et al. Multiple mechanisms for CRISPR-Cas inhibition by anti-CRISPR proteins. *Nature* (2015) 526, 136–139.
- 95) Pawluk A, et al. A new group of phage anti-CRISPR genes inhibits the type I-E CRISPR-Cas system of *Pseudomonas aeruginosa*. *mBio*. (2014) Apr 15;5(2):e00896. doi: 10.1128/mBio.00896-14. PMID: 24736222; PMCID: PMC3993853.
- 96) van Houte S, et al. The diversity-generating benefits of a prokaryotic adaptive immune system. *Nature*. (2016) Apr 21;532(7599):385-8. doi: 10.1038/nature17436. Epub 2016 Apr 13. PMID: 27074511; PMCID: PMC4935084.
- 97) Pawluk A, et al. Inactivation of CRISPR-Cas systems by anti-CRISPR proteins in diverse bacterial species. *Nat Microbiol*. (2016) Jun 13;1(8):16085. doi: 10.1038/nmicrobiol.2016.85. PMID: 27573108.
- 98) Pawluk A, et al. Naturally Occurring Off-Switches for CRISPR-Cas9. *Cell*. (2016) Dec 15;167(7):1829-1838.e9. doi: 10.1016/j.cell.2016.11.017. Epub 2016 Dec 8. PMID: 27984730; PMCID: PMC5757841.
- 99) Rauch BJ, et al. Inhibition of CRISPR-Cas9 with Bacteriophage Proteins. *Cell*. (2017) Jan 12;168(1-2):150-158.e10. doi: 10.1016/j.cell.2016.12.009. Epub 2016 Dec 29. PMID: 28041849; PMCID: PMC5235966.
- 100) Koonin EV and Makarova KS. Anti-CRISPRs on the march. *Science*. (2018) Oct 12;362(6411):156-157. doi: 10.1126/science.aav2440. PMID: 30309933.
- 101) Zhuo C, et al. Spatiotemporal control of CRISPR/Cas9 gene editing. *Signal Transduct Target Ther*. 2021 Jun 20;6(1):238. doi: 10.1038/s41392-021-00645-w. PMID: 34148061; PMCID: PMC8214627.

- 102) Yang NJ and Hinner MJ. Getting across the cell membrane: an overview for small molecules, peptides, and proteins. *Methods Mol Biol.* (2015) 1266:29-53. doi: 10.1007/978-1-4939-2272-7_3. PMID: 25560066; PMCID: PMC4891184.
- 103) Otvos L Jr and Wade JD. Current challenges in peptide-based drug discovery. *Front Chem.* (2014) Aug 8;2:62. doi: 10.3389/fchem.2014.00062. PMID: 25152873; PMCID: PMC4126357.
- 104) Clementi ME, et al. Antibodies against small molecules. *Ann Ist Super Sanita.* (1991) 27(1):139-43. PMID: 1958021.
- 105) Lee SW, et al. Identification and Optimization of Novel Small-Molecule Cas9 Inhibitors by Cell-Based High-Throughput Screening. *J Med Chem.* (2022) Feb 24;65(4):3266-3305. doi: 10.1021/acs.jmedchem.1c01834. Epub 2022 Feb 10. PMID: 35142491.
- 106) Maji B, et al. A High-Throughput Platform to Identify Small-Molecule Inhibitors of CRISPR-Cas9. *Cell.* (2019) May 2;177(4):1067-1079.e19. doi: 10.1016/j.cell.2019.04.009. PMID: 31051099; PMCID: PMC7182439.
- 107) Ran FA, et al. Genome engineering using the CRISPR-Cas9 system. *Nat Protoc.* (2013) Nov;8(11):2281-2308. doi: 10.1038/nprot.2013.143. Epub 2013 Oct 24. PMID: 24157548; PMCID: PMC3969860.
- 108) Mehlem A, et al. Imaging of neutral lipids by oil red O for analyzing the metabolic status in health and disease. *Nat Protoc.* (2013) Jun;8(6):1149-54. doi: 10.1038/nprot.2013.055. Epub 2013 May 23. PMID: 23702831.
- 109) Lo RC and Kim H. Histopathological evaluation of liver fibrosis and cirrhosis regression. *Clin Mol Hepatol.* (2017) Dec;23(4):302-307. doi: 10.3350/cmh.2017.0078. Epub 2017 Dec 20. PMID: 29281870; PMCID: PMC5760001.
- 110) Byers SL, et al. Mouse estrous cycle identification tool and images. *PLoS One.* (2012) 7(4):e35538. doi: 10.1371/journal.pone.0035538. Epub 2012 Apr 13. PMID: 22514749; PMCID: PMC3325956.
- 111) Caligioni CS. Assessing reproductive status/stages in mice. *Curr Protoc Neurosci.* (2009) Jul;Appendix 4:Appendix 4I. doi: 10.1002/0471142301.nsa04is48. PMID: 19575469; PMCID: PMC2755182.
- 112) Cora MC, et al. Vaginal Cytology of the Laboratory Rat and Mouse: Review and Criteria for the Staging of the Estrous Cycle Using Stained Vaginal Smears.

Toxicol Pathol. (2015) Aug;43(6):776-93. doi: 10.1177/0192623315570339. Epub 2015 Mar 3. PMID: 25739587.

113) Nikolac Gabaj N, et al. Comparison of three different protocols for obtaining hemolysis. Clin Chem Lab Med. (2022) Feb 23;60(5):714-725. doi: 10.1515/cclm-2021-1227. PMID: 35212494.

114) Guilloux JP, et al. Integrated behavioral z-scoring increases the sensitivity and reliability of behavioral phenotyping in mice: relevance to emotionality and sex. J Neurosci Methods. (2011) Apr 15;197(1):21-31. doi: 10.1016/j.jneumeth.2011.01.019. Epub 2011 Jan 26. PMID: 21277897; PMCID: PMC3086134.

115) Love MI, et al. Moderated estimation of fold change and dispersion for RNA-seq data with DESeq2. Genome Biol. (2014) 15(12):550. doi: 10.1186/s13059-014-0550-8. PMID: 25516281; PMCID: PMC4302049.

116) Krämer A, et al. Causal analysis approaches in Ingenuity Pathway Analysis. Bioinformatics. (2014) Feb 15;30(4):523-30. doi: 10.1093/bioinformatics/btt703. Epub 2013 Dec 13. PMID: 24336805; PMCID: PMC3928520.

117) Langfelder P and Horvath S. WGCNA: an R package for weighted correlation network analysis. BMC Bioinformatics. (2008) Dec 29;9:559. doi: 10.1186/1471-2105-9-559. PMID: 19114008; PMCID: PMC2631488.

118) Dutheil S, et al. High-Fat Diet Induced Anxiety and Anhedonia: Impact on Brain Homeostasis and Inflammation. Neuropsychopharmacology. (2016) Jun;41(7):1874-87. doi: 10.1038/npp.2015.357. Epub 2015 Dec 14. PMID: 26658303; PMCID: PMC4869056.

119) De Souza CT, et al. Consumption of a fat-rich diet activates a proinflammatory response and induces insulin resistance in the hypothalamus. Endocrinology. (2005) Oct;146(10):4192-9. doi: 10.1210/en.2004-1520. Epub 2005 Jul 7. PMID: 16002529.

120) Lenert ME, and Burton MD. Acute effects of a high-fat diet on estrous cycling and body weight of intact female mice. Neuropsychopharmacology. (2022) Jan;47(1):418-419. doi: 10.1038/s41386-021-01164-6. PMID: 34453116; PMCID: PMC8617026.

121) Lenert ME, et al. Homeostatic Regulation of Estrus Cycle of Young Female Mice on Western Diet. J Endocr Soc. (2021) Feb 1;5(4):bvab010. doi: 10.1210/jendso/bvab010. PMID: 33733019; PMCID: PMC7947973.

122) Billington CJ, et al. Effects of intracerebroventricular injection of neuropeptide Y on energy metabolism. *Am J Physiol* (1991) 260:R321–R327.

123) Chao PT, et al. Knockdown of NPY expression in the dorsomedial hypothalamus promotes development of brown adipocytes and prevents diet-induced obesity. *Cell Metab* (2011) 13:573–583.

124) Shi YC, et al. Arcuate NPY controls sympathetic output and BAT function via a relay of tyrosine hydroxylase neurons in the PVN. *Cell Metab* (2013) 17:236–248.

125) Egawa M, et al. Neuropeptide Y suppresses sympathetic activity to interscapular brown adipose tissue in rats. *Am J Physiol* (1991) 260:R328–R334

126) Zhang W, et al. Hypothalamus-adipose tissue crosstalk: neuropeptide Y and the regulation of energy metabolism. *Nutr Metab* (2014) Jun 10;11:27. doi: 10.1186/1743-7075-11-27. PMID: 24959194; PMCID: PMC4066284.

SUPPLEMENTAL MATERIALS:

FIGURES:

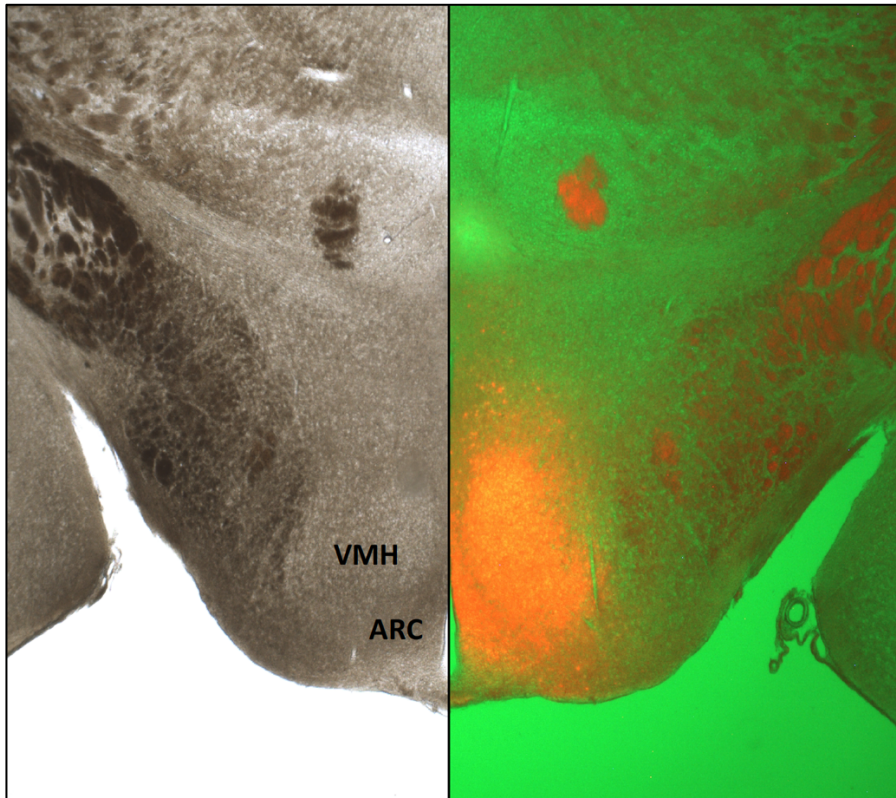


Figure 1: Validation of the injection site. The infected area (on the right) is detected using a fluorescence microscope (Invitrogen EVOS FL Auto 2.0 Imaging System) 20x TX-Red to trace the mCherry orange fluorescence in the designed guides. The highlighted area perfectly matches the hypothalamic area of the arcuate nucleus (ARC) and ventromedial hypothalamus (VMH), which are the main hypothalamic areas involved in metabolic control (shown on the left).

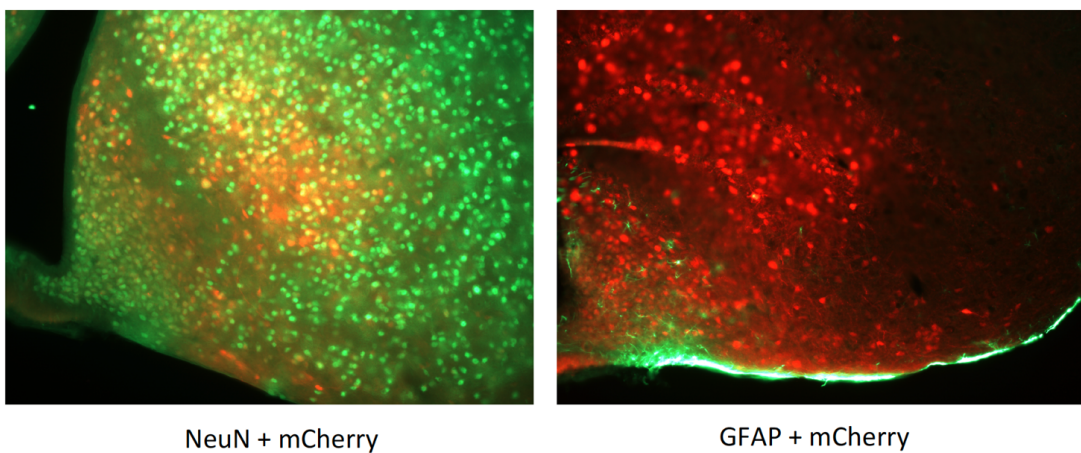


Figure 2: Demonstration that the knockout occurs only in the neurons of the hypothalamus and not in glial cells. The presence of the guide is detected using the mCherry red fluorescence. Neurons are detected in green (on the left) using Mouse anti-NeuN antibody (1:100, Millipore MAB377). Mature Astrocytes are detected in green (on the right) using Rabbit anti-GFAP antibody (1:500, Sigma G9269). Secondary antibodies used: 405 Goat anti-mouse (1:500, Invitrogen) and 488 Goat anti-rabbit (1:500, Invitrogen).

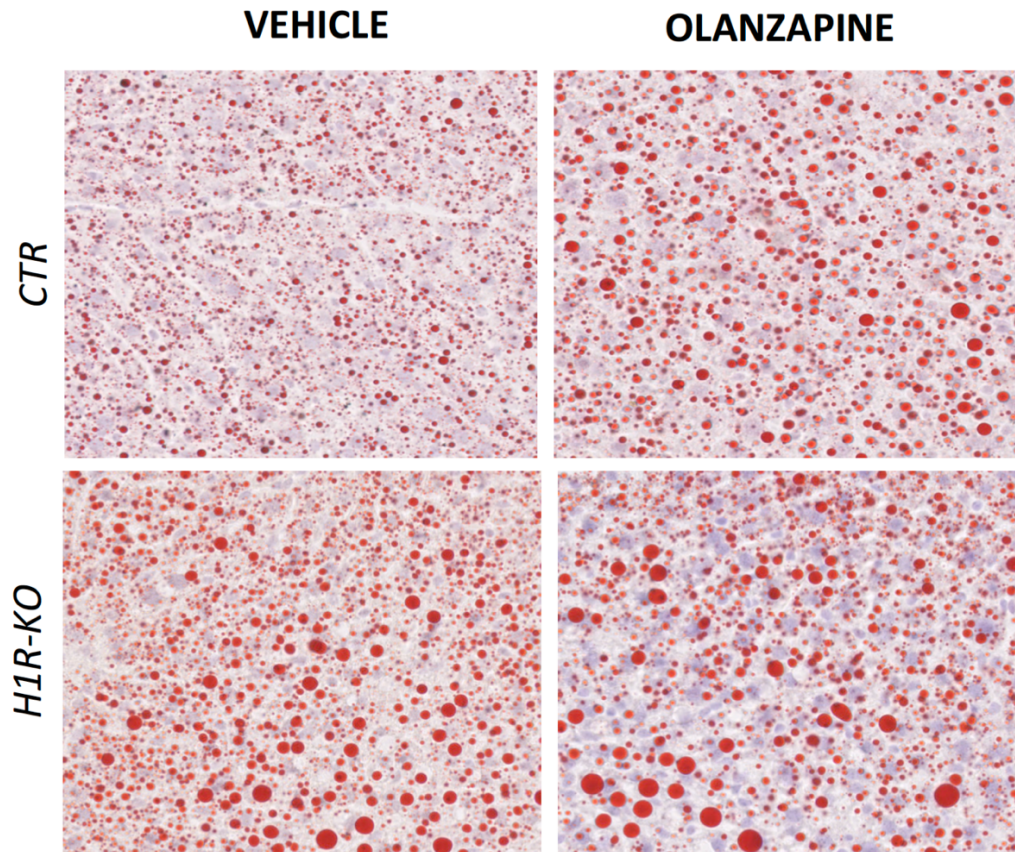


Figure 3: Different fat deposition patterns (in red) in liver sections of H1R-KO mice compared to the Controls, fed with HFD, after 25 days of treatment with Olanzapine or Vehicle. Oil-Red- O staining. Magnification 20x.

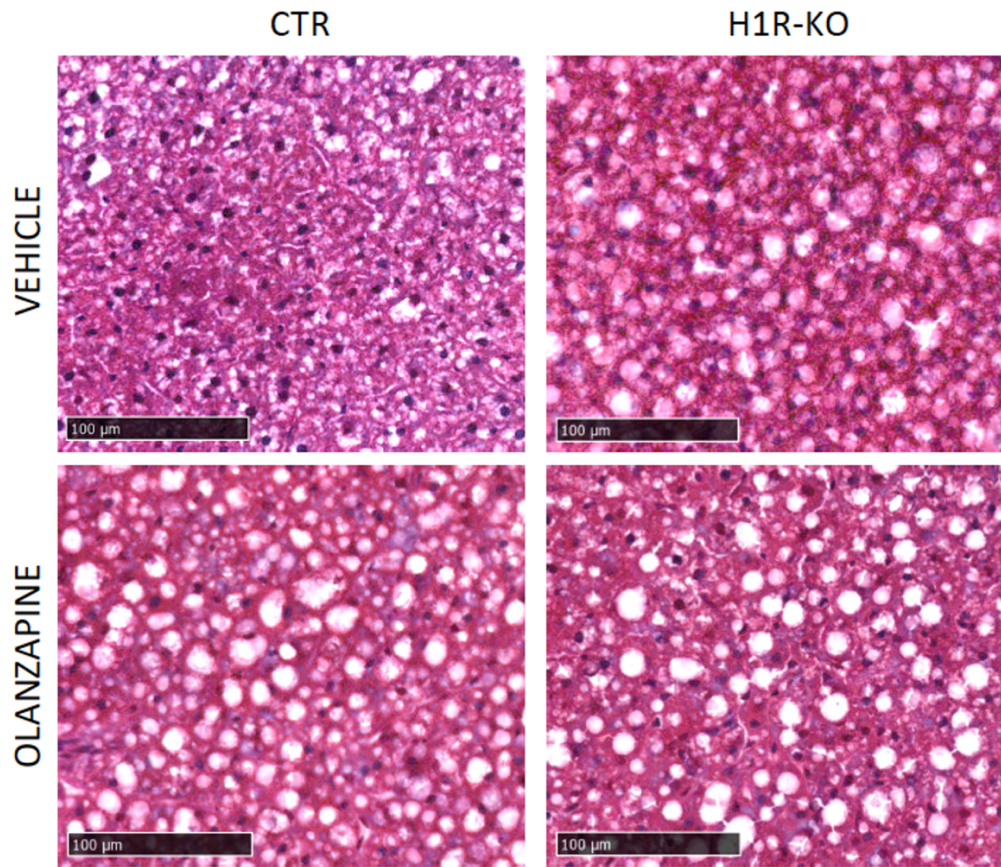


Figure 4: Fibrosis patterns (collagen fibres deposition in blue) in liver sections of H1R-KO mice compared to the Controls, fed with HFD, after 25 days of treatment with Olanzapine or Vehicle. Masson's Trichrome staining. Magnification 20x.

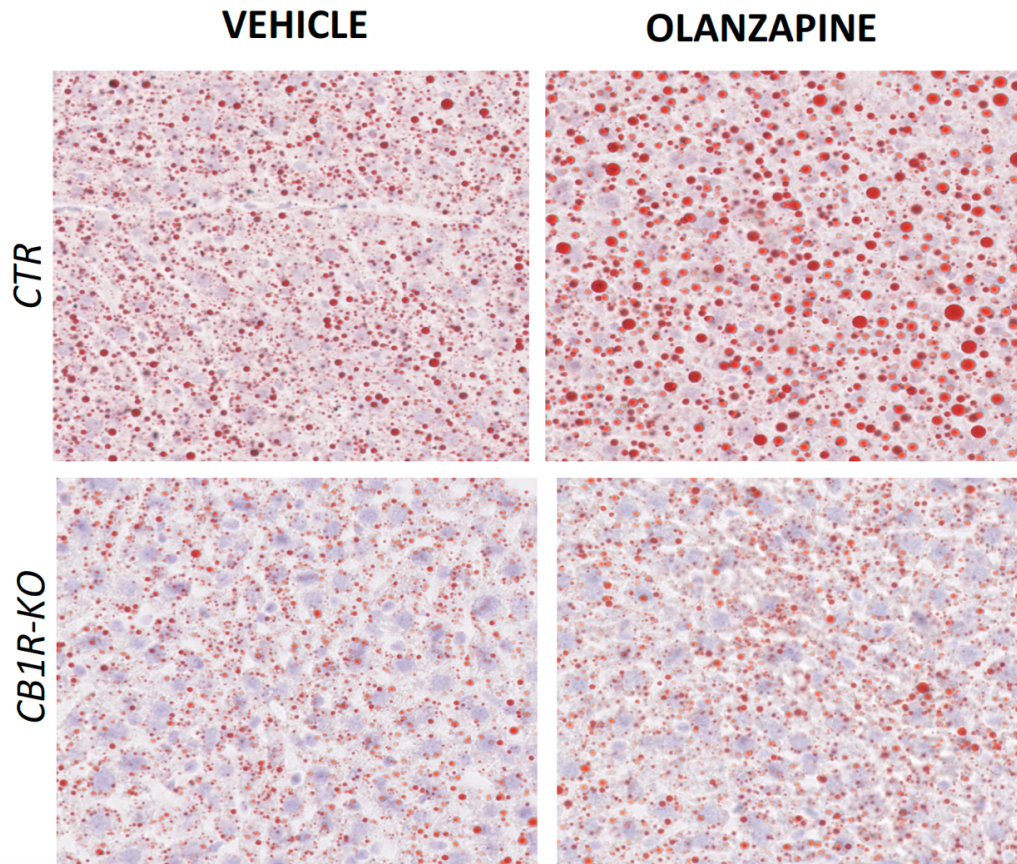


Fig.5 Different fat deposition patterns (in red) in the liver sections of CB1R-KO mice compared to the Controls, fed with HFD, after 25 days of treatment with Olanzapine or Vehicle. Oil-Red- O staining. Magnification 20x.

From the identification of a druggable target for the OL-induced MetS to the development of a new therapeutic approach using CRISPR/Cas7-11S

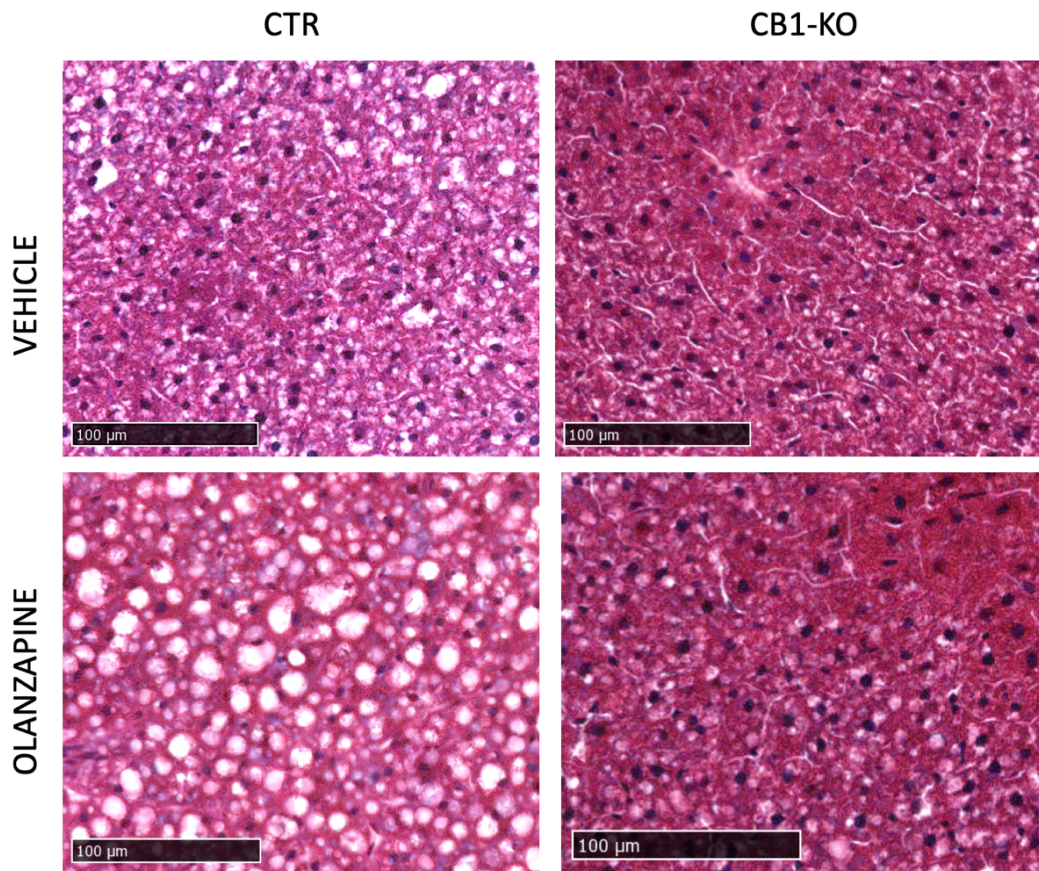


Fig.6 Fibrosis patterns (collagen fibres deposition in blue) in liver sections of CB1R-KO mice compared to the Controls, fed with HFD, after 25 days of treatment with Olanzapine or Vehicle. Masson's Trichrome staining. Magnification 20x.

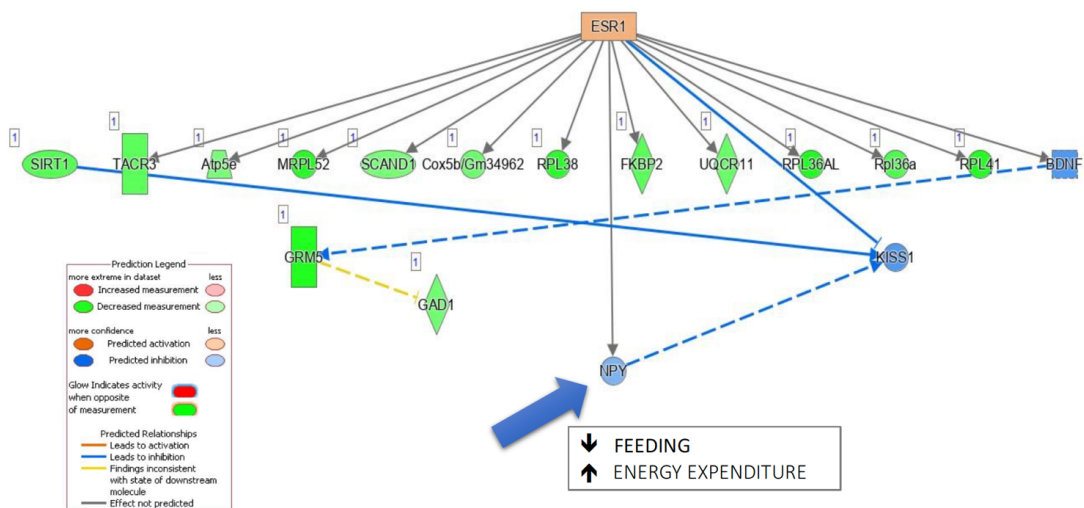


Fig.7 High-fat diet modulation of hypothalamic response in the normal control condition. IPA analysis of DEG between CTR-SD vs CTR-HFD

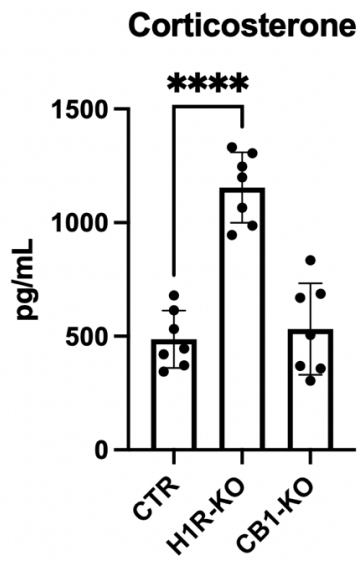


Fig.8 Corticosterone evaluation in serum in mice fed with standard diet (H1R-KO, CB1R-KO and Controls). DetectX Corticosterone Enzyme Immunoassay Kit (Arbor Assays #K014-H5). One-way ANOVA (* $p < 0.05$; ** $p < 0.01$; *** $p < 0.001$; **** $p < 0.0001$).

TABLES:

Drug class	Second-generation antipsychotics								First-generation antipsychotics			
	AMI	ARI	ASE	CLO	OLA	PALI	RIS	QUE	SER	ZIP	HAL	PER
D ₂	1.3 ^b	0.66 ^{ab}	1.3 ^b	210	20	2.8	3.77	770	2.7	2.6	2.6	1.4 ^b
5-HT _{1A}	>10,000 ^c	5.5 ^{ab}	2.5 ^b	160	610	480	190	300	2,200	1.9 ^{ab}	1,800	421
5-HT _{2A}	2,000 ^c	8.7 ^b	0.06 ^b	2.59	1.5	1.2	0.15	31	0.14	0.12	61	5 ^b
5-HT _{2C}	>10,000 ^c	22 ^b	0.03 ^b	4.8	4.1	48	32	3,500	6.0	0.9	4,700	132 ^b
α ₁	7,100 ^c	26 ^b	1.2 ^b	6.8	44	10	2.7	8.1	3.9	2.6	17	10
α ₂	1,600 ^c	74 ^a	1.2 ^b	158	280	80	8	80	190	154	600	500
H ₁	>10,000 ^d	30 ^b	1.0 ^b	3.1	0.08	3.4	5.2	19	440	4.6	260	8
M ₁	N/A	6,780 ^b	8128 ^b	1.4 ^b	2.5 ^b	>10,000 ^b	>10,000 ^b	120 ^b	5,000	300 ^b	>10,000 ^b	1,500
M ₂	N/A	3,510 ^b	4.5 ^b	204 ^b	622 ^b	>10,000 ^b	>10,000 ^b	630 ^b	N/A	>3,000 ^b	>10,000 ^b	N/A
M ₃	N/A	4,680 ^b	4.67 ^b	109 ^b	126 ^b	>10,000 ^b	>10,000 ^b	1,320 ^b	2,692 ^b	>1,300 ^b	>10,000 ^b	1,848 ^b
M ₄	N/A	1,520 ^b	5.09 ^b	27 ^b	350 ^b	>10,000 ^b	>10,000 ^b	660 ^b	N/A	>1,600 ^b	>10,000 ^b	N/A

Notes: Adapted with permission from Correll CU, From receptor pharmacology to improved outcomes: individualizing the selection, dosing, and switching of antipsychotics, *Eur Psychiatry*, 2010;25(Suppl 2):S12–S21, Copyright © 2010, Elsevier Masson SAS. All rights reserved.⁷⁹ Data represented as the equilibrium constant (K_i; nM), ie, nanomolar amount of the antipsychotic needed to block 50% of the receptors in vitro. Therefore, a lower number denotes stronger receptor affinity and binding. ^aPartial agonism. ^dData from cloned human brain receptors. ^cData extracted from rat. ^eData extracted from guinea pig.

Abbreviations: AMI, amisulpride; ARI, aripiprazole; ASE, asenapine; CLO, clozapine; HAL, haloperidol; OLA, olanzapine; PALI, paliperidone; PER, perphenazine; QUE, quetiapine; RIS, risperidone; SER, sertindole; ZIP, ziprasidone; N/A, not applicable.

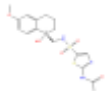
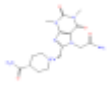
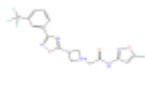
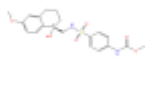
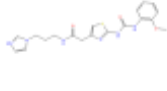
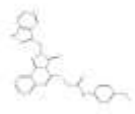
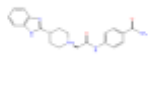
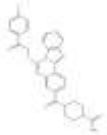
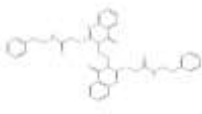
Table 1: Receptor binding profile and plasma half-life (t_{1/2}) of antipsychotic drugs.

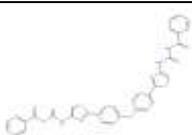
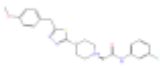
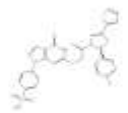
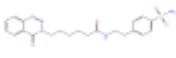
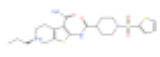
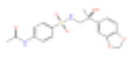
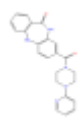
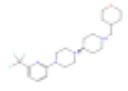
IPA ANALYSIS		
DATASET NAME	GENE SET	N. OF GENES AFTER FILTERING FOR LOW EXPRESSED GENES
DATASET 1	Differential expressed genes between CTR fed with Standard Diet and CTR fed with High Fat Diet (DEG-CTR-SDvsCTR-HFD)	593 genes
DATASET 2	Differential expressed genes between CTR fed with High Fat Diet and H1R-KO fed with High Fat Diet (DEG-CTR-HFDvsH1R-KO-HFD)	459 genes
DATASET 3	Differential expressed genes between H1R-KO fed with High Fat Diet treated with vehicle and H1R-KO fed with High Fat Diet treated with Olanzapine (DEG-H1R-KO-HFD-VvsH1R-KO-HFD-OL)	221 genes
DATASET 4	Differential expressed genes between CTR fed with High Fat Diet treated with Olanzapine and CB1R-KO fed with High fat diet treated with Olanzapine (DEG-CTR-HFD-OLvsCB1R-KO-HFD-OL)	128 genes

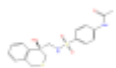
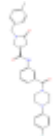
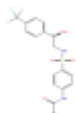
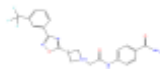
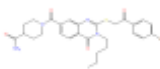
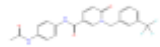
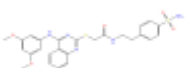
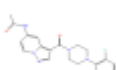
From the identification of a druggable target for the OL-induced MetS to the development of a new therapeutic approach using CRISPR/Cas7-11S

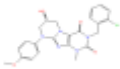
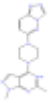
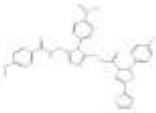
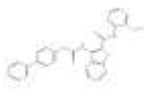
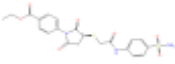
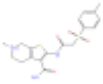
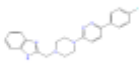
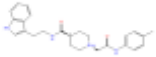
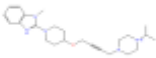
WGCNA ANALYSIS		
DATASET NAME	GENE SET	N. OF GENES AFTER FILTERING FOR LOW EXPRESSED GENES
DATASET 5	Control mice treated with Olanzapine	9752 genes
DATASET 6	CB1R-KO mice treated with Olanzapine	8323 genes

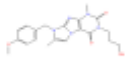
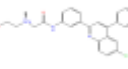
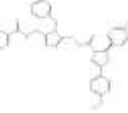
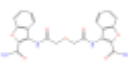
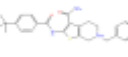
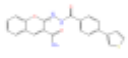
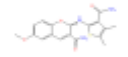
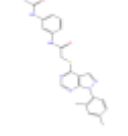
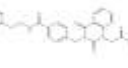
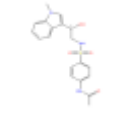
Table 2. Overview of dataset used for the computational analysis.

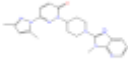
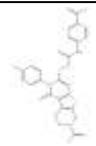
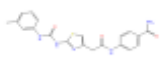
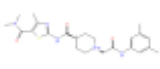
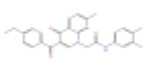
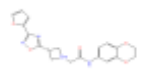
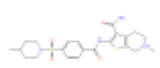
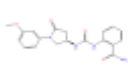
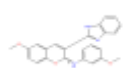
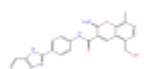
Structure	Title	Docking Score	Glide Gscore	CAS	QPlogBB	QPPMDCK
	F6521-8617	-6.868	-6.885	2034526-68-4	-1.867	67.345
	F1890-0022	-6.504	-6.545	896802-36-1	-2.025	2.431
	F6064-3403	-6.512	-6.561	1351658-06-4	-1.170	578.742
	F6521-8606	-6.428	-6.428	2034405-54-2	-1.855	70.998
	F2096-1095	-6.298	-6.552	921469-98-9	-1.564	374.311
	F6548-3559	-6.275	-6.275	1023482-99-6	-1.011	729.526
	F6521-4430	-6.186	-6.186	2034407-30-0	-1.562	165.425
	F2602-0077	-6.140	-6.310	887215-43-2	-1.326	15.830
	F0916-4099	-6.987	-6.990	443348-06-9	-1.985	150.483
	F3407-3998	-6.961	-6.961	689771-84-4	-2.623	176.136

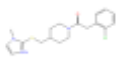
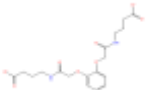
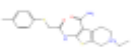
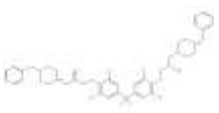
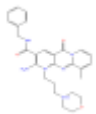
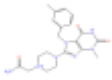
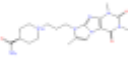
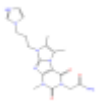
	F1366-3035	-6.938	-6.938	865248-43-7	-3.622	18.690
	F0816-0340	-6.672	-7.263	397288-98-1	-1.212	2026.694
	F6609-6483	-6.544	-6.547	1326875-30-2	-0.475	832.877
	F5496-2191	-6.491	-6.691	1251612-00-6	-0.388	293.352
	F0568-0753	-6.488	-6.554	534596-88-8	-2.334	94.782
	F0916-6794	-6.428	-6.428	440330-89-2	-2.672	25.692
	F2727-0018	-6.353	-6.476	1177746-19-8	-1.284	48.326
	F5857-3253	-6.321	-6.321	1396884-94-8	-1.515	110.431
	F6240-6584	-6.319	-6.430	440120-46-7	-0.977	220.703
	F3395-0110	-6.310	-6.447	2034524-18-8	1.414	1230.788

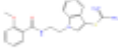
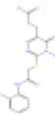
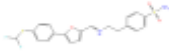
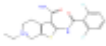
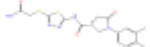
	F6556-0810	-6.290	-6.290		-1.397	194.442
	F6617-2715	-6.277	-6.277	1984056-09-8	-0.985	787.784
	F6200-2309	-6.273	-6.273	1351641-20-7	-1.290	605.656
	F6064-3404	-6.264	-6.281	1351643-60-1	-1.920	152.436
	F0912-3628	-6.250	-6.250	403729-66-8	-2.653	85.335
	F2744-1294	-6.245	-6.245	1005305-92-9	-1.142	742.848
	F6548-4739	-6.228	-6.228	688356-45-8	-2.105	139.185
	F3407-0441	-6.218	-6.218	1242998-43-1	-1.138	156.953
	F3395-0229	-6.215	-6.366	2549053-08-7	0.467	71.820
	F6513-3509	-6.211	-6.211	2034245-63-9	-0.791	447.541

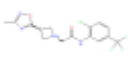
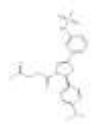
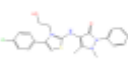
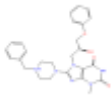
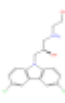
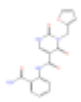
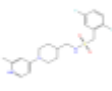
	F2013-0141	-6.208	-6.208	848206-58-6	-0.651	907.504
	F6713-4901	-6.204	-6.204	2380188-07-6	-0.730	293.828
	F0514-1083	-6.204	-6.204	393583-90-9	-2.080	146.423
	F6472-7228	-6.187	-6.187	1796958-67-2	-0.328	882.348
	F0666-0220	-6.180	-6.180	887892-75-3	-0.679	1158.476
	F1740-0137	-6.176	-6.176	868154-99-8	-3.504	5.682
	F2536-0156	-6.170	-6.333	1185173-06-1	-0.632	42.572
	F6713-6036	-6.168	-6.427	2380190-19-0	0.159	511.481
	F2356-0780	-6.164	-6.332	941928-93-4	-0.692	106.857
	F6608-3879	-6.158	-6.158	2640977-96-2	0.810	244.609

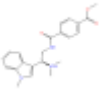
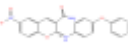
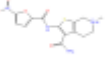
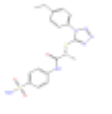
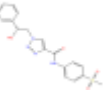
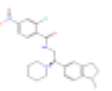
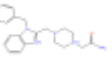
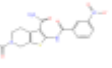
	F2582-0195	-6.135	-6.135	876902-45-3	-1.275	245.390
	F3371-0144	-6.130	-6.146	1018050-89-9	-0.610	262.533
	F0514-4984	-6.125	-6.125	393783-29-4	-1.442	358.535
	F0834-1154	-6.097	-6.097	477295-66-2	-3.039	6.498
	F0526-1182	-6.090	-6.194	1216838-71-9	-0.798	91.228
	F6782-3362	-6.086	-6.127	2640980-61-4	-1.288	183.784
	F6660-0187	-6.075	-6.075	2321343-51-3	-1.300	174.991
	F1874-0967	-6.063	-6.063	872861-93-3	-1.200	378.380
	F0922-0585	-6.060	-6.060	899922-66-8	-1.657	268.421
	F6200-3261	-6.058	-6.058	1448029-62-6	-1.668	90.843

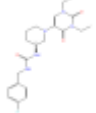
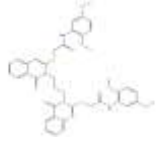
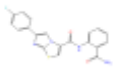
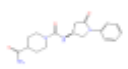
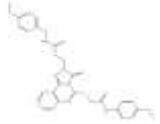
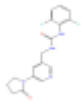
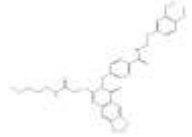
	F6713-1897	-6.038	-6.207	2380059-14-1	-0.313	749.150
	F3222-2466	-6.030	-6.030	1189986-87-5	-1.600	244.622
	F2096-0927	-6.023	-6.023	921469-16-1	-2.358	50.520
	F5772-6957	-6.021	-6.271	1203373-90-3	-0.759	123.694
	F3411-1560	-6.021	-6.021	894887-23-1	-1.135	402.981
	F6064-8462	-6.015	-6.032	1428350-87-1	-0.802	412.432
	F0539-0097	-6.013	-6.177	449767-18-4	-1.608	11.855
	F2024-1006	-6.013	-6.013	894021-97-7	-1.758	61.055
	F6660-0996	-6.004	-6.004	1164474-00-3	-0.087	2388.008
	F6411-5714	-5.988	-6.162	931745-11-8	-2.039	52.226

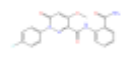
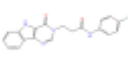
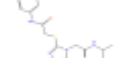
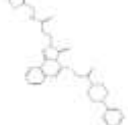
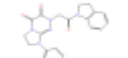
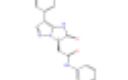
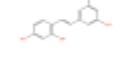
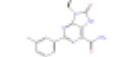
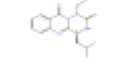
	F3268-0134	-5.984	-6.192	941233-06-3	-1.432	160.567
	F6374-1415	-5.897	-5.995	1428363-73-8	-0.090	4717.140
	F0716-0029	-7.274	-7.278	328104-81-0	-3.826	0.324
	F2537-0116	-6.729	-6.893	1330300-68-9	-0.385	258.220
	F0777-1198	-6.610	-7.487	325473-69-6	-0.103	145.094
	F1673-2006	-6.546	-6.732	867136-61-6		
	F2636-0262	-6.522	-6.568	898463-54-2	-1.371	10.170
	F3289-1204	-6.232	-6.236	923109-72-2	-1.339	12.497
	F3234-0546	-6.208	-6.448	938916-93-9	-1.609	59.307
	F6571-0336	-6.017	-6.121	2034391-51-8	0.186	1644.404

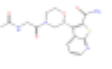
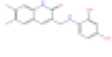
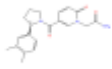
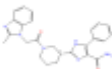
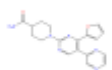
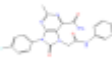
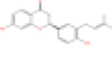
	F1386-0199	-5.981	-6.052	1052409-46-7	-1.264	338.081
	F2712-0120	-7.021	-7.021	886955-26-6	-2.582	4.441
	F3375-0118	-6.518	-6.518	326876-37-3	-1.280	775.588
	F6252-5108	-6.378	-6.396	2034392-95-3	-0.594	90.301
	F2713-0909	-6.326	-6.441	881432-87-7	-0.734	87.580
	F0526-1349	-6.312	-6.476	1216587-45-9	-0.327	206.054
	F3226-1041	-6.307	-6.311	573705-39-2		
	F1877-1392	-6.279	-6.279	893924-32-8	-2.170	40.403
	F0828-0069	-6.278	-6.278	474648-30-1	-2.025	226.351
	F0526-1468	-6.271	-6.434	1215696-84-6	-0.776	84.584

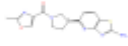
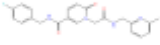
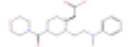
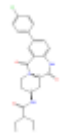
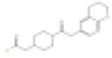
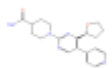
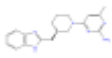
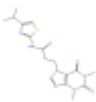
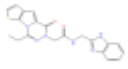
	F2461-0135	-6.257	-6.421	1216692-85-1	-0.788	56.384
	F6064-0391	-6.255	-6.272	1327202-86-7	-0.341	3968.562
	F0652-0198	-6.252	-6.252	852141-65-2	-2.318	9.903
	F2734-0442	-6.251	-6.251	928199-38-6		
	F0856-0360	-6.248	-6.248	474877-84-4		
	F2019-0479	-6.222	-6.222	1216857-82-7	-0.641	195.170
	F3144-0096	-6.206	-6.239	887200-41-1	-1.162	39.787
	F1021-0525	-6.198	-6.207	301160-67-8	-0.052	991.800
	F0696-1421	-6.151	-6.169	1396880-95-7	-1.957	24.022
	F6454-2418	-6.051	-6.051	2034286-77-4	-0.602	1385.066

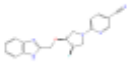
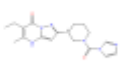
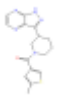
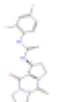
	F5476-0563	-6.000	-6.060	1396800-81-9	-0.497	125.079
	F6660-1227	-5.978	-5.978	313397-62-5	-1.936	47.359
	F0526-1439	-5.961	-6.125	1177444-66-4	-1.865	4.206
	F3090-2332	-5.951	-5.951	887347-59-3	-2.514	19.801
	F6240-2262	-5.919	-5.919	1396855-69-8	-2.224	28.515
	F2291-0889	-5.876	-5.876	921893-31-4	-0.367	18.790
	F6556-6423	-5.865	-5.901	2309747-88-2	-0.229	128.427
	F5621-0362	-5.863	-6.965	1172519-80-0	-0.331	15.572
	F1298-0526	-5.861	-5.861	864927-45-7	-2.463	11.953
	F0648-0134	-5.845	-5.845	852047-45-1	-2.764	5.421

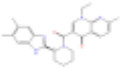
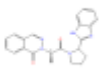
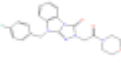
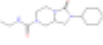
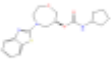
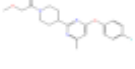
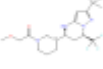
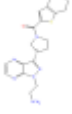
	F6523-1095	-6.891	-6.893	2034347-77-6	-0.731	318.953
	F6479-4338	-6.627	-6.627	2034616-78-7	-0.706	478.381
	F6674-6479	-6.466	-6.466		-1.015	622.408
	F3407-4002	-6.349	-6.349	689762-21-8	-2.653	192.649
	F5269-0502	-6.286	-6.286	1049450-52-3	-0.709	843.362
	F2024-0222	-6.284	-6.284	887465-20-5	-1.268	101.017
	F6548-3739	-6.254	-6.254	1106720-77-7	-1.740	354.659
	F6562-2165	-6.213	-6.213	2097929-05-8	-0.662	610.064
	F6561-1319	-6.205	-6.208	2034537-25-0	-0.545	681.485
	F3168-2395	-6.193	-6.193	688062-34-2	-1.931	323.142

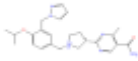
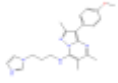
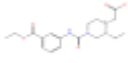
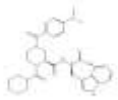
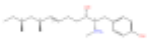
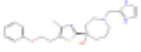
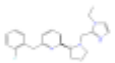
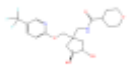
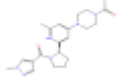
	F2213-0715	-6.159	-6.159	921793-10-4	-1.224	190.848
	F3398-2028	-6.114	-6.114	1207001-18-0	-0.705	868.967
	F2644-0581	-6.095	-6.095	949763-67-1	-1.107	267.274
	F2258-0234	-6.085	-6.115	923195-47-5	-1.181	384.716
	F6548-1612	-6.081	-6.081	1104842-08-1	-1.431	349.184
	F2334-0250	-6.068	-6.068	941888-33-1	-0.829	363.139
	F6278-0001	-6.059	-6.059	1305287-49-3	-1.017	241.903
	ARN18225_Z_01	-5.770	-5.770		-1.726	48.699
	ARN5869_Z_01	-5.678	-5.678		-1.662	55.326
	ARN17682_Z_01	-5.923	-5.923		-1.625	49.901

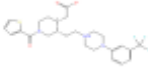
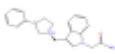
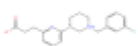
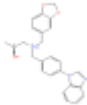
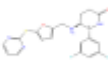
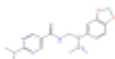
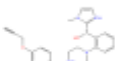
	ARN8622_Z_01	-5.519	-5.519		-1.556	58.791
	ARN7185_Z_01	-5.526	-5.526		-1.501	65.970
	ARN7993_Z_01	-5.691	-5.736		-1.479	76.222
	ARN7071_Z_01	-5.791	-5.791		-1.396	77.514
	ARN4141_Z_01	-5.608	-5.608		-1.345	103.899
	ARN10163_Z_01	-5.702	-6.063		-1.318	133.022
	ARN17286_Z_01	-5.556	-5.557		-1.207	69.870
	ARN8128_Z_01	-5.570	-5.570		-1.197	136.097
	ARN4250_Z_01	-5.624	-5.624		-1.185	258.570
	ARN18395_Z_01	-5.952	-5.952		-1.149	194.850

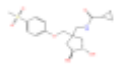
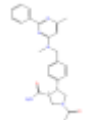
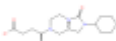
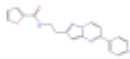
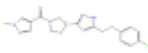
	ARN4183_Z_01	-5.710	-5.710		-1.094	224.028
	ARN9954_Z_01	-6.236	-6.236		-1.044	191.712
	ARN8991_Z_01	-5.554	-5.590		-1.022	455.493
	ARN18861_Z_01	-5.867	-5.889		-1.012	83.732
	ARN22805_Z_01	-5.515	-5.515		-0.991	707.763
	ARN3274_Z_01	-5.562	-5.565		-0.900	81.816
	ARN4233_Z_01	-5.649	-5.649		-0.891	210.717
	ARN9812_Z_01	-5.669	-5.824		-0.886	285.296
	ARN10255_Z_01	-5.884	-5.884		-0.813	682.705
	ARN8369_Z_01	-5.716	-5.743		-0.806	597.812

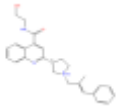
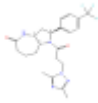
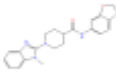
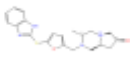
	rep_IIT_20211112.sdf	-6.097	-6.098		-0.773	77.830
	ARN20577_Z_01	-5.756	-5.759		-0.712	96.913
	ARN18693_Z_01	-5.616	-5.633		-0.670	668.205
	ARN19027_Z_01	-5.517	-5.563		-0.637	426.100
	ARN8036_Z_01	-6.013	-6.092		-0.570	470.857
	ARN8576_Z_01	-5.545	-5.545		-0.476	671.727
	ARN5025_Z_01	-5.760	-5.779		-0.471	626.893
	ARN5059_Z_01	-5.640	-5.681		-0.386	690.114
	ARN3030_Z_01	-5.568	-5.568		-0.370	942.400
	ARN20512_Z_01	-5.717	-5.717		-0.343	1226.601

	ARN5945_Z_01	-5.748	-5.811		-0.324	1103.629
	ARN9535_Z_01	-5.587	-5.587		-0.304	241.107
	ARN8402_Z_01	-5.533	-5.585		-0.217	1253.886
	ARN5941_Z_01	-5.551	-5.551		-0.212	2134.089
	ARN19045_Z_01	-5.904	-5.904		-0.173	1026.080
	ARN18126_Z_01	-6.006	-6.006		-0.040	100.853
	ARN19047_Z_01	-5.725	-5.732		0.033	2634.014
	ARN7105_Z_01	-5.825	-5.825		0.034	3676.622
	ARN6147_Z_01	-5.747	-5.747		0.209	7583.660
	ARN7100_Z_01	-5.998	-6.004		-0.785	70.319

	ARN6778_Z_01	-6.025	-6.032		-0.738	74.008
	ARN8661_Z_01	-6.005	-6.237		-0.364	1739.969
	ARN18081_Z_01	-5.828	-5.828		-2.612	10.228
	ARN20502_Z_01	-5.677	-5.680		-1.725	21.070
	ARN18680_Z_01	-6.256	-6.256		-1.920	102.328
	ARN18070_Z_01	-6.151	-6.160		-0.964	113.040
	ARN9581_Z_01	-6.176	-6.589		-0.220	258.335
	ARN7612_Z_01	-6.030	-6.309		0.504	1243.533
	ARN18960_A_01	-7.564	-7.564		-0.879	836.506
	ARN9444_Z_01	-7.670	-7.670		-0.661	483.324

	ARN0113_Z_02	-5.571	-5.572		-0.486	199.300
	ARN20614_Z_01	-8.220	-8.259		-0.450	147.176
	ARN4019_Z_01	-7.813	-7.896		-0.358	249.377
	ARN4721_J_01	-7.821	-7.843		-0.350	111.284
	ARN2809_Z_01	-8.023	-8.046		-0.344	53.161
	ARN3688_J_01	-7.479	-7.559		-0.139	297.700
	ARN10521_Z_01	-7.504	-7.638		-0.137	387.582
	ARN4022_Z_01	-7.856	-7.861		-0.127	575.338
	ARN4585_Z_01	-8.175	-8.298		-0.094	274.587
	ARN3883_Z_01	-6.467	-6.691		-0.074	402.459

	ARN18955_Z_01	-6.392	-6.392		-2.223	33.616
	ARN9578_Z_01	-6.238	-6.324		-1.445	156.225
	ARN19043_Z_01	-6.398	-6.401		-1.312	24.919
	ARN17848_Z_01	-6.130	-6.130		-1.212	262.500
	ARN19157_Z_01	-6.559	-6.559		-1.160	53.531
	ARN2797_Z_01	-6.378	-6.379		-0.962	305.622
	ARN4216_Z_01	-6.295	-6.301		-0.941	388.162
	ARN9772_Z_01	-5.993	-6.404		-0.780	908.343
	ARN8408_Z_01	-5.994	-6.048		-0.669	663.085
	ARN6228_J_01	-6.340	-6.768		-0.628	106.520

	ARN7192_Z_01	-6.042	-6.047		-0.618	131.521
	ARN9189_Z_01	-6.297	-6.297		-0.587	1064.875
	ARN9955_A_01	-6.536	-6.547		-0.321	84.745
	ARN10089_Z_01	-6.665	-6.693		-0.272	1295.132
	ARN10296_Z_01	-6.121	-6.159		-0.074	2112.201
	ARN3986_J_01	-6.427	-6.432		0.035	320.219
	ARN8468_Z_01	-6.035	-6.088		0.043	2217.997
	ARN20688_Z_01	-6.305	-6.329		0.198	569.625
	ARN4607_Z_01	-6.402	-6.552		0.211	73.620